

UNIVERSITY OF CINCINNATI

May 10, **20** 00

I, Chao-Heng Tseng,

**hereby submit this as part of the requirements for the
degree of:**

Doctorate of Philosophy

In:

Environmental Engineering

It is entitled Enhanced Pulsed Corona Method for the
Removal of SO₂ and NO_x from Combustion Gas in a Wet
Electrostatic Precipitator

Approved by:

Tim C. Keener

Paul L. Bishop

Soon-Jai Khang

Yuen-Koh Kao

Enhanced Pulsed Corona Method for the Removal of SO₂ and NO_x from Combustion Gas in a Wet Electrostatic Precipitator

A dissertation submitted to the

Division of Research and Advanced Studies
of the University of Cincinnati

in partial fulfillment of the
requirements for the degree of

DOCTORATE OF PHILOSOPHY (Ph.D.)

in the Department of Civil and Environmental Engineering
of the College of Engineering

2000

by

Chao-Heng Tseng

B.S. Mechanical Engineering, National Taiwan University

M.S. Environmental Engineering, National Taiwan University

Ph.D. Environmental Engineering, University of Cincinnati

Committee Chair: Dr. Tim C. Keener

Abstract

This research investigated the removal of sulfur dioxide (SO_2 , up to 3000 ppm) and nitrogen oxides (NO_x , up to 1000 ppm) in a bench-scale pulsed corona enhanced wet electrostatic precipitator (wESP). High level of SO_2 (up to 70%) was removed by using water and pulsed corona discharge (45 kV, 40 watt) without any additives. SO_2 removal efficiency increased with gas residence time, water flow rate, inlet SO_2 concentration, and applied corona power. Corona discharge forced the charged SO_2 to reach equilibrium with the water. The primary removal mechanisms for SO_2 are the selective charging of SO_2 molecules and the wet wall absorption. A n-CSTR/mass transfer model was developed for this wESP system. The overall SO_2 removal efficiency and the overall SO_2 mass transfer coefficient of the wESP can be predicted from wESP system parameters and operational conditions.

NO_x removal efficiency increased with gas residence time, inlet NO_x concentration, and applied corona power. Without any additives, the maximum De- NO_x efficiency were 20% and 5% in an air stream and in a 3%- O_2 simulated flue gas, respectively. The maximum NO_x removal in this simulated flue gas was 40% due to the formation of NH_4NO_3 aerosols with the injection of O_3 and NH_3 (without ammonium sulfur aerosols). High NO_x removals (~80%) were measured when the in-situ ammonium sulfur aerosols were formed in simulated flue gas that contained NH_3 , SO_2 , and ozone. It was determined that the in-situ ammonium sulfur aerosols served as a highly efficient adsorbent with tremendous surface area which enhanced the oxidation of NO , as well as the formation of NH_4NO_3 .

A batch reactor was also constructed to study the SO_2 mass transfer and removal mechanisms. The results showed that a positive pulsed corona achieved the maximum pollutant removal rate as compared to any other types of coronas. The overall mass transfer was enhanced by 160% with a power density of 685 watt/m^3 . A thin film mass transfer model was developed by introducing both the gas and liquid side electrostatic enhancement factors. It is believed that both the gas side and the liquid side boundary layer thicknesses were reduced by the corona discharge.

Acknowledgments

First, I would like to thank my advisor, Dr. Tim C. Keener, for giving me an opportunity to be a part of his research group. Without his invaluable advice and guidance along the way, I would never have reached as far as I have. I would also like to thank my co-advisor, Dr. Soon-Jai Khang, for all his insights and suggestions. I am grateful to have worked with the Drs. Keener and Khang, and fellow students in our research group.

A great deal of helps has contributed by Dr. Paul L. Bishop and Dr. Yuen-Koh Kao. And special thanks are due two of my wonderful partners in this research: Karen Larkin, who shared many experiment works with me at the first two years, and Joo-Youp Lee, with whom I finished the most theory part at the last two years.

Last but not the least, I appreciate the love and support from my family in Taiwan, brothers and sisters at Cincinnati Chinese Church, Dr. and Mrs. Louie, and Yin-Chun Cathy Chen, my significant one. Praise to the Lord our Heavenly Father and Jesus my Savior.

Chao-Heng
in Cincinnati, May 2000

Table of Contents

1. INTRODUCTION	7
1.1 Sulfur Dioxide and Nitrogen Oxides	7
1.2 Current Control Technology	9
1.3 Introduction of Pulsed Corona Technology	10
1.3.1 Power Technologies	10
1.3.2 Corona Discharge in an ESP	12
1.3.3 Pulsed Corona Discharge Technology	15
1.3.4 Electron Beam Technology	17
1.3.5 Corona Polarity	18
1.3.6 Wet Electrostatic Precipitator	19
1.4 Research Objectives	21
2. LITERATURE REVIEW	23
2.1 Electron Attachment	23
2.2 Ozone Oxidation	25
2.2.1 Ozone Generation	25
2.2.2 SO ₂ Removal	26
2.2.3 NO _x Removal	27
2.3 Radical Reactions	28
2.3.1 SO ₂ Removal	29
2.3.2 NO _x Removal	29
2.4 Corona Wind Enhanced Mass Transfer	30
2.5 Ammonia Injection	32
2.5.1 SO ₂ Removal with Ammonia Injection	32
2.5.2 NO _x Removal with Ammonia Injection	34
2.5.3 The Byproducts of SO ₂ and NO _x Removal with Ammonia Injection	37
2.5.4 Ammonia Recovery	38
2.6 Other Factors	39
2.6.1 Other Alkaline in the Gas or Liquid Phase	39
2.6.2 O ₂ , CO ₂ and Water Vapor in the Gas Phase	39
2.6.3 Temperature Effects	40
2.6.4 Particles in the Gas Phase	41
2.6.5 Wet Scrubbing Methods for NO _x removal	42
3. EXPERIMENT DESCRIPTION	43
3.1 Methodology	43
3.2 Wet ESP System	44
3.2.1 Wet ESP System Setup	47
3.2.2 Wet ESP Experimental Procedure	54
3.3 Batch SO₂ Absorption System	55
3.3.1 Batch Reactor Setup	55

3.3.2	Batch Reactor Experimental Procedure	58
3.4	Water Analysis	59
3.4.1	Gravimetric Method with Drying of Residue for Sulfate Ion	59
3.4.2	Iodometric Method for Sulfite Ion	60
3.4.3	Ion Chromatography	61
3.4.4	Water Quality	64
4.	THEORY AND MODELING	66
4.1	Gas Flows in the wESP	66
4.2	The Motion of Charged Particles and Ions in ESPs	70
4.3	Chemistry of SO₂	72
4.3.1	Henry's Law	72
4.3.2	Oxidation of SO ₂	72
4.3.3	Dissociation of SO ₂	73
4.4	Chemistry of NO_x	75
4.4.1	Henry's law	75
4.4.2	Gas Phase Reactions of Nitrogen Oxides	76
4.4.3	Removal of Nitrogen Oxides	77
4.5	Equilibrium State N-CSTR Model of wESP	78
4.6	Electrostatics Enhanced Mass Transfer N-CSTR Model of wESP	81
4.7	Thin Film Mass Transfer Theory of SO₂ Absorption	85
4.7.1	Determination of Overall Mass Transfer Coefficient K _{OG}	85
4.7.2	Mass Transfer Modeling at Gas Phase Boundary Layer	88
4.7.3	Mass Transfer Modeling at Liquid Phase Boundary Layer	89
4.7.4	Determination of Local Mass Transfer Coefficients and Dissociation Enhancement Factor	93
4.8	Electrostatic Enhancement Factors	96
4.8.1	Determination of Electrostatic enhancement Factors	97
5.	SO₂ REMOVAL IN WESP	100
5.1	Removal vs. Electrical Properties	100
5.1.1	Removal Efficiency vs. Corona Voltage and Power	101
5.1.2	Modeling Results of Electrostatics Enhanced Mass Transfer N-CSTR Model in wESP	103
5.2	Pollutant Concentration and Flow Conditions	105
5.2.1	SO ₂ Concentration	105
5.2.2	Gas and Liquid Flow Rate	106
5.3	Ozone Injection	107
5.3.1	In-Situ Ozone	107
5.3.2	Ozone Injection	109
5.4	Ammonia Injection	113
5.5	Fates of Sulfur	115
5.5.1	pH in the Water of wESP	115
5.5.2	Concentrations of Sulfite and Sulfate	117
5.5.3	Sulfur Mass Balance	119

<u>6.</u>	<u>NO_x REMOVAL IN WESP</u>	121
<u>6.1</u>	<u>In Nitrogen</u>	122
<u>6.2</u>	<u>In Air</u>	123
6.2.1	Without Ozone or Ammonia Injections	123
6.2.2	With Ozone Injection	125
6.2.3	With Ammonia Injection Only (without Ammonium-Sulfur Aerosol)	127
<u>6.3</u>	<u>In Simulated Flue Gas</u>	128
6.3.1	With Ammonia Injection Only	128
6.3.2	With Ozone Injection Only	130
6.3.3	With Ammonia and Ozone Co-Injection (without Ammonium Sulfur Aerosol)	130
<u>6.4</u>	<u>Enhanced Effect of In-situ Ammonium Sulfur Aerosols</u>	132
6.4.1	Molecules of NO Removed per Molecule of Ozone	136
6.4.2	Ammonia Slippage	138
<u>6.5</u>	<u>Ultimate Analysis of the Ammonium Salt Aerosols</u>	138
<u>6.6</u>	<u>Summary of wESP Performance</u>	140
<u>6.7</u>	<u>Fates of Nitrogen</u>	142
6.7.1	Concentrations of Nitrite and Nitrate in Water	142
6.7.2	Mass Balance of Nitrogen	145
<u>7.</u>	<u>SO₂ REMOVAL RESULTS OF BATCH TESTS</u>	147
<u>7.1</u>	<u>Gas Mixing</u>	147
<u>7.2</u>	<u>Liquid Mixing</u>	149
<u>7.3</u>	<u>Pulsing</u>	149
<u>7.4</u>	<u>Polarity</u>	150
<u>7.5</u>	<u>Corona Power</u>	152
<u>7.6</u>	<u>Chemical Dissociation Enhancements and Electrostatic Enhancements</u>	155
<u>7.7</u>	<u>Comparison of the Mass Transfer Enhancement due to the Corona Effect and the Physical Gas-Phase Mixing</u>	160
<u>8.</u>	<u>CONCLUSIONS</u>	161
<u>9.</u>	<u>REFERENCE</u>	165
<u>10.</u>	<u>APPENDICES</u>	170

List of Figures

<u>Figure 1.1 SO_x Emissions in USA in 1997</u>	8
<u>Figure 1.2 NO_x Emissions in USA in 1997</u>	8
<u>Figure 1.3 Schematic Diagram of a Typical Wire-to-Plate ESP</u>	13
<u>Figure 1.4 Typical Field Strength in a Wire-to-Plate ESP</u>	13
<u>Figure 3.1 Schematic Diagram of Wet-ESP System</u>	45
<u>Figure 3.2 Top View of wESP System</u>	46
<u>Figure 3.3 Front View of wESP System</u>	46
<u>Figure 3.4 Side View of wESP System</u>	47
<u>Figure 3.5 High Voltage Pulsing Module</u>	52
<u>Figure 3.6 The Overall View of the Batch Reactor System</u>	56
<u>Figure 3.7 Typical Chromatogram of a Standard Solution</u>	63
<u>Figure 3.8 Typical Chromatogram of the Water Sample from wESP</u>	63
<u>Figure 4.1 Bulk Gas Velocity in the wESP</u>	67
<u>Figure 4.2 Local Reynolds Number, R_{ex}, in the wESP</u>	67
<u>Figure 4.3 The Boundary Layer Profiles in the wESP</u>	69
<u>Figure 4.4 The Profiles of Mass Transfer Coefficient in the wESP</u>	69
<u>Figure 4.5 Most Possible Reaction Paths of NO_x Removal</u>	78
<u>Figure 4.6 The Equilibrium State N-CSTR model</u>	79
<u>Figure 4.7 Gas-liquid Interface Mass Transfer</u>	82
<u>Figure 4.8 One CSTR in Electrostatics Enhanced Mass Transfer N-CSTR Model</u>	83
<u>Figure 4.9 Thin Film Mass Transfer Theory in the Batch Reactor</u>	85
<u>Figure 4.10 Typical Result of a Batch Reactor Test</u>	87
<u>Figure 4.11 Removal of the Liquid Side Mass Transfer Resistance</u>	94
<u>Figure 4.12 Electrostatic Enhancement Factors of Mass Transfer Coefficients</u>	97
<u>Figure 5.1 SO₂ Concentration in ESP under Dry Condition</u>	100
<u>Figure 5.2 SO₂ Removal Efficiency vs. Inlet SO₂ Concentration in wESP</u>	102
<u>Figure 5.3 SO₂ Removal Efficiency vs. Corona Power in wESP</u>	102
<u>Figure 5.4 Overall Mass Transfer Coefficient vs. Corona Power in wESP</u>	103
<u>Figure 5.5 Mass Transfer Coefficient vs. Corona Power and Inlet SO₂ concentration in wESP</u>	104
<u>Figure 5.6 SO₂ Removal vs. Gas Residence Time in wESP</u>	106
<u>Figure 5.7 SO₂ Removal vs. Gas/Liquid Volumetric Flow Ratio in wESP</u>	107
<u>Figure 5.8 Relationship between In-situ Ozone and Power in wESP</u>	108
<u>Figure 5.9 Relationship between In-situ Ozone, Gas Residence Time and Corona Power</u>	109
<u>Figure 5.10 SO₂ Removal vs. Ozone Injection in the SO₂/Air Stream</u>	110
<u>Figure 5.11 SO₂ Removal vs. Corona Discharge in the SO₂/Air Stream</u>	111
<u>Figure 5.12 SO₂ Removal vs. Ozone Injection in SO₂/NO_x/Air Stream</u>	112

<u>Figure 5.13 SO₂ Removal vs. Corona Discharge in SO₂/NO_x/Air Stream</u>	112
<u>Figure 5.14 SO₂ removal vs. Ammonia Injection in SO₂/Air Stream</u>	113
<u>Figure 5.15 SO₂ removal vs. Ammonia Injection and Corona Discharge in SO₂/Air Stream</u>	114
<u>Figure 5.16 pH in Phases of wESP at Low and High SO₂ Inlet Concentration</u>	116
<u>Figure 5.17 Sulfite and Sulfate Concentrations of Water Samples in Six Positions</u>	118
<u>Figure 6.1 NO Removal in Dry ESP</u>	121
<u>Figure 6.2 NO Removal Efficiency vs. Corona Power in Air</u>	124
<u>Figure 6.3 NO and NO_x Removal vs. Input NO_x Concentration and Gas Residence Time in Air</u>	124
<u>Figure 6.4 The NO and NO_x Removal vs. Ozone Injection in Air-NO_x Stream</u>	125
<u>Figure 6.5 The NO and NO_x Removal vs. Ozone Injection in NO_x/Air and SO₂/NO_x/Air Streams</u>	126
<u>Figure 6.6 The NO_x Removal in SO₂/NO_x/Air Stream</u>	127
<u>Figure 6.7 NO and NO_x Removal vs. Ammonia Injection in Air</u>	128
<u>Figure 6.8 NO_x Removal with Ammonia Injection in Simulated Flue Gases</u>	129
<u>Figure 6.9 The NO_x Removal vs. Ammonium and Ozone in Simulated Flue Gas</u>	132
<u>Figure 6.10 The Improved NO_x Removal vs. Ammonium and Ozone in Simulated Flue Gas</u>	134
<u>Figure 6.11 The Improved NO_x removal Efficiency vs. Ammonium Sulfur Aerosols</u>	134
<u>Figure 6.12 Molecules of NO Removed per Molecule of Ozone</u>	137
<u>Figure 6.13 Removal Mechanisms of NO and NO_x in Air</u>	141
<u>Figure 6.14 Removal Mechanisms of NO and NO_x in 3%-O₂ Simulated Flue Gas</u>	141
<u>Figure 6.15 Removal Mechanisms of NO and NO_x with More Additives in 3%-O₂ Simulated Flue Gas</u>	142
<u>Figure 6.16 Increased Nitrite and Nitrate Concentrations of wESP tests in Air, N₂ and Simulated Flue Gas</u>	143
<u>Figure 6.17 Nitrite and Nitrate Concentrations of Water Samples of Six Positions</u>	144
<u>Figure 7.1 Overall Mass Transfer Coefficient vs. Gas Mixing Fan Speed</u>	148
<u>Figure 7.2 Overall Mass Transfer Coefficient vs. Gas Phase Mixing</u>	148
<u>Figure 7.3 Overall Mass Transfer Coefficient vs. Liquid Phase Mixing</u>	149
<u>Figure 7.4 The Effect of Pulsing on the SO₂ Mass Transfer in Batch Reactor</u>	150
<u>Figure 7.5. Schematic of Corona Discharge Processes</u>	151
<u>Figure 7.6 Mass Transfer Coefficient vs. Corona Polarity and Power in Batch Reactor</u> ..	152
<u>Figure 7.7 Overall Mass Transfer Coefficients vs. Corona Power of Batch Tests</u>	153
<u>Figure 7.8 Electrostatic Enhancement Factors vs. Corona Power</u>	158
<u>Figure 7.9 Mass Transfer Resistances vs. Corona Power</u>	159
<u>Figure 10.1 Distribution of Sulfite Ions vs. pH of solution</u>	176

List of Tables

<u>Table 1.1 Air Quality Standards and Industrial Exposure Standards</u>	9
<u>Table 1.2 Comparison of Corona Discharge Technology and Electron Beam Technology</u> .	11
<u>Table 1.3 The Ionization and Dissociation Energies of Gas Molecules</u>	15
<u>Table 3.1 Summary of the wESP Experiment Parameters</u>	43
<u>Table 3.2 Summary of Batch Reactor Experimental Parameters</u>	44
<u>Table 3.3 Total Sulfur Analysis of Batch Reactor Tests</u>	58
<u>Table 3.4 Analysis Methods for Sulfur and Nitrogen Compounds in the Liquid Phase</u>	59
<u>Table 3.5 Reproducibility of Ion Chromatograph Analysis of Tap Water</u>	64
<u>Table 3.6 Quality of Water Used in the wESP and Batch Tests</u>	65
<u>Table 4.1 Electrical Mobility of Electrons, Ions, and Aerosol Particles at Standard Conditions</u>	71
<u>Table 4.2 Summary of the Calculation of Thin Film Mass Transfer Theory</u>	96
<u>Table 4.3 Summary of the Calculation of Electrostatic Enhancement Factors</u>	99
<u>Table 5.1 Experimental and Equilibrium Modeling Results of pH Value in Six Phases</u>	115
<u>Table 5.2 Sulfur Mass Balance of Iodometric Sulfite Tests and Gravimetric Sulfate Tests Results</u>	119
<u>Table 5.3 Mass balance of Sulfur by Ion Chromatograph Method</u>	120
<u>Table 6.1 Test Removal of Nitrate Oxide in a Nitrogen Stream and in Air</u>	122
<u>Table 6.2 Ultimate Analysis of the Ammonium Salt Aerosols Collected at wESP</u>	139
<u>Table 6.3 Summary of Maximum Removal Efficiency in the wESP</u>	140
<u>Table 6.4 Mass balance of Nitrogen by Ion Chromatograph Method</u>	145
<u>Table 7.1 Summary of Overall Mass Transfer Coefficients of Batch Tests</u>	154
<u>Table 7.2 Mass Transfer Coefficients and Resistances and Chemical Dissociation Enhancement Factor for Non-Corona Tests</u>	155
<u>Table 7.3 Mass Transfer Coefficients and Resistances and Electrostatic enhancement Factors</u>	157
<u>Table 10.1 Summary of Literature Reviews</u>	170
<u>Table 10.2 Molecular Reactions</u>	171
<u>Table 10.3 Reactions of Ammonia with SO₂</u>	173
<u>Table 10.4 Henry's Constants into Water</u>	174
<u>Table 10.5 Henry's Constant of SO₂</u>	174
<u>Table 10.6 Liquid Phase Reactions</u>	175
<u>Table 10.7 Dissociation Reactions of Sulfite and Sulfate</u>	176
<u>Table 10.8 Solubility of Gases in water</u>	177
<u>Table 10.9 Diffusivity of Ions in Water</u>	177
<u>Table 10.10 Solubility Study of Calcium and Ammonium Salts</u>	178
<u>Table 10.11 Radicals and Electrons Related Reactions</u>	179

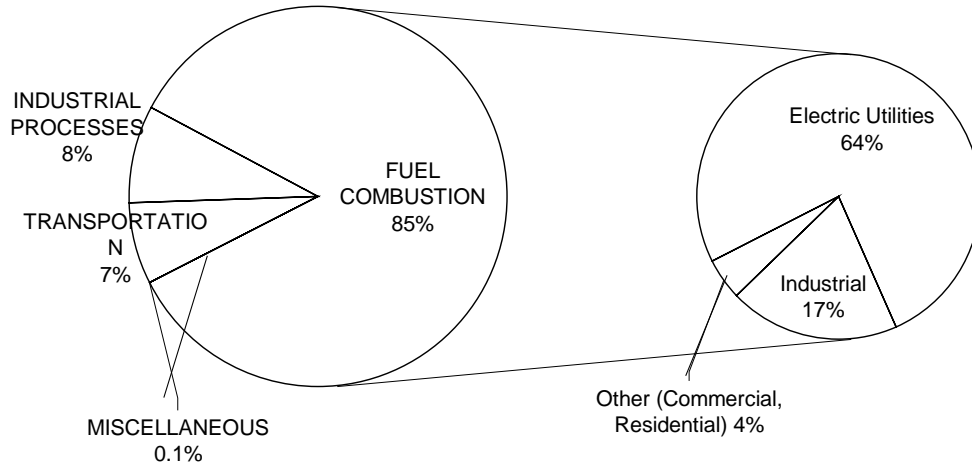
1. INTRODUCTION

1.1 Sulfur Dioxide and Nitrogen Oxides

Sulfur dioxide (SO_2) and total nitrogen oxides (NO_x , the combined sum of NO and NO_2) are strong respiratory irritants that can cause health damage at high concentrations. These pollutants lead to acid deposition and fine aerosols ($\text{PM}_{2.5}$). NO_x is a primary precursor of photochemical smog as well. SO_2 is formed from the sulfur content in fuels. NO_x is formed from both nitrogen in the air (thermal NO_x) and in the fuel (fuel NO_x) in the combustion processes. NO_x can be easily distinguishable by its telltale brown plume out of the stack if the NO_2 ratio is high. Most of the combustion sources emit SO_2 and NO_x at the same time.

Based on the data from the US EPA, 85% of SO_2 and 45% of NO_x emissions come from the stationary combustion sources as shown in Figure 1.1 and Figure 1.2 [1]. The Clean Air Act Amendments of 1990 have made the control of SO_2 and NO_x emissions a prominent national issue. The current air quality standards and industrial standards are listed in Table 1.1 [2,3]. The wide range of emission standards are caused by the different standards for different plant sizes, and based on specifications such as the type of coal used and boiler type [3]. In 1998, the US EPA issued a New Source Performance Standard for NO_x , setting a stringent 0.15 lb/mmbtu NO_x emission limit for new or modified industrial and utility boilers [3]. Back-end NO_x control techniques will become increasingly necessary as regulations are made even stricter.

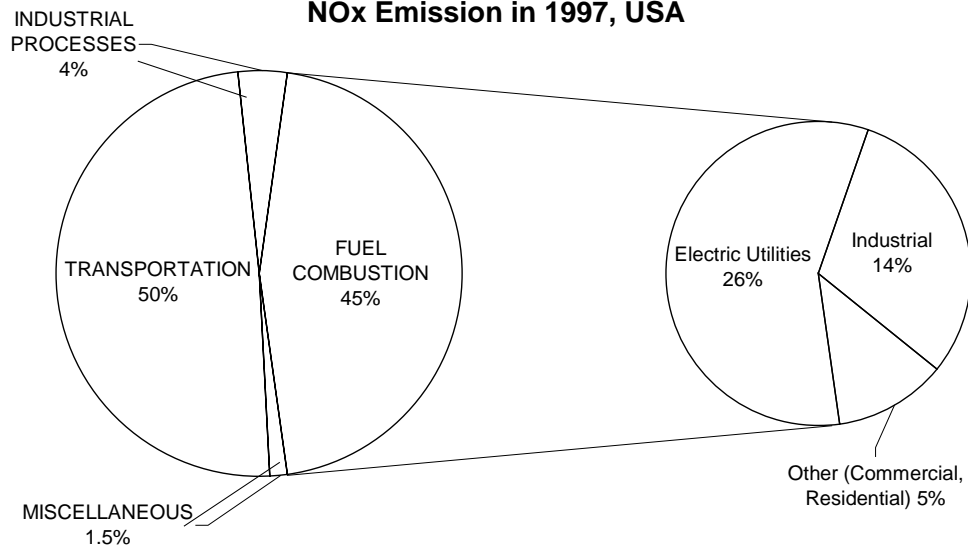
SOx Emission in 1997, USA



Total SOx Emissions: 20,371 thousand short tons
 Data from 1997 National Air Quality and Emissions Trends Report, US EPA

Figure 1.1 SOx Emissions in USA in 1997

NOx Emission in 1997, USA



Total NOx Emissions: 23,582 thousand short tons
 Data from 1997 National Air Quality and Emissions Trends Report, US EPA

Figure 1.2 NOx Emissions in USA in 1997

Table 1.1 Air Quality Standards and Industrial Exposure Standards

	Permitted Ambient Concentrations (NAAQS)	Permitted Industrial Concentrations (TWA and STEL)	Range of National Emission Standards	
			New Plants	Existing Plants
SO ₂	80 µg/m ³ (0.03 ppm), annual average 365 µg/m ³ (0.14 ppm), 24-h average	2 ppm, 8-h average 5 ppm, 15-min peak	750 ~ 1480 mg/m ³ (6% O ₂)	1480 mg/m ³ (6% O ₂)
NO _x expressed as NO ₂	100 µg/m ³ (0.053 ppm), annual average	3 ppm, 8-h average 5 ppm, 15-min peak	615 ~ 980 mg/m ³ (6% O ₂)	-----

NAAQS (National Ambient Air Quality Standards), TWA (time-weighted average), and STEL (short term exposure limit) [2,3]

1.2 Current Control Technology

The SO₂ control techniques utilized by most coal-fired power stations are wet or dry scrubber processes, where alkaline materials are injected into the flue gas streams to neutralize SO₂. The extensive uses of wet scrubbing processes have presented challenging problems for high-sulfur coal applications since the 1970s.

NO_x removal presents a significant challenge, since they are present in low to moderate concentrations (100 ~ 700 ppm) at high volumetric rates. Combustion modification systems usually reduce the NO_x emissions by about 20 ~ 50% [4]. Currently, the most used back-end NO_x control techniques are the selective or selective non-catalytic reduction (SCR or SNCR) processes.

Dry electrostatic precipitators (ESPs) have long been used by the utility industry as the preferred method for controlling particulates. The basic idea is to give the particles an electrostatic charge and then place them into an electrostatic field that drives the particles to a collecting wall (Figure 1.3). ESPs are effective on smaller particles than other particle removal devices. In wet electrostatic precipitators (wESPs), a thin water film flows down the surface of

the collection wall to carry particles away continuously, as well as to absorb acidic gases. However, instead of to control acidic gases, wESPs have been traditionally used to control tacky particulates or in other situations where high ash resistivity is a severe problem.

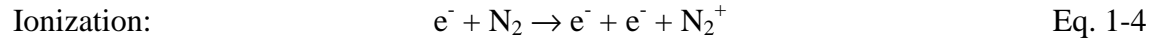
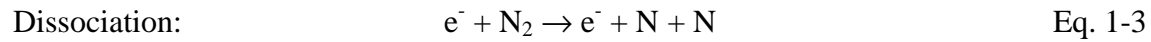
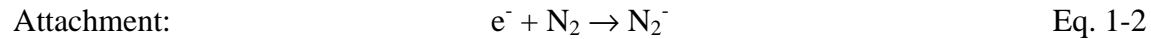
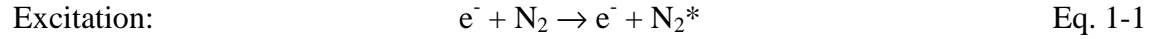
The economical method for the simultaneous removal of SO₂ and NO_x still represents a significant technical challenge that could ultimately determine the use of certain types of fossil fuels for energy production. Integrated emission control systems are needed to effectively control particles, acid gases and metal vapors in a cost efficient manner.

1.3 Introduction of Pulsed Corona Technology

Alternative postcombustion cleaning technologies have been developed. These technologies include an innovative method which utilizes a low-cost wESP to remove gaseous pollutants and particulate matter. Simultaneous removal of NO_x and SO_x by corona discharge in a wESP requires smaller installation spaces and less investment costs than conventional combinations of scrubbing De-SO_x and catalytic De-NO_x processes. Pulsed corona technology has been investigated as a means for controlling many gaseous pollutants, including NO_x, SO_x, HCl, CO,^[5] CO₂,^[6] mercury vapor,^[5, 7] Dioxin,^[5, 8] Freon,^[5, 7] PBC ^[5] and other organic compounds (odors) ^[5].

1.3.1 Power Technologies

When an electric field (DC, AC or pulsed) is applied to a gas, energetic electrons are discharged. These electrons transfer energy to gas molecules through collisions, resulting in excitation, attachment, dissociation, or ionization ^[9].



Plasma, a quasi-neutral mixture of electrons, radicals, and positive and negative ions, is generated when the electrons are discharged. Non-thermal plasma (cold plasma) process operates by producing plasma where the majority of the electrical energy accelerates the energetic electrons without accelerating or heating the ions. This condition is used in both conventional dry and wet electrostatic precipitators [9].

Table 1.2 Comparison of Corona Discharge Technology and Electron Beam Technology

	Corona Discharge	Electron Beam
Operational Pressure	Atmosphere	Vacuum
Electron Generation	Internal (within Polluted Gas)	External
Electron Energy*	~ 10 eV	$10^5 \sim 10^6$ eV
Capital Cost	Lower	Higher
Operational Cost	Higher	Lower
Disadvantage	Electrode Corrosion	Dirty Electron Injection Window; X-ray Hazard

* 1 eV = 1.6×10^{-19} J

Basically, there are two major methods of applying cold plasma to the pollution control as shown in Table 1.2: corona discharge technology, in which energetic electrons are generated within polluted gas, and electron beam technology, in which electrons are externally generated. Other less-used technologies include dielectric barrier discharges (dielectric bed discharges),

ferroelectric pellet bed [9], and surface discharge induced plasma chemical process (SPCP). It is still not clear which type of power technology is most efficient for various pollutants, concentrations, and situations. This research utilized pulsed corona discharge technology in a wESP.

1.3.2 Corona Discharge in an ESP

In the corona discharge process, high voltage electrodes are immersed in the atmospheric-pressure gas with either a positive or negative polarity, holding a voltage of typically 40 kV (Figure 1.3). The distance from the wire to the plate is about 3 ~ 7.5 inches (7.6 ~ 19 cm) [2, 68]. The electrical field strength near the plate is the ratio of the voltage to the wire-to-plate spacing, about 2.7 ~ 4 kV/cm. However, all the electrical flow that reach the plate comes from the wires and the surface area of the wires is much lower than that of the plate; thus, by the conservation of charge, the driving potential near the wires must be much larger, typically 50 to 100 kV/cm, as shown in Figure 1.4 [2, 10]. The empirical corona breakdown field strength E_b for plain wire is given by the following expression [10]:

$$E_b = 30 + 12.7\sqrt{d_w} \quad \text{Eq. 1-5}$$

where d_w is the wire diameter in cm. For a wire diameter of 2 mm, the breakdown field strength is 58.4 kV/cm. This means that if the corona voltage was maintained at 60 kV, gas becomes conductive in the region around the wires within a radius of approximately 1 cm.

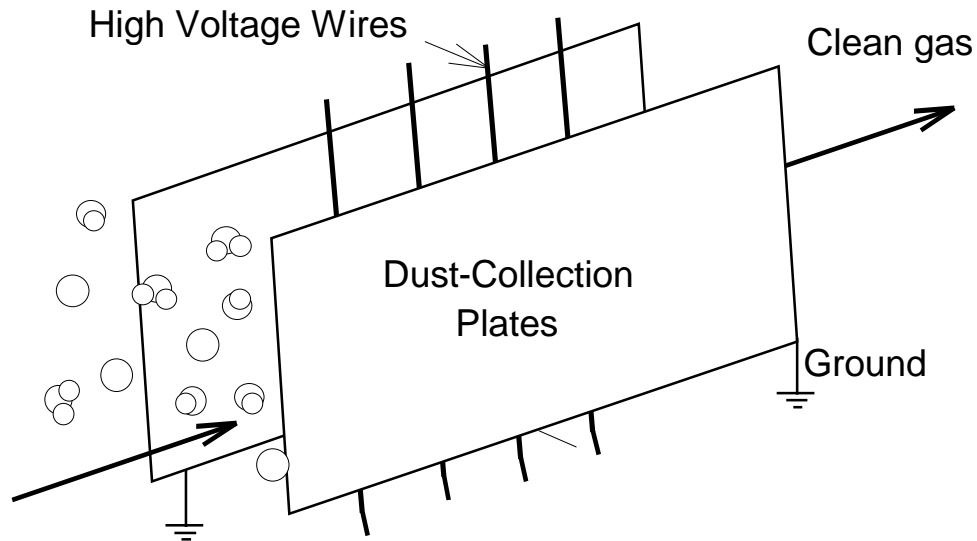


Figure 1.3 Schematic Diagram of a Typical Wire-to-Plate ESP

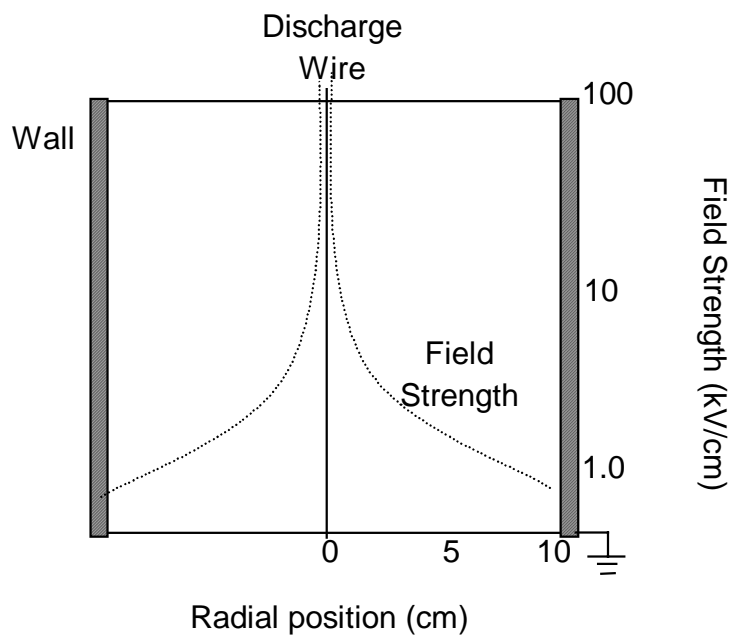


Figure 1.4 Typical Field Strength in a Wire-to-Plate ESP

Accelerated by electrical field, the high-energy electrons ionize molecules, release more electrons, and cause an electron current called an electron avalanche. The low-energy electrons are accelerated from a very low level of kinetic energy as they drift along the high voltage region

(corona region) until they collide with a gas molecule and immediately lose energy through excitation, attachment, dissociation, or ionization. Both negative and positive coronas are distinguishable by their violet color and are seen as a glowing gas ring surrounding the discharge wires. After transferring its energy to the molecule, the electron is re-energized by the electrical field. This process is repeated so that the energy of electrons is not wasted as compared with the electron-beam processes.

If the wire is positive, the electrons will move rapidly to the wire and the positive ions will stream away from the wire to the wall in an "ion wind." If the wire is negative, the positive ions will go to the wire and the electrons will be repelled toward the wall. In either case, the ions migrate from the wire to the wall in high concentrations ($10^6 \sim 10^9$ per cm^3) and at high initial velocities (~ 75 m/s) for the typical conditions of 1 mm wire dia., 10 cm wire-to-plate spacing at 50 kV as shown in Figure 1.4 [10, 68]. Electron velocity slows down with the decreasing field strength. Therefore, low-energy electrons exist in corona discharges (~ 10 eV) as compared to electron beam discharges where high-energy electrons (keV \sim MeV) are produced [9].

Based on the same delivered power, corona discharges are more efficient than electron-beam discharges [11]. As shown in Table 1.3, both the bond dissociation energies and ionization potentials of O_2 (5.1 eV, 12.1 eV) and H_2O (5.2 eV, 12.6 eV) are much lower than those of N_2 (9.8 eV, 15.5 eV) [12, 13]. The ionization and dissociation rates for N_2 are lower than for both O_2 and H_2O [11]. Therefore, ionizing N_2 is less efficient than ionizing O_2 in producing useful radicals (O , OH , HO_2) for oxidation. In corona discharge, low-energy electrons dissociate and ionize O_2 and H_2O at higher rates than N_2 , which produces radicals in more efficient ways [11]. The high-energy electron beam wastes energy to ionize N_2 . And the energy of low-energy

electrons is wasted because electrons cannot be re-accelerated again in the electron beam process.

Table 1.3 The Ionization and Dissociation Energies of Gas Molecules

	Bond Dissociation Energy		Ionization Energy
	kcal/mol [12]	eV per molecule [12, 13]	eV per molecule [12]
N ₂	226 (N-N)	9.8	15.5
O ₂	118 (O-O)	5.1	12.1
H ₂ O	118 (H-OH)	5.2, 5.4 (H-OH)	12.6
SO ₂	N.A.	5.70 (SO-O), 5.71 (S-O ₂)	12.34
NO	N.A.	N.A.	9.25
NO ₂	73 (NO-O)	N.A.	12.0
NH ₃	103 (NH ₂ -H)	3.0 (NH ₂ -H), 4.7 (NH-H ₂)	10.15
HCl	N.A.	4.5 (H-Cl)	N.A.
H ₂ S	N.A.	3.2 (H ₂ -S), 3.7 (HS-H)	N.A.
CO ₂	N.A.	5.5 (CO-O)	N.A.

1 eV = 3.82*10⁻²³ kcal; 1 eV/molecule = 23 kcal/mol

N.A.: not available

1.3.3 Pulsed Corona Discharge Technology

Unlike conventional plasma processes that are performed in a low-pressure gas atmosphere, a pulsed corona generates highly non-equilibrium plasma with very high electron energy and low ion-molecular energy without sparking or arcing. Only electrons enable non-elastic collisions with neutral molecules and produce active radicals, such as O[·], O₃, OH[·], H[·], NH₂[·], and N[·]. In conventional non-pulsed plasma processes, low gas pressures were used to minimize the gradual heat transfer from electrons to ions and molecules through collision processes. By pulsing the high voltage, only electrons can be accelerated to gain sufficient energy to generate radicals, whereas ions and molecules, since they have a much larger mass, cannot be sufficiently accelerated to get a concurrent energy loss. More energetic electrons

produce more free radicals for pollutant oxidation or removal reactions. Therefore, a pulsed corona generates a highly non-equilibrium plasma with a very high electron energy and a low ion-molecular energy at atmospheric pressure.

The pulsed ESP was first used to optimize particulate precipitation efficiency by precisely controlling duration and pulse frequency in 1952 [14]. Pulsed power allows the ESP to achieve higher peak voltages and sparking voltages, by which precipitation efficiency and overall electrical efficiency can be increased without increasing the collection area. Furthermore, pulsing also led to higher overall electrical efficiency of 70%.

In the early 1980's, pulse electric fields are found to be effective in increasing the efficiency of electrons. Meanwhile, the possible removal of SO_x and NO_x by means of corona discharge was confirmed [15]. Later studies revealed that a pulsed corona exhibits a higher removal efficiency than a DC corona for the simultaneous removal of NO_x and SO_x [5, 15, 16]. In 1981, researchers at the University of Tokyo applied the pulse corona to generate energetic electrons in the plasma [2, 16]. The technologies were called Pulse-induced Plasma Chemical Process (PPCP) and Surface discharge induced Plasma Chemical Process (SPCP) in their works.

Dry pulsed-corona methods for the simultaneous removal of NO_x and SO_x have been investigated at lab-scale in a collaborated study in Japan and the U.S.A. [11]. The Italian National Power Company (ENEL) conducted small pilot plant tests of dry pulse corona processing for the simultaneous removal of NO_x, SO_x, and particulate from the flue gas (100 Nm³/hr) of a coal-fired power plant [15]. Now pulsed corona technology has been investigated as a means for controlling many gaseous pollutants, including NO_x, SO_x, HCl, CO [5], CO₂ [6], mercury vapor [5, 7], Dioxin [5, 8], Freon [5, 7], PBC [5], VOC and odors [5].

1.3.4 Electron Beam Technology

In the electron beam process, electrons are accelerated by high voltage in a vacuum region before being injected through a thin foil window which serves as a vacuum seal [9]. The high-energy electrons (as high as 1 MeV) produce a large volume of plasma as they collide with the gas molecules in the atmospheric-pressure flue gas stream. The basic idea behind this technology is using the plasma generated by the very high-energy electron beam to produce ions and radicals. These ions and radicals, particularly the OH[•] radical, oxidizes SO₂ and NO to SO₃, NO₂, and NO₃. By adding ammonia, these high oxidation-state gases are neutralized and converted to ammonium sulfate and ammonium nitrate. These dry byproducts are removed by following conventional particulate removal devices, such as a ESP or bag-house, and could be used for agricultural fertilizer.

The reducing of NO_x in combustion flue gas by UV light was observed in 1972 [15]. In the late 1970s, Japanese researchers found that electron beams were an effective simultaneous treatment for sulfur dioxide and nitrous oxide from combustion flue gas [15]. In the following years, the effects of electron beam were fully investigated and applied to pilot plants and demonstration plant level in Japan [17]. Many pilot plant tests with gas flow rates as large as 25,000 Nm³/h, have been conducted around the world. This process was well investigated to produce models in good agreement with the experimental results.

However, this high voltage electron beam process requires heavy shielding from x-rays. The high capital cost is also another major disadvantage of the conventional MeV-type electron beam accelerators [9]. These limitations motivated researchers into alternate electrical-discharge-based technologies. Recent research efforts are applying pulsing technology to

improve the electron beam process. Compact low-energy (less than 200 keV) electron beam accelerators have been developed to increase the competitiveness of this technology.

1.3.5 Corona Polarity

De-SO_x Possibility

Masuda reported that SO₂ was removed from gas streams only by positive pulsing in a dry pulse-induced plasma chemical process [16]. Mizuno et al. also demonstrated that the positive pulsed streamer corona has a better SO₂ removal performance than the negative corona [11]. They concluded that a positive polarity produces more uniform streamers that extend farther out from the electrode, thereby creating a larger and more uniform treatment volume.

De-NO_x Possibility

Masuda demonstrated that De-NO_x is possible by both positive and negative pulsing [16]. NO is oxidized to NO₂ in a pulsed corona discharge with a field intensity of 10 ~ 12 kV/cm. The NO removal efficiency in a negative pulse corona is a function of the specific power of pulsing (P/Q) divided by the inverse of the square root of the gas residence time. The removal rates in positive pulsed coronas are more than one order of magnitude higher than those with negative pulsing coronas [16]. However, as far as the removal based on the same energy input is concerned (gNO/kWh), there is no difference between polarities [5, 16]. The works of Chakrabarti et al. also demonstrated that a positive pulsed corona has a higher efficiency for NO_x removal [18].

NO_x can also be generated from nitrogen within a corona discharge. However, the amount of NO_x generation is very small. In a gas flow rate of 2 L/min, the NO_x generation from

corona wire is approximately 1 ppm at room temperature, and increases to 30 ppm as the corona wire was heated to a temperature of 600°C [19].

Corona Volume

The positive corona produces longer streamers and a greater corona volume that fills the gas phase fully and ionizes a larger volume at the same energy level [15]. Therefore, a larger active volume is resulted in the positive corona discharge. Negative corona appears only in a small region around the discharge wires. The available corona space in positive discharges is about 10 times more than that of negative coronas [5].

Power Consumed in Mercury Removal

The power consumed was raised with the increasing flue gas temperature and voltage for mercury removal in PPCP. Moreover, the power consumed was always substantially higher for a positive corona than for a negative corona [7]. As far as the mercury removal amount was concerned, however, no difference was observed in the corona polarity up to 200°C, while the negative polarity performed better at temperatures beyond 300°C [7].

1.3.6 Wet Electrostatic Precipitator

Wet electrostatic precipitators (wESPs) have been traditionally used to control tacky particulates or in other situations where high ash resistivity is a severe problem. Wet ESPs have typically been applied with tubular collector surfaces, although any configuration may be operated with wet walls instead of dry walls. Several wet-type electrostatic reactors have been

developed in the laboratory: wet reactor with thin water/absorbent film on the wall; semi-wet reactor with water-hold wall-attached membrane filter; and spray reactor [18, 20].

Wet-type ESPs have the following advantages over dry-type ESPs:

- No dust layer can be built, especially for the aerosol liquid, tars, and oil mists contained in flue gases.
- No problems with back-corona, spark-over, and rapping re-entrainment.
- Earlier onset of discharge in wet systems. [18]
- Experiments [18, 20] has shown that for the removal of NO_x by corona discharge, wet-type reactors performed better than the dry-type ESPs and spray-type reactors because the chemical reactions involving water and its radicals enhance the removal of NO_x [18].
- Operating at lower temperatures, the treated gas volumetric flow is less and the required equipment volume is also smaller.

In addition, wESPs can have several advantages when compared to other control systems currently in use. These advantages include:

- Low pressure drops (0.1 ~ 0.5 inches water [68], comparing with 3~10 inches for air filters [31,] ~ 10 inches for wet scrubber [2], and 45 ~ 60 inches for venturi scrubber [4]) and low power requirements
- The potential for the simultaneous removal of acid gases and heavy metal vapors.
- The absorption of ammonia can prevent ammonia leakage if ammonia is used in the system.
- High removal efficiency of Dioxin (90%), as well as the potential removal of other pollutants, can be obtained in a wet type plasma reactor [8]

However, the wet-type ESPs may have several disadvantages:

- Generation of liquid waste
- Corrosion
- Neutralizing materials, such as limestone, are needed

1.4 Research Objectives

The potential of gas removal in ESPs is neither currently being used nor fully understood. The precise nature of the charge-induced effects is as yet unclear. This research explores the feasibility of combining the pulsed-corona methods with the wet wall absorption and the optional ammonia and/or ozone injection by studying the removal of SO₂ and NO_x from simulated combustion gas in a pulsed corona enhanced wESP.

The experimental objectives of this research are as follows:

1. To construct a bench-scale wire-plate wESP system and a batch absorption system.
2. To optimize both SO₂ and NO_x removal by adjusting system parameters and experimental conditions of the wESP.
3. To examine the fates of sulfur and nitrogen in the removal process.

The theoretical objectives of this research are as follows:

1. To determine the primary removal mechanisms of SO₂ and NO_x.
2. To develop a mathematical model for overall removal efficiency that incorporates the mass transfer and electrostatic effects.

3. To compare the theoretical simulation results to the experimental results in order to explore the removal mechanisms and the effects of system parameters on resultant overall removal efficiency.

2. LITERATURE REVIEW

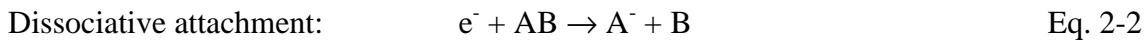
All the possible SO₂ and NO_x removal mechanisms have been studied in this chapter, including electron attachment, ozone oxidation and radical reactions, corona wind enhanced mass transfer, effect of ammonia injection, etc.

2.1 Electron Attachment

The phenomenon of electron attachment has been studied as one of the primary mechanisms responsible for removing gaseous pollutants in wESPs. There are two mechanisms for electron attachment based on the electron energy levels. The two mechanisms are as follows:



and



The presence of these two electron attachment mechanisms is dependent on the electron energy, as well as the gas molecular structure and electron affinity. Most of the work done in this area is vague because there is no clear way to measure either of these attachments.

In three-body attachment, low-energy electrons are generated in a corona discharge with voltages ranging from 3 ~ 15 kV. When electrons attach on pollutant molecules, such as SO₂ or NO, negative ions (SO₂⁻, NO⁻) are formed. Negative ions of pollutants are then separated by an electric field.

In dissociative attachment, high-energy electrons break up the gas molecules. The decomposition of the pollutant molecules may directly lead to the removal of pollutants. The dissociation of the surrounding gases forms radicals that react with pollutants through either

oxidation or reduction pathways. The dissociative recombination of ions in ion-molecular reactions can also generate radical species [6].

Ionic reactions may also play an important role in the discharge chemistry [22]. The probabilities of ion reactions are a few orders magnitude higher than the probabilities of radical reactions [21, 23]. And the reaction rates of electron-ion related reactions are 10 to 10^8 times greater than those for neutral species reactions [6]. Therefore, the effective production or loss of ion species becomes comparable with neutral reactions, even though the ionic density is much less than that of neutral species.

The first study of electron attachment of NO and SO₂ in SO₂ or NO gases under low pressure was conducted by Bradbury and Tatel [13, 24] who found that negative ions are formed in the presence of low velocity electrons. The attachment probability for SO₂ is minimum at $E/N = 40$ Townsend (Td) [13]. E/N is the ratio of the electric field strength E to the number density of the gas N . Lakdawala and Moruzzi [25] concluded that the three body attachment of SO₂ exists at $E/N < 40$ Td and the dissociative attachment exists at $E/N > 40$ Td in SO₂ and SO₂/O₂ mixtures at 0.5 ~ 6 torr. The attachment probability for NO linearly increases with an increase in pressure, thereby forming negative ions (NO⁻) [24]. It was suggested that the three-body attachment exists because an increase in pressure increases the fraction of all the collisions.

Tamon et al. demonstrated that electron attachment was responsible for SO₂ removal in a gas stream [26]. The maximum removal efficiency of 120 ppm SO₂ was 98%. They found that the removal efficiency increased with increases of oxygen and water vapor concentration. To explain their findings, it is assumed that one negative ion of oxygen (O₂⁻ or O⁻) or hydroxyl radical (OH⁻) forms an ion-cluster with several SO₂ molecules [26]. Although fewer electrons hit

the pollutant molecules directly, one single radical generated by one electron can still remove several pollutant molecules, which enhances the overall removal efficiency.

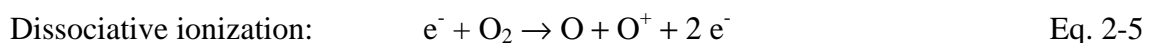
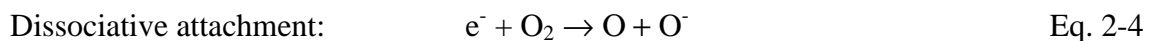
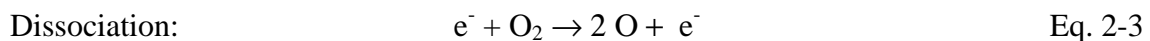
The formation of large negative SO₂ ion clusters in SO₂/O₂ gas mixtures was observed in a drift tube mass spectrometer [25]. In the presence of oxygen, O⁻, SO⁻, and S⁻ ions are formed because of the spread of energy of the available electrons. These ions rapidly form clusters with neutral SO₂ molecules. The typical negative ion clusters are O⁻(SO₂)₂, O⁻(SO₂), SO⁻(SO₂)₂, SO₂⁻(SO₂)₂, and S⁻(SO₂)₂ at a pressure of 0.7 torr. The increase of removal efficiency by the addition of water vapor was attributed to the formation of OH⁻(SO₂)_n cluster. Larger ion clusters are formed at higher pressures. Moreover, the clustering reaction can be generated in a core particle that consists of up to 30 H₂O or NH₃ molecules [27].

2.2 Ozone Oxidation

2.2.1 Ozone Generation

Generally, ozone is an unwanted by-product of ESPs. However, it is possible to use high concentrations of ozone as a chemical oxidizer, resulting in the removal of SO₂ and NO_x. Simachev et al. [28] and Lozovskii et al. [29] demonstrated in a pilot plant that the co-injection of ozone/ammonia into a wet scrubber simultaneously desulfurized and denitrified with an efficiency of 96% at 1:1 ozone to NO ratio.

The ozone generation in a corona discharge begins with the generation of oxygen free radicals through the following reactions [6, 30].



Then, Oxygen free radicals react with oxygen to generate ozone.



where $\text{M} = \text{N}_2$ or O_2 .

Commercial silent-discharge type ozone generators have an energy yield of 50 ~ 90 gO_3/kWh for dry air and 180 gO_3/kWh for pure oxygen gas [6, 16]. Since the theoretical limit of energy yield is 1200 gO_3/kWh , 92% of the energy is lost as heat [6]. Negative coronas produce about 10 times as much ozone as positive coronas [10, 19, 31]. This is the reason that indoor ESPs use positive coronas.

In lower temperature conditions, a substantial enhancement in ozone generation can be expected because the ozone losing processes are enhanced by the increase of gas temperature [6]. Ozone decomposes when the temperature of flue gas is higher than 80°C [32]. Heating the corona discharge wire may also reduce the ozone generation [19, 33].

The in-situ ozone generation was not observed in every the corona-discharge-based gas cleaning processes because different experimental conditions were used [42].

2.2.2 SO_2 Removal

The ozone can oxidize SO_2 to form sulfur trioxide.



Reaction rate constant: $k < 4.8$ @300K [29]

SO_3 is very soluble in water and easily reacts with water to form sulfuric acid. However, comparing with the reaction of ozone to NO , the reaction of ozone to SO_2 is slow and does not

easily take place. Slater and Rissone mentioned that at temperatures below 423 K, the direct interaction between ozone and SO₂ to form sulfur trioxide does not take place [34]. Lozovskii et al demonstrated that with typical contact times for gas scrubbing systems (less than 5 seconds), ozone did not oxidize SO₂ in the gas phase, regardless of the ratios of O₃/SO₂ concentrations [29].

Dissolved ozone in water might contribute to the oxidation of sulfite to sulfate within the water. However, ozone is not easy to dissolve in water. The Henry's constant of ozone is greater than O₂ and NO, but less than SO₂ and NO₂ (Table 10.4).

2.2.3 NO_x Removal

NO can be oxidized to NO₂ by free oxygen and ozone. These reactions take place in less than 0.1 sec [28]. The reactions of NO oxidation by ozone are listed below:



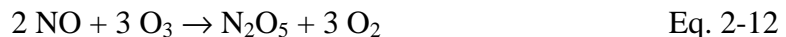
Reaction rate constant: $\log k = 10 \sim 11$ @300K [35]



Ozone oxidizes NO_x into other forms of nitrogen oxides, such as nitrogen trioxide and dinitrogen pentoxide through the following reactions [30].



Reaction rate constant: $\log k = 7.5 \sim 11$ @300K [35]



These nitrogen oxides easily react with water to form nitric acids, thus removing the original pollutants from the flue gas stream.

Lozovskii et al demonstrated that with an ozone/NO concentration ratio less than 1, NO was oxidized to NO₂ in the gas phase ($t < 0.1$ sec) in a flue gas stream with SO₂ and NO [29]. Ozone oxidized NO first and the oxidation rate of SO₂ was 10% lower. The oxidation of NO by ozone in the gas scrubbing system was independent to the liquid spraying conditions because the oxidation is fast and only in the gas phase alone.

Masuda and Nakao demonstrated that for a coal-burning boiler with 300 MW capacity and total gas flow rate of 10⁶ Nm³/hr, the oxidation of NO requires a power of about 7.5 MW if a 50 gO₃/kWh ozone generators is used [16].

2.3 Radical Reactions

When a corona discharge is applied to a flue gas, energetic electrons are created, transferring energy to the dominant gas molecules (N₂, O₂, H₂O, CO₂) by collisions. These collisions result in the formation of primary radicals (O·, N·, OH·, etc.), positive and negative ions and excited molecules. After the formation of primary radicals, the electron-ion, ion-ion reactions, and electron detachments create more secondary radicals (O₂·, HO₂·, etc) [36]. Large amount of O·, O₂·, OH·, and H· radicals are easily generated in coronas. In flue gas applications, these radicals may oxidize SO₂ and NO, or react with them to form aerosols. Since the formation energy of the radicals is on the order of 10 eV, the energy of the electrons in a corona discharge is approximately equal to the energy needed for radical formation. The first attempt of measuring oxidizing radical OH· in a corona discharge has been proposed by either threshold ionization mass spectroscopy or laser absorption spectroscopy [37].

2.3.1 SO₂ Removal

In plasma, the ion-molecule reactions enhance the oxidation of SO₂ to SO₃ [38]. SO₂ might be oxidized by O⁻ to SO₃, or reacts with O₂⁻ to form SO₂⁻ in associative detachment reaction [25].



However, not all the study reported the gas-phase oxidation of SO₂ because different experimental conditions were used [39, 40].

2.3.2 NO_x Removal

NO can be oxidized to NO₂ and N₂O₅ when the corona field exceeds the ordinary level of precipitator operation, E = 4.5 ~ 9.0 kV/cm, with the existence of O₂ and H₂O [16, 30]. It was reported that 67% of NO was oxidized by ozone; and the remaining 33% was oxidized by radicals such as OH[·], O[·], O₂[·] etc. However, detailed reaction mechanisms were not mentioned. The following empirical formula was derived for the oxidation efficiency of NO in their tubular electrostatic precipitator [16, 30]:

$$\eta = 1 - \exp\left(-\frac{K \cdot P}{Q \cdot C} \cdot \frac{L}{D}\right) \quad \text{Eq. 2-15}$$

where K is a constant, P is corona power, Q is gas flow rate, C is the inlet NO concentration, L is the length of the tubular ESP, and D is the diameter of the ESP. These results show that DC

corona oxidation of NO in a dry ESP could have quite a high technical potential, but would require a high energy consumption (78.1 MW out of a 300 MW coal-burning boiler) [16].

In a low oxygen stream, NO can be reduced to N₂ by reducing radicals such as N[•] in a dry corona discharge [21, 41].



In Mizuno's wESP tests, half of the removed NO was dissociated into N₂ and O₂, with the rest of the NO was absorbed by the water [20]. However, increasing the concentration of O₂ reduced the NO_x reduction efficiency [44]. Therefore, NO can only be reduced under low O₂ concentration, which may not be practical in the application of flue gas treatment where excess air usually exists.

2.4 Corona Wind Enhanced Mass Transfer

The corona wind, which has a velocity of 0.6 ~ several m/s [68], is caused by the Coulomb force exerted onto gas ions and the collisions of ions and neutral gas molecules [45]. The secondary flow induced by the corona wind can be observed at the discharge gap flowing toward the grounded plate electrode both for the cases of pulsed coronas and DC coronas [37]. The velocity of the corona wind increased with the square root of the current [45, 46]. The corona wind can reduce the effective thickness of the gas/liquid boundary layer, enhance the mixing between radicals and pollutant molecules, and increase the mass transfer of SO₂ to the liquid phase [16, 37, 47].

Masuda and Nakao reported that SO₂ is not oxidized in a DC corona field and the removal is due to the corona wind [16]. The removal efficiency at a given corona power per

volumetric flow rate (P/Q , $W\text{-hr}/m^3$) rises with the increasing diameter of the corona wires, possibly because this requires an increased voltage to maintain an equal corona current and thereby enhances the corona wind at the same P/Q value.

Corona wind generating condition can be determined by the Electrohydrodynamics (EHD) number [48]. In an inertial flow, the EHD number is determined as the ratio of electric pressure ($\sim\kappa\epsilon_0 E^2$) to inertial pressure ($\sim\eta U^2$).

$$N_{\text{EHD}} = \frac{\kappa\epsilon_0 E^2}{\eta U^2} \quad \text{Eq. 2-17}$$

where

$\kappa = 1$, dielectric constant for gases

$\epsilon_0 = 8.854 * 10^{-12}$ farads/m, permittivity of free space

$E = 2 * 10^5$ V/m, electrical field of 20 kV (the typical onset voltage in this wESP)

$\eta = 1.2 \text{ kg}/m^3$, density of gas

$U = 0.061$ m/sec, velocity of gas flow

Therefore, the EHD number of this wESP system ($N_e = 178$) exceeds unity. When the EHD number is larger than 1, the gas flows are much more likely to respond to electrostatics, which is so called "the corona wind effect."

Corona discharge can improve the rate of SO_2 absorption into water [11]. The electrical potential gradient on solution changed the diffusion constants of diffusion ions [9]. Corona wind can increase the heat transfer rates as much as six times [46]. Khang indicated that the maximum electrostatic enhancement factors of heat transfer and mass transfer were 3.3 and 9.3, respectively [47]. These results indicate that the mass transfer enhancement was not only due to the corona wind but also due to the selective charge of SO_2 molecule clusters.

2.5 Ammonia Injection

Ammonia (NH₃) was used to neutralize the sulfurous and nitrous acids produced in some gas-cleaning processes by the plasma [44]. Moreover, NH₃ causes many other gas phase reactions with SO₂ and NO_x in the presence of water as discussed further in this section.

2.5.1 SO₂ Removal with Ammonia Injection

Wet Flue Gas Desulfurization Without Corona Discharge

In the SO₂/NH₃/H₂O gas mixture, SO₂ reactions lead to the formation of white crystallite material [52, 53]:



Or ammonia reacts directly with SO₃ to produce aerosol products.



Ammonium sulfite (NH₄)₂SO₃ and bi-sulfite NH₄HSO₃ are unstable at high temperature (> 70°C) and can easily decompose and release NH₃ and SO₂ [54]. Therefore, they are not suitable for agricultural uses unless they are oxidized to the form of sulfate.

Commercial developments in the late 1990s suggested the use of NH₃ solution in conventional wet flue gas desulfurization (FGD) in the position downstream of an ESP [49, 50].

In wet scrubbing processes, starting from the dissolution of SO_2 into water droplets, all reactions take place in the soluble phase.

The ammonia byproduct, mainly ammonium sulfate $(\text{NH}_4)_2\text{SO}_4$, mixed with ammonium nitrate and a small portion of co-collected fly ash, is fully acceptable for agricultural products. The advantage of using ammonium sulfate over other fertilizers is the presence of both nitrogen and sulfur, which is ideal for high alkaline soils. Because of the continued use of non-sulfur fertilizers [50, 51], larger crop yields tend to remove increasing amounts of sulfur from the soil. Therefore, the fertilizers containing sulfur are becoming more popular. By recycling the by-products, the ammonia-based wESP system can be free from wastewater generation or zero-effluent operation.

In conclusion, the advantages of wet FGD with NH_3 reagent include [50]:

- It produces high value ammonia byproduct for agricultural uses.
- It may avoid the generation of solid waste.
- It can be free from wastewater generation or zero-effluent operation.

The drawbacks of wet FGD with NH_3 reagent include:

- Visible stack discharge arising from ammonium aerosol (commonly observed in the early use of ammonia reagent in the wet FGD as a blue plume). This can be avoided by reducing the operation pH, and compensated by using a high liquid/gas flow ratio to reduce the ammonia vapor pressure and gas-phase formation of ammonium aerosols.
- Liquid carryover with $\text{SO}_3/\text{H}_2\text{SO}_4$, which may happen in any wet scrubbing system, causes corrosion effects and the visible emission of sulfuric acid mist in high-sulfur fuel applications. So the pre-treatment of raw gas for removing SO_3 is needed in some high-sulfur fuel applications.

- Some portion of the byproducts are ammonium sulfite $(\text{NH}_4)_2\text{SO}_3$ and bi-sulfite NH_4HSO_3 , which are unstable at high temperature ($> 70^\circ\text{C}$) and decompose and release NH_3 and SO_2 [54].

Flue Gas Desulfurization With Corona Discharge

Dinelli et al. indicated that the SO_2 removal is governed mainly by the thermochemical reaction of ammonia and enhanced further by the corona process [15]. Ning et al. demonstrated that at 112°C , 97.4% of 690 ppm SO_2 were removed with a 1939 ppm NH_3 injection, forming less thermo-stable byproducts [54]. But the same SO_2 removal efficiency was reached with a less NH_3 injection (1215 ppm) under 33.4 kV (7 ~ 10 kV/cm) corona discharge, indicating that the thermo-stability of the byproducts was enhanced by corona discharge. It was believed that ammonium salts exist in the form of sulfate rather than sulfite under corona discharge due to the oxidation of SO_2 [54]. Some important reactions of ammonia with SO_2 in the gas phase are listed in Table 10.3.

2.5.2 NO_x Removal with Ammonia Injection

There are primarily two processes for NO_x control: the reduced nitrogen and the oxidative processes. Ammonia is involved in both of these processes.

Reduction

Ammonia is widely used as a reducing agent in the conventional selective catalytic reduction (SCR, $300 \sim 450^\circ\text{C}$) and selective non-catalytic reduction (SNCR, $900 \sim 110^\circ\text{C}$) processes [2, 4]. The injection of the reducing nitrogen compounds with NH_2 functional group is effective in reducing NO_x by up to 70%.

In a plasma induced radicals De-NO_x process, amidogen radicals (NH₂·), which may be formed by NH₃ or urea, is the primary reducing agent [43]. The generation of radicals occurs only in high energy plasma applications, such as electron beam process, and usually not in the corona discharge process [16]. The most important reaction path [15, 18, 21] for the formation of NH₂· radicals is from the dissociation of NH₃ (at an electrical field > 11.5 kV/cm [16]). The major attack on NH₃ is by OH· radicals.



Reaction rate constant: $k = 8.32 \times 10^{-17} \cdot T^{1.6} \cdot \exp(-480/T)$, cm³/sec [43, 55, 56]



[43, 56]



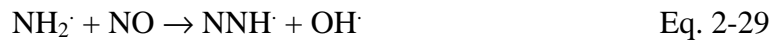
[56]



Then NH₂· radicals reduce NO to N₂.



[21, 41, 43, 56]



[56]



[56]



[15]

NH[·] radicals can be formed as well [15, 18, 21]. Then the NH[·] radicals reduce NO to N₂ [18, 21].

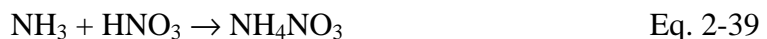
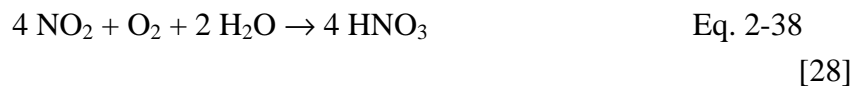
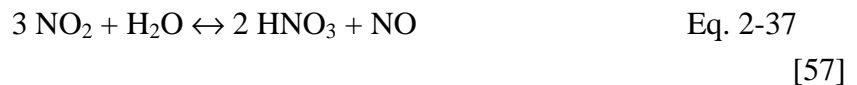
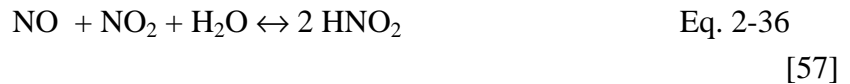


However, the reduction of NO_x only occurs for low O₂ condition. The OH[·] radicals are provided from injecting H₂O vapor, not from O₂. With the presence of O₂, the oxidation of NO_x might occur rather than the reduction.

Oxidation

There is no reaction between NH₃ and NO at low temperatures. NO is oxidized to NO₂ by O₂ and O₃ or by O[·] and OH[·] radicals in a plasma [5]. With the presence of water vapor, NO₂ reacts with NH₃ and forms the final product: NH₄NO₃ [5, 6, 32]. Two reaction mechanisms have been proposed:

(1) NO₂ is oxidized to nitric acids first, then react with NH₃ to form NH₄NO₃.



(2) In a plasma process, $\text{NH}_2\cdot$ radicals are formed from the dissociation of NH_3 as discussed in the previous section, and fix NO_2 into ammonium nitrate [5].

The reaction rates of above reactions are not available. However, the competition was observed between NO_2 to NH_3 and SO_2 to NH_3 [16]. SO_2 may be removed effectively only after NO_2 has been removed, which suggests that the reaction rate of NO_2 to NH_3 is faster than that of SO_2 to NH_3 .

Masuda et al. mentioned that ammonia enhanced the removal of NO_2 , but not NO , because there is no reaction between NH_3 and NO at room temperature [16]. Mizuno et al. demonstrated that in a dry ESP at the temperature range, ammonia effected only the De- NO_2 efficiency, not the De- NO efficiency from room temperature to 150°C [20]. This is because that the conversion of NO to NO_2 does not depend on ammonia, but mainly on the concentration of free oxygen radicals [21]. In the co-presence of ammonia and water vapor, however, both the NO and NO_x removal efficiencies were enhanced proportional to the temperature and power input, because the $\text{OH}\cdot$ radicals formed from water vapor oxidize the NO to NO_2 [20].

Since De- NO_x in dry ESPs performed better with the presence of ammonia and water vapor [6], wESPs with ammonia injection provides a better NO_x removal [18, 20]. NO_x was converted mainly to NH_4NO_3 aerosols in the streamer corona with the presence of ammonia [21, 58]. It was later confirmed by infrared spectroscopy that NH_4NO_3 is the final product of the $\text{NO}_x/\text{NH}_3/\text{H}_2\text{O}$ reaction during corona discharge [18].

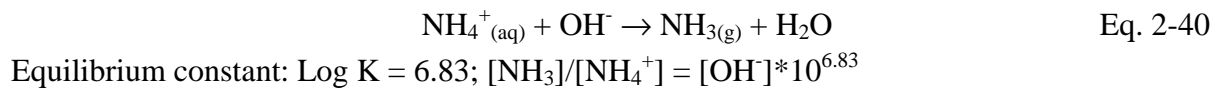
2.5.3 The Byproducts of SO_2 and NO_x Removal with Ammonia Injection

Onda et al. conducted experiments in a simulated flue gas with NO_2 , SO_2 , NH_3 , and H_2O in a dry pulsed corona reactor [37]. The compositions of collected materials were 49 mol% of

$(\text{NH}_4)_2\text{SO}_4$ and 47 mol% of $2\text{NH}_4\text{NO}_3 \cdot (\text{NH}_4)_2\text{SO}_4$. The particle diameter was around 61.5 μm , which seemed to consist of many smaller grains [37]. Kanazawa et al. reported that in a corona discharge De-NO_x process, the diameters of the aerosol particles (mainly NH_4NO_3) were in the range of sub-micron to a few micron [42]. These solid by-products are soluble in water and can be easily removed from gas stream. Chang reported that the shape of by-products NH_4NO_3 and $(\text{NH}_4)_2\text{SO}_4$ became more crystal-like in the downstream of the reactor [40, 42].

2.5.4 Ammonia Recovery

The Henry's law constant of ammonia is 16.22 $\text{cm}^3\text{-atm/mol}$ at 25°C [59]. A study was conducted about the ammonia recovery from the liquid of a combined lime/ammonia spray dryer by a stripping process [60]. The major ammonia recovery reaction is as below.



It can be derived from the above equation that when the pH value in water solution is 9, the gaseous ammonia is equal to $67.6 * [\text{NH}_4^+]$. That means more than 95% of the ammonia is in the form of molecular ammonia, which can be released by stripping. In general, the ammonia regeneration rates increase as the G/L ratios, temperatures, and solids concentrations increase. With temperature $> 45^\circ\text{C}$ and $\text{pH} > 9$, the ammonia recovery efficiency can be higher than 90% [60].

2.6 Other Factors

2.6.1 Other Alkaline in the Gas or Liquid Phase

Dinelli et al. indicated that in a dry pulse corona system, a dry hydrated lime (calcium hydroxide, $\text{Ca}(\text{OH})_2$) injection has no effect on the NO_x removal, but doubled the SO_2 removal [15]. And an ammonia injection enhanced both the SO_2 and NO_x removal with a greater extent of SO_2 removal than the hydrated lime injection [15].

Alkaline in the liquid phase can enhance the absorption of SO_2 and NO_2 . In a pulse-corona wESP study, however, the same De- NO_x performance was found by replacing water with NaOH or ammonia solution [20]. When water is used as the absorbent, the De- NO_x performance remained unchanged if the water pH value dropped below 3.

2.6.2 O_2 , CO_2 and Water Vapor in the Gas Phase

Oxygen and water can greatly enhance the oxidation and removal of NO in a corona discharge [16, 21, 30]. The increase of air relative humidity favors the positive glow formation [62]. Corona breakdown voltage decrease as the humidity increases [61]. However, ion mobility decreases as the humidity increases. Corona current is lower in humid air [61].

Studies showed that either the absorption of SO_2 into water was enhanced by the presence of a corona [39, 41, 63], or that the removal efficiency of SO_2 in a corona discharge increased in the presence of water vapor [26, 64]. When liquid water was sprayed from electrified nozzles, its SO_2 absorption capacity increases dramatically. Charged water droplets from electrified nozzles can remove substantial amounts of SO_2 and certain noxious gaseous species far exceeding the level that attributed to saturation [39].

The existence of electronegative gases, especially CO₂, lowered NO_x removal rate due to the reduction of the discharge current [42].

2.6.3 Temperature Effects

In wet systems, the solubility of SO₂ and NO_x in water decreases as the temperature increases. In dry systems, better SO₂ removal was obtained at lower temperatures with dry ammonia injection (75% at 100°C and 90% at 70°C) [15]. ENEL [5] showed that higher temperatures lowered the SO₂ removal efficiency [37], but the De-NO_x remained unchanged. Another study showed that the temperature effect is negligible in the dry De-NO_x process [20]. In the presence of ammonia and water vapor, however, both De-NO and De-NO_x efficiencies were enhanced proportionally to the temperature.

A study of theoretical modeling showed that the evolutions of the radicals and pollutants are substantially affected by the gas temperature rise due to the thermal shock wave [36]. The temperature rise ranged from the initial value of 27°C up to 472°C near the anode in a time scale of 140 ns. The temperature rise reduces the gas density and limits some reactions responsible for the radical formation. Ozone density also drops due to the reaction $O_2^* + O_3 \rightarrow 2 O_2 + O$, which is more efficient in higher temperature. This reaction competes with other reactions (such as $NO + O_3 \rightarrow NO_2 + O_2$) and limits the NO reduction. Later experiments confirmed that in a negative corona, the ozone concentration was reduced by 80% at 270°C, and it became zero at 500°C [19]. For a positive corona where ozone generation is about one order of magnitude lower, the corresponding temperatures were 380°C and 600°C respectively.

Heating corona wires not only reduces ozone generation, but also causes the generation of NO_x, primarily NO₂ [19]. For a negative corona, the NO_x generation remained at a very low

level up to a wire temperature of 300°C, beyond which it increased sharply with the temperature. For a positive corona, the NO_x generation occurred from room temperature onward, and it became saturated beyond 300°C at a low concentration level.

2.6.4 Particles in the Gas Phase

The presence of fly-ash particles improves SO₂ and NO_x removal [63], and the presence of SO₂ improves particle removal. Particles provide a surface for the SO₂ reactions as a catalyst, which improves the SO₂ removal. SO₃ can be scavenged from the gas phase to the particle surface and trapped there [5], so that the reverse reaction of SO₃ into SO₂ by electron bombardment is greatly hampered. Meanwhile, unstable radiochemical products from SO₂ and NO_x condense on the surface of the particles and are stabilized by a reaction with the absorbed water on the particle surface [63]. Moreover, the condensation of SO₃ on the particle surface makes the particles more conductive and lowers the resistivity of particles, which reduces back corona and improves the particle removal [2, 63]. In order to reduce the resistivity of particles, flue gas conditioners are added into the ESPs sometimes. Coal ash is basic, so SO₃ conditioner is usually added. Portland cement is acidic, and a basic conditioner like NH₃ is usually added [2].

Gas ions induce aerosol formation, such as the formation of ammonium salts [6, 22]. The action of the ions lowers the threshold of nucleation and increases the nucleation rate due to the influence of the central force field. The typical deposition speed of ions to the surface of the aerosols has been observed to be a few times to an order of magnitude faster than with neutral species. A clustering reaction can be generated in a core particle that consists of up to 30 H₂O or NH₃ molecules (e.g., X⁺(H₂O)₃₀ or Y⁺(NH₃)₃₀) [6, 27].

The heterogeneous gas-particle surface reaction rate can also be enhanced in a corona environment [6]. The gas-particle reaction of a charge-free aerosol particle is controlled by gas phase diffusions and internal particle diffusions. For the corona environments, the electrical field induced drift motion of ionic species near the charged aerosol particle is more important than the gas phase physical diffusions [6]. Therefore, a substantial enhancement of the gas-particle surface reaction rate can be expected.

The corona discharge was significantly stabilized by the accumulation of particles on the electrodes in a long term continuous operation, which can improve both the NO_x removal efficiency and the energy efficiency (gNO_x removed per kWh) [42].

2.6.5 Wet Scrubbing Methods for NO_x removal

Some new wet scrubbing technologies were studied for the simultaneous removal of NO_x and SO_x [3]. The following technologies are used in order to add the capability of NO_x removal onto the existing capability of SO₂ removal:

- Prior to the wet absorption step, oxidize NO to NO₂ in the gas phase by injecting methanol into the rear cavity of the boiler to gain oxidation-absorption scrubbing.
- Add ferrous chelating compounds to the scrubbing solution to catalyze the wet absorption of NO with subsequent chemical reduction of collected NO to molecular nitrogen in an absorption-reduction scrubbing.
- Use a strong liquid-phase oxidizing agent, such as KMnO₄ or NaClO₂, to oxidize NO to NO₂ in the scrubber in an absorption-oxidation scrubbing.

3. EXPERIMENT DESCRIPTION

3.1 Methodology

A bench-scale pulse-enhanced wESP was used to measure the SO₂ and/or NO_x removal in a continuous flow system [65]. The removal efficiencies of SO₂ and/or NO_x were measured experimentally at a steady state for various gas residence time, water flow rate, inlet SO₂ concentration, and applied corona power. Various combinations of ozone and ammonia were injected into the wESP system to enhance the SO₂ and NO_x removal. Experiments were conducted in pure nitrogen, air, and simulated flue gases with 3% or 6% oxygen content. Table 3.1 summarizes the wESP experimental parameters.

Table 3.1 Summary of the wESP Experiment Parameters

Properties	Typical Value	Variable Range	Unit
System Geometry			
Plate-plate spacing	0.20		m
Collection Area	0.186		m ²
Electrical Properties			
Polarity	negative / positive		
Volatge	0 ~ 60		kVolt
Current	0 ~ 2.5		mAmp
Pulsing Frequence	70 ~ 90	10 ~ 90	Hz
Volume	0.019		m ³
Gas Properties			
Air Flow Rate	132, 113, 75	47 ~ 188	L/min
Gas Residence Time in the Corona Discharge Region	8.6, 10, 15	7.5 ~ 24	sec
SO ₂ concentration	2000, 2500	0 ~ 3000	ppm
NO concentration	500, 800, 1000	0 ~ 1200	ppm
NO ₂ concentration	50, 80, 100	0 ~ 120	ppm
Water Properties			
Water Flow Rate	3.79	1.89 ~ 9.46	L/min
L/G	0.050 ~ 0.029	0.050 ~ 0.029	m ³ / m ³

A batch reactor was constructed to conduct batch reaction studies, such as the amount and removal rate of pollutants, in a controlled environment for further study of removal mechanisms. The removal rates of SO₂ were measured experimentally for various gas and liquid mixing conditions, with various polarities and powers of the applied corona discharge. Experiments were conducted in both the pure nitrogen/de-ionized water system and the air/tap water system. The NaOH solution was used to eliminate the liquid phase mass transfer resistance. These tests are particularly useful in determining how the mass transfer is influenced. Table 3.2 summarizes the batch reactor experimental parameters.

Table 3.2 Summary of Batch Reactor Experimental Parameters

Properties	Typical Value	Unit
System Geometry		
Collection Area	0.0103	m ²
Gas Volume	0.030	m ³
Water Volume	0.001	m ³
Electrical Properties		
Polarity	negative	
Volatge	0 ~ 50	kVolt
Current	0 ~ 2.5	mAmp
Gas Properties		
NO concentration	800 ~ 1000	ppm
SO ₂ concentration	2000 ~ 5000	ppm

3.2 Wet ESP System

The wESP system consisted of a mixing chamber, inlet and outlet ducts, a collecting area in the top section for pollutant removal studies, a bottom section for the collection and sampling

of the water, and an outlet duct to exhaust the processed gas. The overall views of this wESP system are shown in Figure 3.1 to Figure 3.4.

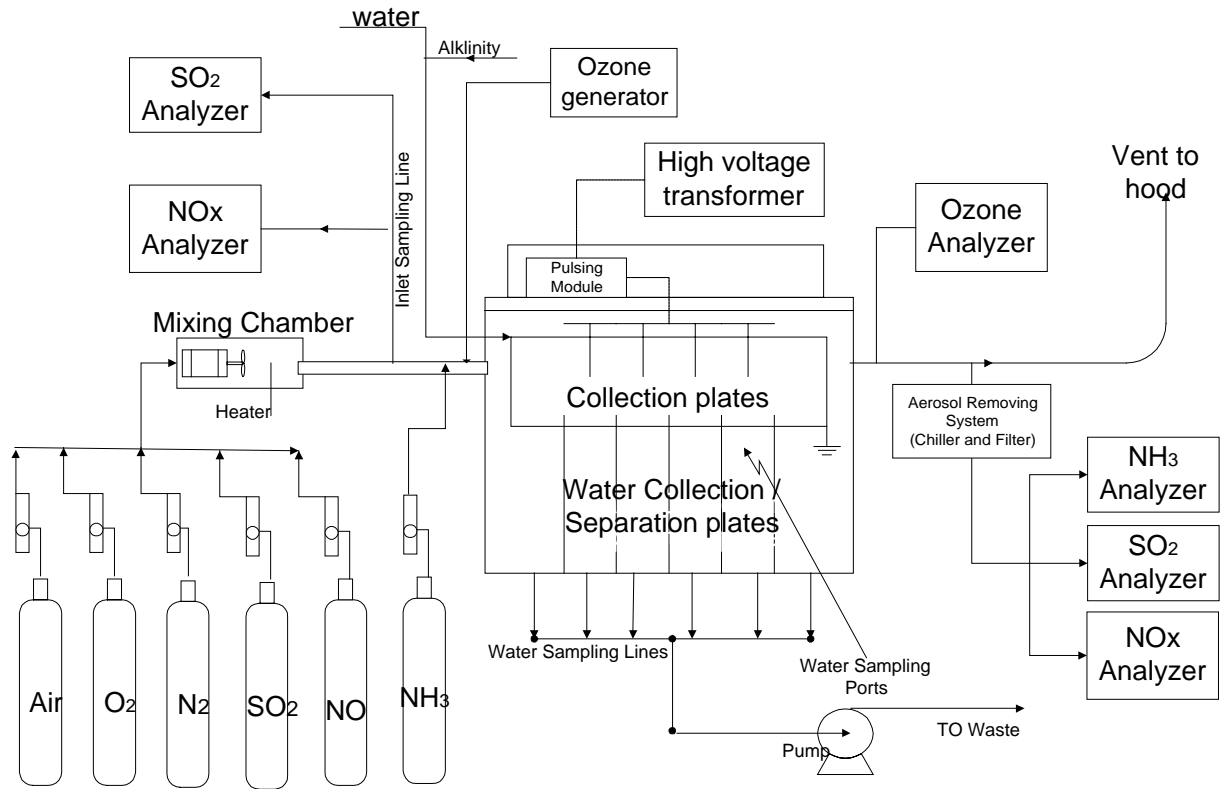


Figure 3.1 Schematic Diagram of Wet-ESP System

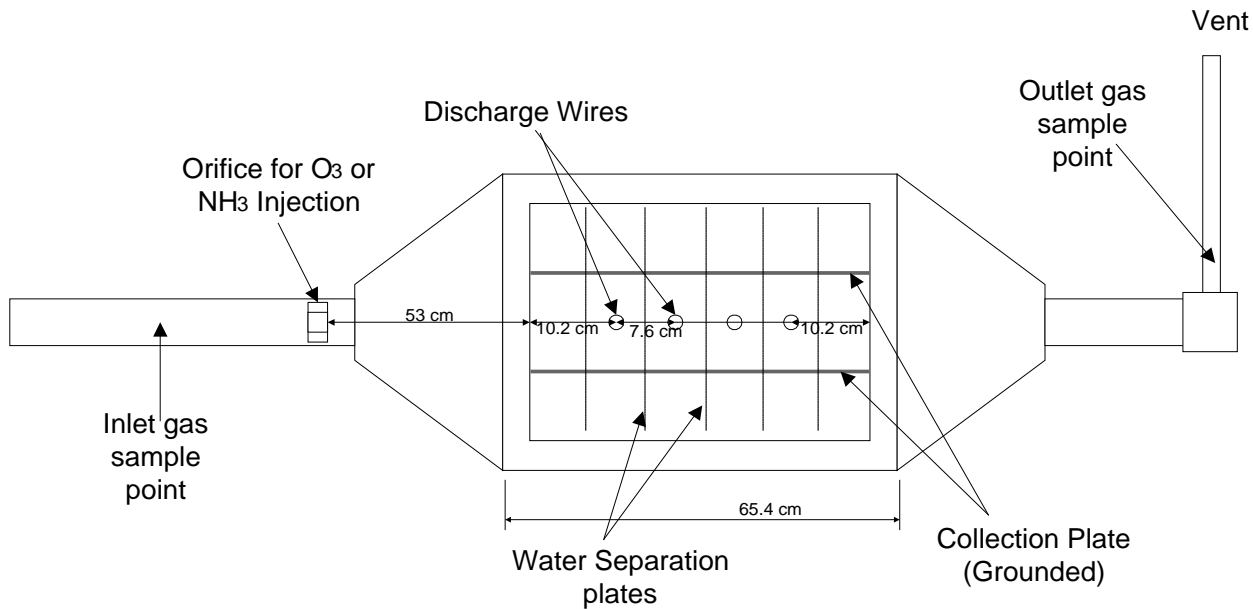


Figure 3.2 Top View of wESP System

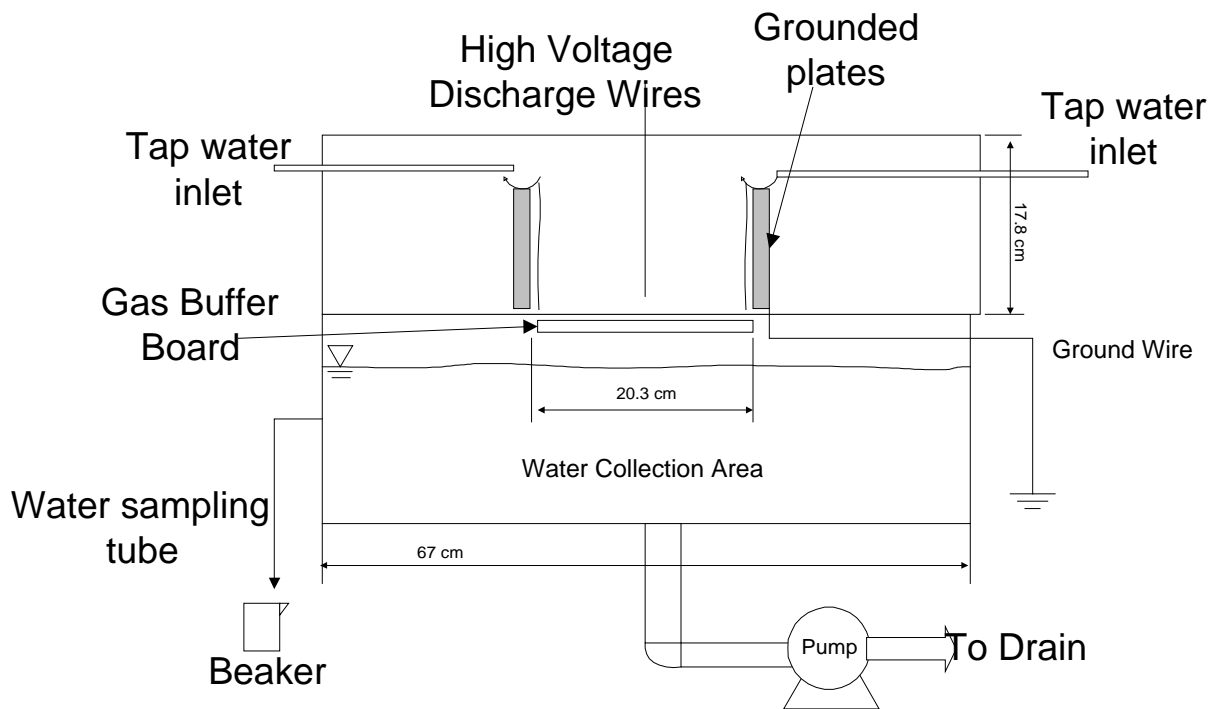


Figure 3.3 Front View of wESP System

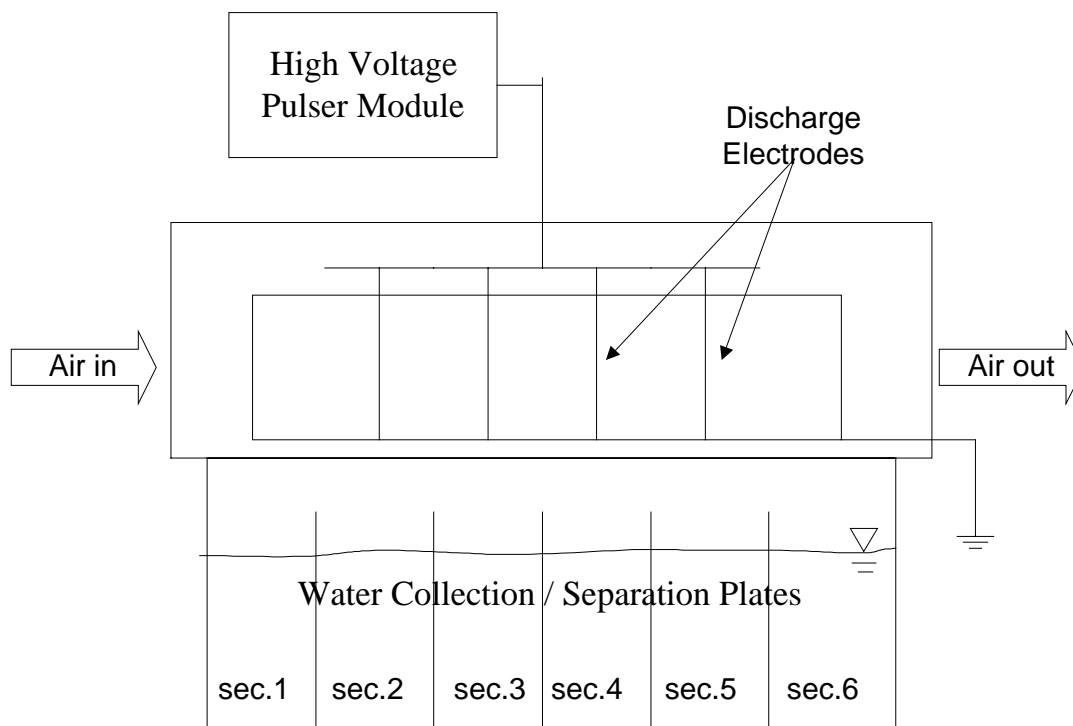


Figure 3.4 Side View of wESP System

3.2.1 Wet ESP System Setup

Air Flow System

Pure SO₂ and/or NO_x were mixed with laboratory compressed air or pure nitrogen in the mixing chamber at room temperature. Airflow rates ranged from 2202 to 1259 cm³/sec with the ideal gas residence times ranged from 8.6 to 15 sec at 25°C. SO₂ concentrations (from 1000 to 3000 ppm) and NO concentrations (from 400 to 1000 ppm) were controlled by the flow meters. In addition, the air/N₂/CO₂ mixtures were made with a air/N₂ volumetric ratio of 1:6, 70% relative humidity to simulate 3%-O₂ and 6%-O₂ flue gases with 11% CO₂ and an ideal gas residence time of 11.5 sec at room temperature. A metal heater was installed in the mixing chamber to control the inlet air temperature. The simulated flue gas flowed through a mixing fan and a buffer for further mixing, then flowed into the inlet duct.

The initial inlet duct diameter was 3.8 cm at the entrance, with 12.7 cm for the rest of the duct. The smaller diameter was used to create greater mixing. As the gas passed through the duct, it went through a section packed with plastic straws to reduce turbulence. Then the gas flow was sampled by the inlet analyzers. The straws forced the gas to move smoothly from the duct to the top section of the wESP. Ammonia injection lines were installed at an orifice in the transition duct 53 cm upstream of the corona region. Air temperature and humidity were measured at the end of the transition duct.

After the transition duct, there was a diffusion screen which dispersed the gas so that it flowed evenly between the grounded plates. As the air passed through the transition zone and the screen, it entered the top part of the wESP. The top and bottom parts both had a width of 67 cm and a length of 65.4 cm and were constructed of 6.35 mm gray PVC. The top box was 17.8 cm tall, which carried the gas and contained the electrodes and the grounded plates. Plate-to-plate spacing was 20.3 cm, with discharge electrode wires spaced 10.2 cm from the inlet and outlet and 7.6 cm apart. Pressure inside the top box was slightly higher than the atmospheric pressure to prevent dilution from outside air. Two Omegalux silicone rubber flexible heaters were placed inside the top box to prevent heat loss and to heat the air temperature to 55 °C.

A simulated flue gas passed through the electrodes and the pollutants were collected by a water film running uniformly over the grounded plates at a flow rate of 3.8 L/min. As the gas left the system, it passed through another transition zone to the outlet duct. The outlet duct's entrance diameter of 14 cm was reduced to 5.1 cm to allow the gas to exit the system through the hood.

Gas Sampling

Teflon tubing was used for the sample lines to limit the reactions with tube material during sampling. A filter system was installed in order to remove aerosols before sampling. Two filter holders were installed in parallel between the chiller system and the on-line analyzers. Filter papers with 0.22 μ m pore diameter were used and switched as needed if the pressure head through one of the filters increased to an unacceptable level.

SO₂ concentrations were sampled at both the inlet and outlet ducts by two non-destructive infrared SO₂ analyzers (PIR-2000 and VIA-300, Horiba Instruments, Inc., Irvine, CA). NO and NO₂ concentrations were sampled at both the inlet and outlet ducts by a chemiluminescence NO-NO₂-NO_x analyzer (Thermo Environmental Instruments 42H analyzer). The amounts of SO₂ and NO_x removal were calculated from the difference between the inlet and the outlet concentrations. The relative standard deviations were 2 ~ 4.5% and 13% for the outlet SO₂ concentrations and SO₂ removal efficiency, respectively.

Ozone was generated by an ozone generator (Welsbach ozonator MD408) and measured by an ozone analyzer (ozone analyzer 1003AH, Dasibi Environmental Corp., Glendale, CA) at the end of the collection plates. The ozone generator utilized an AC corona discharge to oxidize pure oxygen into ozone. Diluted ozone concentration inside wESP was up to 312 ppm.

Outlet ammonia was sampled at 20 cm downstream of the corona region at the outlet duct by an NDIR high concentration ammonia analyzer (PIR-2000, Horiba Instruments, Inc., Irvine, CA) with the detection limit of 100 ppm. Standard gases of 2883 ppm SO₂, 774 ppm NO, 1013 ppm NO₂, and 974 ppm ammonia were used as span gases during calibration. All of the data acquired from the analyzers were recorded on computer using a Strawberry Tree data acquisition

program. This enabled data collection in real time for comparison of inlet and outlet SO₂ and NO_x concentrations to give an instant value of the overall collection efficiency.

Particle Removal

For the removal of particulate matters, smoke tests were conducted after the construction of the wESP. Tests showed that the wESP system could reduce opacity from about 100% at the inlet to about 0% at the outlet. However, in some tests with ammonium aerosols formation or high water temperature ($> 35^{\circ}\text{C}$), fewer particles were removed because the corona power was lost due to the sparks from the corona wires to the deposited aerosols or water vapor on the wESP top. This unwanted sparking greatly reduced the corona voltage and power, thus reducing both the particle and gas removal efficiency. The escaped particles interfered with the outlet gas sampling and analyzing.

Therefore, a chiller-filter system was installed between the wESP outlet sampling point and the on-line analyzers. The chiller system is used to condense aerosols and water vapor in order to prevent water vapor from entering the analyzers. It consists of two single pass double-pipe condensers in series. The sampled exhaust gas was cooled to -1°C by flowing through the inner tubes of the condensers from bottom to top, with the coolant flowing in the opposite direction. A filter system was installed in order to remove the aerosols before sampling. Two filter holders in parallel were installed between the chiller system and the on-line analyzers. Filter papers with a 0.22 μm pore diameter were used. When the pressure head through one of the filters increased to an unacceptable level, the sampling line was switched to the other clean filter.

The collected ammonium salt aerosols were analyzed by a CHNS Determinator (Leco CHNS-932, Leco Corp., St. Joseph, MI) for C, H, and N contents and a total sulfur analyzer (Leco SC-132 model 781-400, Leco Corp., St. Joseph, MI) for the sulfur content.

Electrical System

Originally, the wESP system had several channels with several sets of electrodes and grounded plates. However, this configuration did not work because there were sparks between the frame of the system and the grounded plates. These sparks limited the power output, thus rendering the tests incomparable with a real system. This problem was corrected by removing the electrodes from the ends of the system (near the inlet and outlet framework) and increasing the plate-to-plate spacing, thereby resulting in just one gas flowing section. The final plate-to-plate spacing was 20.3 cm, with discharge electrode wires spaced 10.2 cm from the inlet and outlet and 7.6 cm apart. This is the wire-to-plate geometry commonly used in a conventional single-stage ESP.

Electrode wires were electrically isolated by glass supports. The original carbon steel electrode wires (2 mm dia.) were replaced with stainless steel wires with short, pointed stubs to generate stronger corona at a lower voltage level. It was experimentally found that for obtaining the same pollutant removal efficiency, the energy consumed by pointed-stubbed electrodes is only 15 ~ 25% of the energy consumed by the plain electrodes.

The corona discharge in the wESP was produced by a commercial high voltage transformer (PS/WR 100 R2.5-11 Series WR, Glassman High Voltage Inc., Whitehouse Station, NJ) which has the capability to produce both positive and negative DC voltage up to 100 kilovolts (kV). The maximum voltage for the system was around 60 ~ 65 kV due to the

limitation of spark over, which was close to the typical sparking potential (59 kV peak potentials) for the case of a wire in a 4-in pipe at atmospheric pressure [68]. The corona power was calculated from the separate measurement of the average voltage and current. Various voltage ranges and both polarities were tested.

A pulsing module was developed and added between the existing DC power supply and the corona discharge electrodes (Figure 3.5). High voltage was pulsed by an auto distributor (from a 1983 Lincoln/Mercury Cougar) that was rotated by a variable speed motor (Cole-Parmer Servodyne Mixer Model 50000-20 with a Servodyne Mixer-Controller). This module was found to be capable of pulsing the voltage with a frequency range of 10 to 90 Hz. Pulsing allows the power level to be increased without undue sparking.

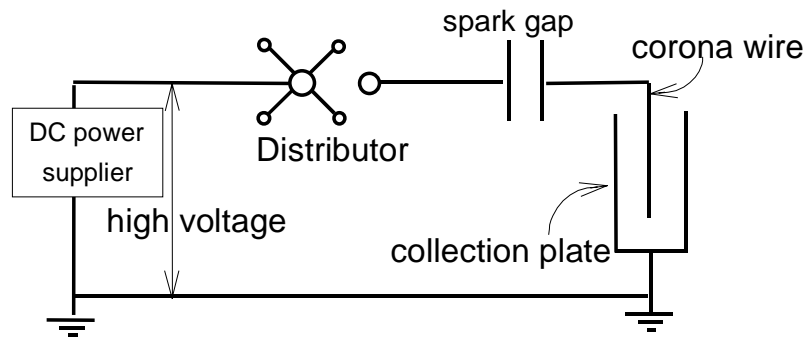


Figure 3.5 High Voltage Pulsing Module

ESP was shielded by aluminum foil to prevent the computer system breakdown due to the electro-magnetic interference from the high voltage pulsing. Before aluminum foil was installed, pulsing corona generates high noise and made the collected data less reliable. This took extra efforts on processing data. Furthermore, data acquisition system was easily shut down at high voltage and experiment had to be halted. With this modification the system can easily achieve higher voltage (70 kV) with acceptable signal interference.

Water Distribution System

Raw tap water carried by Tygon tubing flowed over the grounded collection plates forming a thin layer on plate surface. By controlling the portion of hot water and cold water, water temperature ranged from 10°C to 40°C. By adjusting a rotameter, water flow rate was set to be a minimum required amount of 3.79 L/min to ensure that water flowed uniformly over the plates. Although no direct measurements were made, the uniformity of the water film was visually observed.

Small portion of water was evaporated inside the wESP and raised the relative humidity of the gas stream from dry condition in the inlet gas to 41.8 ~ 43.2 %RH in the outlet gas. Alkalinity was adjusted by injecting sodium hydroxide (NaOH) solution into tubing from a syringe pump. This injection system could raise water pH value up to 10.6 and lasted for only 5 minutes.

The bottom section of the ESP collected the water that ran over the grounded collection plates and carried the pollutants driven to these plates. As the water flowed over the plates and fell into the bottom box, it was divided into six sections, which separated the water into six phases. Water samples were taken at steady state. The steady state was verified by the gas phase SO₂/NO_x concentrations, which usually took about 10 minutes after an experimental condition was set. We waited until the gas-phase concentration reached a steady state and added additional 20 minutes in order to ensure that the water concentrations reached a steady state as well.

After the system reached a steady state, water was sampled from each section and represented a step-by-step reaction occurring in the wESP. The first phase corresponded to the first sixth of gaseous residence time in the box, the second section corresponded to the second

sixth of time phase in the box, etc. Corona discharge electrodes were located above the second, third, fourth and fifth phases. Water analysis is described in detail in section 3.4.

3.2.2 Wet ESP Experimental Procedure

In a typical wESP experiment, the O₃, NO_x and SO₂ analyzers were warmed up and calibrated first. SO₂ analyzers were calibrated with a 3000 ppm SO₂ gas. NO_x analyzer is calibrated with a 1000 ppm NO gas and a 800 ppm NO₂ gas. The O₃ analyzer has an internal calibration system. The wESP was purged with the either compressed air or N₂ in order to flush out any unwanted gaseous constituents. Then pure SO₂ and/or NO is introduced to the gas stream to make up a specific concentration. The SO₂/NO_x tanks were opened and set at a certain flow rate by a rotameter with a needle valve.

Water flow over the plates was initiated to ensure that a smooth film of water was covering the plates and reaching a desired water level in the bottom box. Sand paper was used on the plate to remove any blockages. Both water level and water temperature were maintained during the test period. Maintaining water level is important as changing the level would result in gas being pushed into or out of the bottom box that directly affects the outlet pollutant concentration. Small sections of the gray PVC were replaced in the bottom box to easily maintain water levels.

Once the analyzers were calibrated, the gas concentrations were steady and recorded, and the water level was reached, the power was initiated. Immediately before initiating the power, the distributor mixer was set, and the Strawberry Tree data collection program was started. During the test, the flow rates of the pollutants, initial concentrations, and the power levels were adjusted and noted in the log books. When the test ended, the analyzers were re-calibrated.

3.3 Batch SO₂ Absorption System

3.3.1 Batch Reactor Setup

Gas Chamber

The original batch reactor was constructed of 0.6 cm plexi-glass. Air mixing was controlled by an external mixer (Gerald H. Keller Co. Mixer Model H3697053 with a GT-21 Motor Controller) using a correlation between a spinning side piece and the actual mixer to predict the rpm's used in a test. However, when working with high voltage, this material is not electrically insulated very well.

A new reactor was constructed of 0.6 cm aluminosilicate non-conductive glass as shown in Figure 3.6 to replace the plexi-glass one. The upper gas chamber, with a volume of 29,743 cm³, contains a mixing fan, a corona discharge wire, a pressure manometer, and a septum for injecting pure SO₂ with a syringe. The gas chamber was pressurized by 100 mmH₂O and held for 20 minutes to check if there is any leak. Air mixing was provided by a CPU cooler (Titan Corp., Taiwan) of which the consumed power was measured. The gas sampling system drew gas out of the gas chamber via a peristaltic pump (Cole-Parmer Model 7553-800 with a Masterflex controller) from a glass tube extended to approximately the middle of the gas chamber to the non-dispersive infrared SO₂ analyzer (Horiba PIR-2000) which is a non-destructive analytical method. The sample was then circulated from the analyzer back into the gas chamber while SO₂ was continuously measured. However, NO_x cannot be continuously measured because the NO_x analyzer converts NO to NO₂ while analyzing. The NO_x analyzer first converts NO₂ to NO at 620°C, then utilizes the chemiluminescence reaction of NO-ozone to convert the entire NO to NO₂ ($\text{NO} + \text{O}_3 \rightarrow \text{NO}_2 + \text{O}_2 + \text{hv}$).

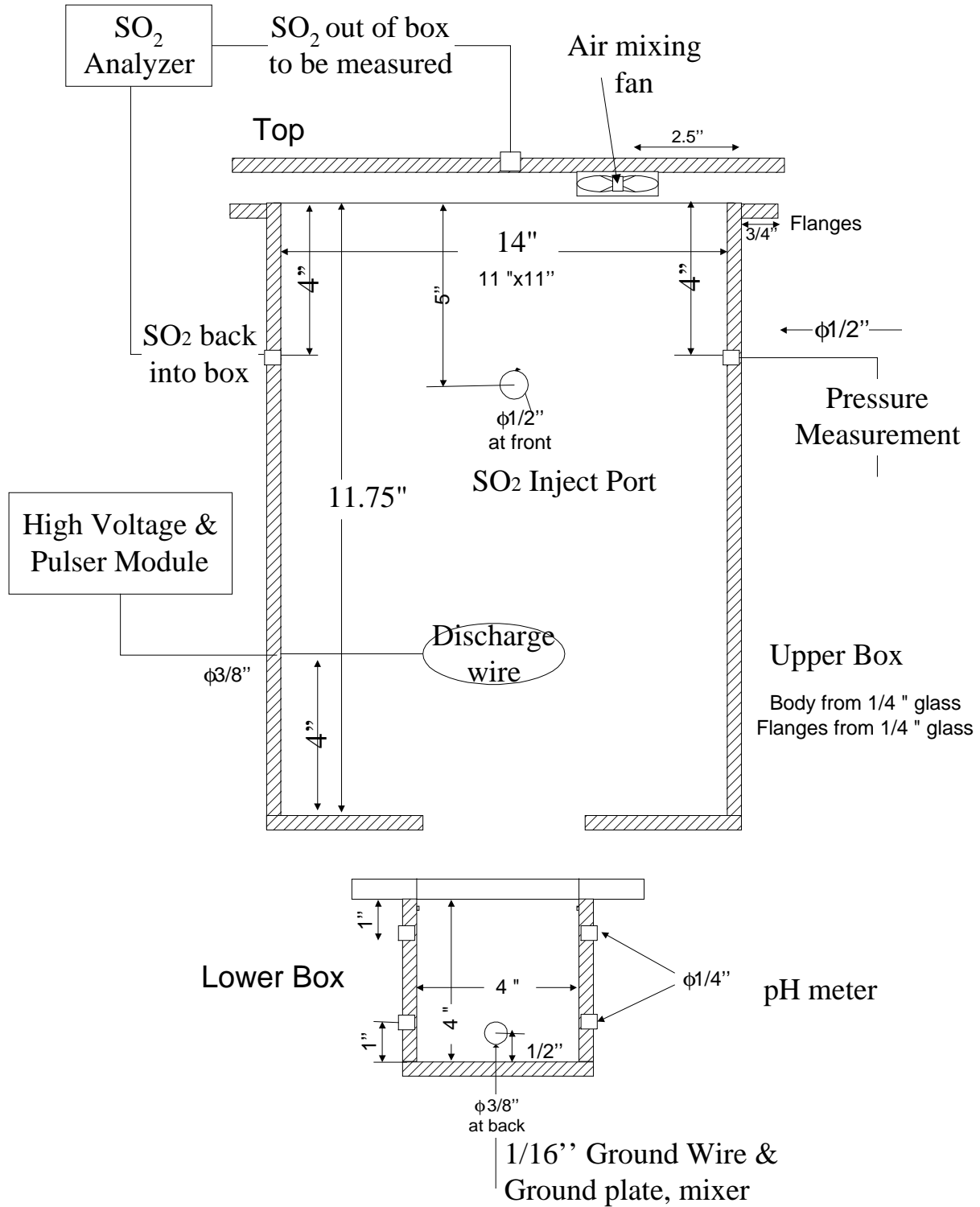


Figure 3.6 The Overall View of the Batch Reactor System

Corona discharge wire was located 10.2 cm above the gas-liquid interface and grounded area, which was the same distance as the wire-to-plate spacing in the wESP system. The wire was wrapped by stainless steel mesh with short, pointed stubs to enhance the corona generation. The same pulsing module as discussed in the section of wESP setup was installed in the batch reactor.

Water Chamber

The bottom water chamber contained the collection water and a mixer to continually mix the water for uniform concentration. This water chamber also contained a grounded plate at the bottom to draw the charged molecules into the water. This plate was electro-plated with gold to prevent corrosion. The discharge wire was initially located approximately 30.5 cm above the grounded plate, but it was found that too much electrons were dissipated away from the grounded plate. Therefore the wire was relocated and stainless steel mesh was put into the water chamber to place the grounded area approximately 10.2 cm from the discharge wire. The de-ionized water used in these tests was boiled to drive off as much oxygen as possible in order to minimize oxidation.

A total sulfur analysis (sulfur concentration in the water by mass percent) was conducted on the batch reactor using a sulfur determinator. The results of two tests indicated that the difference of sulfur mass balance was around 10~13% as shown at Table 3.3. These results verified that the SO₂ was not absorbed onto any tubing or the reactor wall, as well as no major leak in the batch system.

Table 3.3 Total Sulfur Analysis of Batch Reactor Tests

	Unit	Test #1	Test #2
In Gas Chamber			
Initial SO ₂ conc.	ppm	5080	4938
Final SO ₂ conc.	ppm	1103	1788
Initial sulfur mass	g	0.2109	0.2050
Final sulfur mass	g	0.0458	0.0742
Total sulfur loss in gas	g	0.1651	0.1308
In Water Chamber			
Total sulfur before test	% w	0.00256%	0.00032%
Total sulfur after test	% w	0.02050%	0.01140%
Total sulfur gain in water	g	0.1882	0.1162
Difference between the loss in gas and the gain in water	%	13.1%	11.8%

3.3.2 Batch Reactor Experimental Procedure

A typical run in the batch reactor is as following. First, the SO₂ and NO_x analyzers were warmed up and calibrated using a gas with a known concentration. As the analyzer was warming up, the gas chamber was purged with nitrogen. Water was boiled to remove dissolved oxygen, and was kept under a nitrogen blanket to prevent absorbing oxygen after boiling. The boiled water was cooled and put into the water chamber. Then the nitrogen purge was shut off and the system was closed. The pressure line was kept off until the last minute to provide an outlet for the nitrogen purge. These tests were conducted under a slightly positive pressure, with no outside air affecting the results.

Once the system was sealed, the sampling valves are turned from calibrate to sample and the air and water mixers were turned on. The pure SO₂ and NO were retrieved from gas cylinders using a 100 mL glass syringe through a septum that is located near the air mixer. For 5000 ppm SO₂ in the reactor, this needs to be done twice to put 200 mL of pure SO₂. At this point, the

distributor was turned on and the power was initiated. The fan was turned off for the duration of the power trials except for some intermittent mixing (generally every 30 minutes).

After each trial, the SO₂ analyzer was re-calibrated and some water was drawn out for pH and total sulfur analysis. A pH electrode was installed in the water chamber for a continuous pH measurement during the tests.

3.4 Water Analysis

The pH was measured for each water sample of each phase as well as the inlet tap water by Fisher Scientific Accumet 825 MP pH meter. Sulfur and nitrogen compounds were determined by analysis methods listed in Table 3.4.

Table 3.4 Analysis Methods for Sulfur and Nitrogen Compounds in the Liquid Phase

Species	Analysis Methods
Sulfate (SO ₄ ²⁻)	Ion Chromatograph or Gravimetric Method with Drying of Residue (Standard Method 4500-SO42-D), [66]
Sulfite (SO ₃ ²⁻)	Ion Chromatograph or Iodometric Method (Standard Method 4500-SO32-B), [66]
Nitrate (NO ₃ ⁻)	Ion Chromatograph
Nitrite (NO ₂ ⁻)	Ion Chromatograph

3.4.1 Gravimetric Method with Drying of Residue for Sulfate Ion

Sulfate (SO₄²⁻) species in water phase was determined by Gravimetric Method with Drying of Residue, in which sulfate is precipitated in a hydrochloric acid (HCl) solution as barium sulfate (BaSO₄) by the addition of barium chloride (BaCl₂).

Hydrochloric acid with a concentration of 1:1 was prepared. This barium chloride solution was made by dissolving 10 g of barium chloride (BaCl₂.2H₂O) in 100 ml of distilled

water. The use of a drying oven, a hot plate and a thermometer, a balance, fritted glass filters with a filtering apparatus, weighing paper, beakers, flasks, and large glass covers for filters were required.

50 ml of the fresh water sample was treated with 1~2 ml HCl solution, poured into a flask, and heated to boiling. After the sample boiled, warm barium chloride solution was added until the precipitation was complete. To ensure the completion of the precipitation, 2 ml of $\text{BaCl}_2 \cdot 2\text{H}_2\text{O}$ was added in excess. The sample was then digested for a minimum of 2 hours at $80 \sim 90^\circ\text{C}$. After weighing the oven-dried filter, the sample was filtered through at room temperature. In case the precipitate did not entirely exit the flask, warm, distilled water was added to the flask to wash the remaining precipitate out. The filter was then placed into a glass cover and dried in an oven overnight, cooled and weighted the next day.

3.4.2 Iodometric Method for Sulfite Ion

Sulfite (SO_3^{2-}) species in water phase was determined by Iodometric Method, in which sample was titrated with a standardized potassium iodide-iodate titrant. Free iodine, liberated by the iodide-iodate reagent, reacts with sulfite. The titration endpoint is signaled by the blue color resulting from the first excess of iodine reacting with a starch indicator.

To prepare for the sulfite test, sulfuric acid (H_2SO_4) was mixed with distilled water at a ratio of 1:1. After the KIO_3 was dry for 4 hours at 120°C , 0.4458 g of it was used in the standard potassium iodide-iodate titrant along with 4.35 g of KI, 310 mg of sodium bicarbonate (NaHCO_3), and 1000 ml of distilled water. EDTA reagent was made by dissolving 2.5 g of disodium EDTA in 100 ml of distilled water. Starch indicator was created by adding 0.5 g of

soluble-potato powder to 100 ml of distilled water. The uses of a balance, weighing paper, beakers, flasks, titration burette and burette holder were required.

Sample was collected from the wESP with minimum contact with air, and fixed immediately by adding 1 ml EDTA solution/100 ml sample. 1 ml of H_2SO_4 and 0.1 g of sulfamic acid crystals ($\text{NH}_2\text{SO}_3\text{H}$) were added to a 250-ml flask. Then, 50 ml of the EDTA-stabilized sample was put into the flask along with 1 ml of the starch indicator solution. The sample was immediately titrated with the standard potassium iodide-iodate titrant (KI-KIO_3) and swirled until a faint permanent blue color developed.

An interesting observation was made during the sulfite testing. If the starch was added to the flask before the water sample, the sample turned blue at the titration endpoint. However, if the starch indicator was added into the flask containing sample with H_2SO_4 and $\text{NH}_2\text{SO}_3\text{H}$, the sample turned yellow instead of blue at the titration endpoint. Tests were then performed to ensure that the order of addition of the water sample and starch had no effect on the sulfite test results because the results of two orders of addition turned out to be the same.

3.4.3 Ion Chromatography

An ion chromatograph unit (Dionex DX-120, Dionex Corp., Sunnyvale, CA) was used to analyze the wESP collection water for ion concentrations. Ion chromatograph performs isocratic ion analysis applications using conductivity detection. The integrated ion chromatograph system includes a pump, injection valve, detector, conductivity cell, columns, and self-regenerating suppressor (SRSTM). Most anions in water can be determined by ion chromatography, including nitrate (NO_3^-), nitrite (NO_2^-), sulfate (SO_4^{2-}) and sulfite (SO_3^{2-}).

Ion chromatograph anions analysis of wESP collection water follows these steps:

1. Set wESP operation conditions. (Typical wESP conditions: 240 CFH Gas flow rate, 1 GPM water flow rate, 45 kV Corona power, 2000 ppm SO₂ and 1000 ppm NO inlet concentration)
2. After the gas concentrations reached a steady state, operate wESP for another 20 minutes in order to ensure that the water concentrations reached a steady state as well.
3. Take water samples of 6 phases from the bottom sampling line of wESP and one sample of tap water.
4. Immediately add EDTA solution 2 ml/50 ml sample as a complexing agent to inhibit sulfite (SO₃²⁻) oxidation by catalysis of some metal ions.
5. Measure the pH values of each phase.
6. Add some NaOH to raise the pH around 7 for better performance of the Ion Chromatograph
7. Seal samples and keep them in a refrigerator before analysis.
8. Setup Ion Chromatograph condition (flow rate, pressure ...) and load analysis method for anions.
9. Filter the samples to remove any solids in order to prevent blocking the IC column. Take 0.5 mL sample and add 2.0 mL de-ionized water to dilute samples by 5 times before injecting into the IC in order to improve accuracy. Drive out all bubbles in the syringe in order to prevent the bubbles blocked inside column.
10. Perform analysis on the Ion Chromatograms and get peak areas.

Commercial standard solutions were purchased and prepared in the range from 0.8 to 150 mg/L. All standard calibration solutions were treated in the same manner as the sample solutions. A typical chromatogram of standard solution is shown below. Calibration curves of nitrate (NO_3^-), nitrite (NO_2^-), sulfate (SO_4^{2-}), sulfite (SO_3^{2-}) and chlorion (Cl^-) are attached at the appendix. IC anion analysis provides very precise results ($R^2 = 0.985 \sim 0.999$).

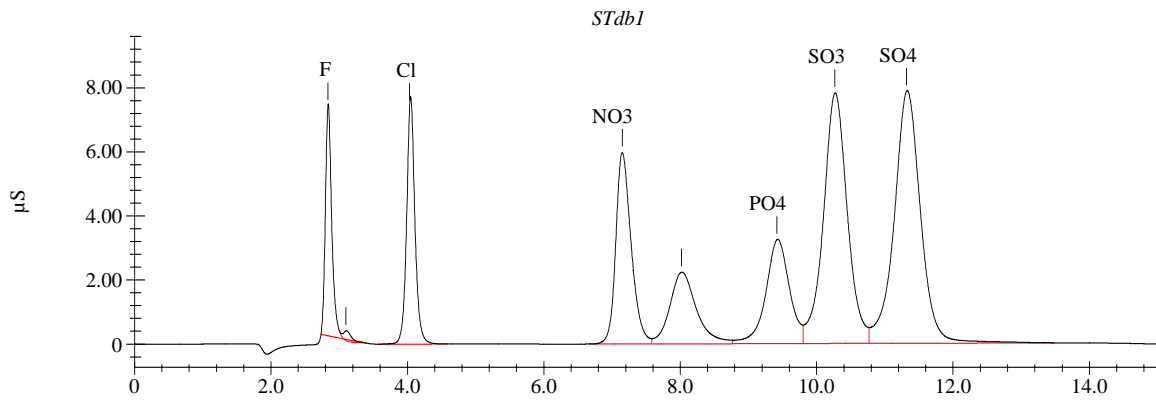


Figure 3.7 Typical Chromatogram of a Standard Solution

Following graph is a typical chromatogram of the water sample from wESP.

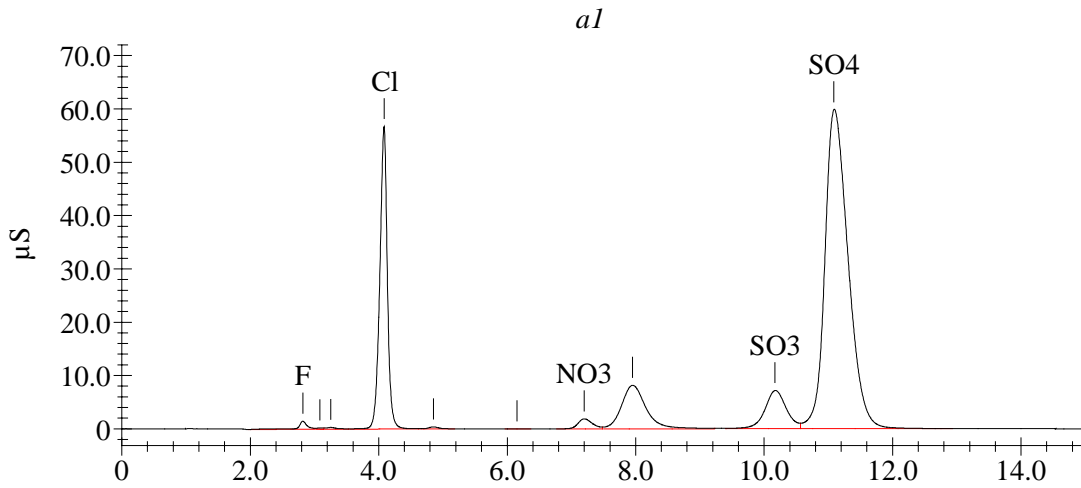


Figure 3.8 Typical Chromatogram of the Water Sample from wESP

The measurements of raw tap water showed a good reproducibility of ion chromatograph analysis as shown in Table 3.5.

Table 3.5 Reproducibility of Ion Chromatograph Analysis of Tap Water

	NO ₃ ⁻	SO ₄ ²⁻	Cl ⁻
Unit	mg/L	mg/L	mg/L
Tap water sample #1	6.96	124	172
Tap water sample #1	6.93	123	171
Tap water sample #2	5.75	137	185
Tap water sample #2	6.33	141	192

3.4.4 Water Quality

The background concentrations of raw water used for wESP and batch tests were measured as shown in Table 3.6. Nitrite and sulfite concentrations were non-detectable. These background concentrations were subtracted from the results obtained for the wESP sample water.

Water was originally boiled to remove dissolved oxygen in batch tests. According to the results shown in Table 3.6, however, the influence on the mass transfer coefficient was little when the different type of water is used. It is reported that the reaction between dissolved oxygen and sulfite is negligible in the absence of catalysts [59].

Table 3.6 Quality of Water Used in the wESP and Batch Tests

	De-ionized water	Boiled de-ionized water	Tap water	Unit
pH	5.00 ~ 5.40	5.35 ~ 6.20	8.25 ~ 8.50	
Na ⁺	7.55 ~ 13.28	N.A.	18.11	mg/L
Ca ²⁺	1.8	N.A.	28	mg/L
Cl ⁻	4.0 ~ 4.2	N.A.	171~192	mg/L
SO ₃ ⁻	N.D.	N.A.	N.D.	mg/L
SO ₄ ²⁻	N.D.	N.A.	123 ~ 141	mg/L
NO ₂ ⁻	N.D.	N.A.	N.D.	mg/L
NO ₃ ⁻	N.D.	N.A.	5.75 ~ 7.34	mg/L
K _{OG} from Batch Tests*	2.63*10 ⁻⁶	2.72*10 ⁻⁶	2.68*10 ⁻⁶	mol/s-cm ² -atm

N.D. = non-detectable; N.A. = not available.

* Batch test conditions: 3000 ppm SO₂ in pure N₂, 22°C gas and water temp., no corona discharge.

** Anion concentrations are from Ion Chromatograph analysis

*** Anion concentrations of boiled DI water have not been measured, but they should be equal to the concentrations of non-boiled DI water.

4. THEORY AND MODELING

This chapter will discuss the gas flows and the motion of charged particles or ions in an ESP, the chemical theory of SO₂ and NO_x removal, and the mass transfer modeling of SO₂ removal in a wESP.

4.1 Gas Flows in the wESP

The Reynolds number of the gas flow and the thicknesses of hydrodynamic and concentration boundary layers can be estimated in the wESP without corona discharge. The local Reynolds number is defined as:

$$Re_x = \frac{xv_b\rho}{\mu} \quad \text{Eq. 4-1}$$

where

x = the distance from the leading edge, cm (< total length of collection plates = 61 cm)

v_b = Bulk gas velocity, cm/sec

ρ = Air density, 0.001205 g/cm³ at 25°C

μ = Air viscosity, 0.000181 g/cm-sec

The bulk gas velocities were measured by a Hot Wire Gas Velocity Meter (Sierra Instruments, Inc., CA). Three different gas flow rates were used to cover the gas residence times from 8.6 ~ 15 sec as shown in Figure 4.1. Based on the measured gas velocity, the local Reynolds number can be calculated as shown in Figure 4.2. It can be concluded that without corona discharge, the flows were in the laminar region since the Re_x was smaller than 200,000 for a flow over a flat plate [81].

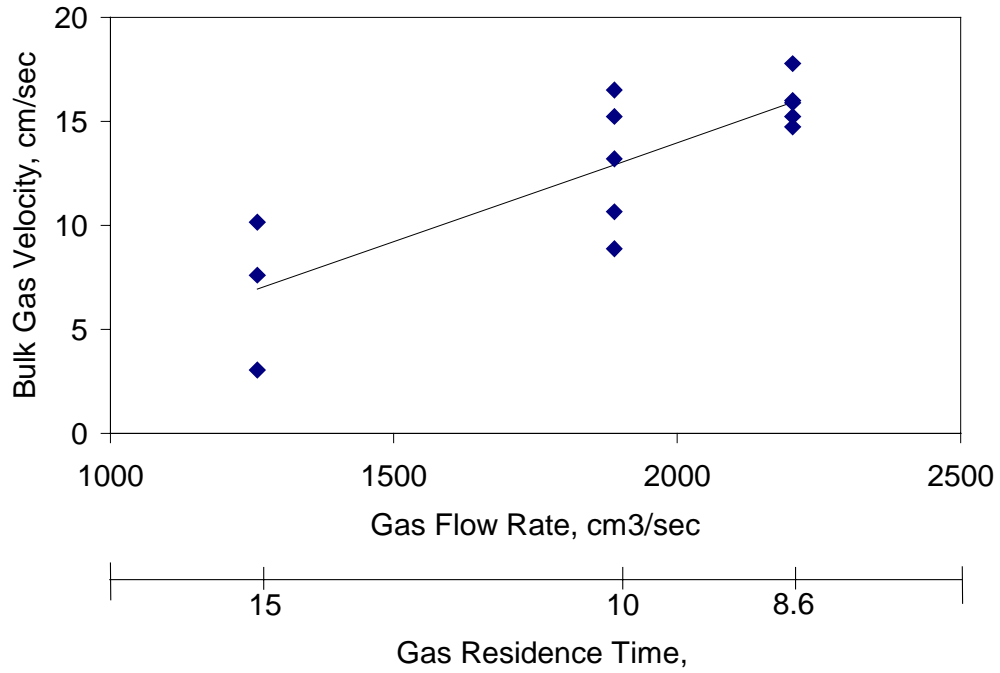


Figure 4.1 Bulk Gas Velocity in the wESP

Wet ESP Conditions: In 20°C air, without corona discharge.

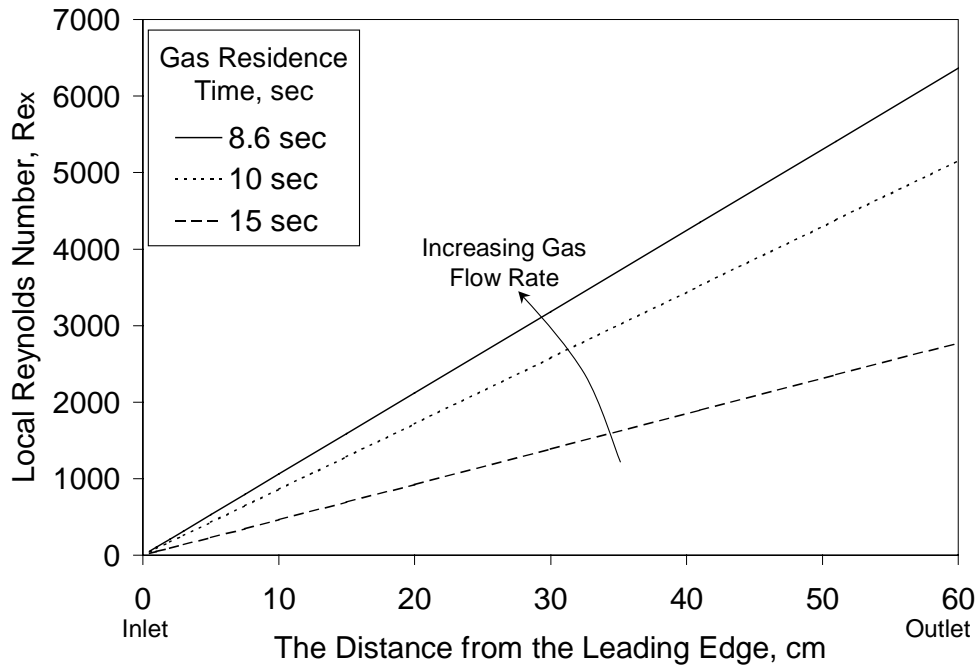


Figure 4.2 Local Reynolds Number, R_{ex} , in the wESP

Wet ESP Conditions: In 20°C air, without corona discharge.

The hydrodynamic boundary layer thickness, δ , is obtained from [81]:

$$\frac{\delta}{x} = \frac{5}{\sqrt{\text{Re}_x}} \quad \text{Eq. 4-2}$$

And the concentration boundary layer, δ_c , is related to the hydrodynamic boundary layer by [81]:

$$\frac{\delta}{\delta_c} = \text{Sc}^{1/3} \quad \text{Eq. 4-3}$$

where Sc is the Schmidt number ($\text{Sc} = \frac{\mu}{\rho D_{\text{SO}_2}}$).

The calculated concentration boundary layers are very close to hydrodynamic boundary layers in the wESP. The differences between the thicknesses of hydrodynamic and concentration boundary layers are less than 0.3%. The boundary layer profiles are shown at Figure 4.3. The convective gas side mass transfer coefficient of the system involving a moving fluid over a flat plate surface can be solved as [81] the following equation and in Figure 4.4:

$$\frac{k_g x}{D_{\text{SO}_2}} = 0.332 \text{Re}_x^{1/2} \text{Sc}^{1/3} \quad \text{Eq. 4-4}$$

When a corona discharge is applied in the gas phase, the conditions of the gas flow change and the above estimation is not valid anymore. According to the analysis in section 2.4, the electrohydrodynamics number of this wESP system ($N_e = 178$) far exceeds unity. Therefore, the gas flow will respond to the electrostatics in a corona discharge. No research quantitatively discussed the electrostatic effect on the mass transfer boundary layers in a corona discharge.

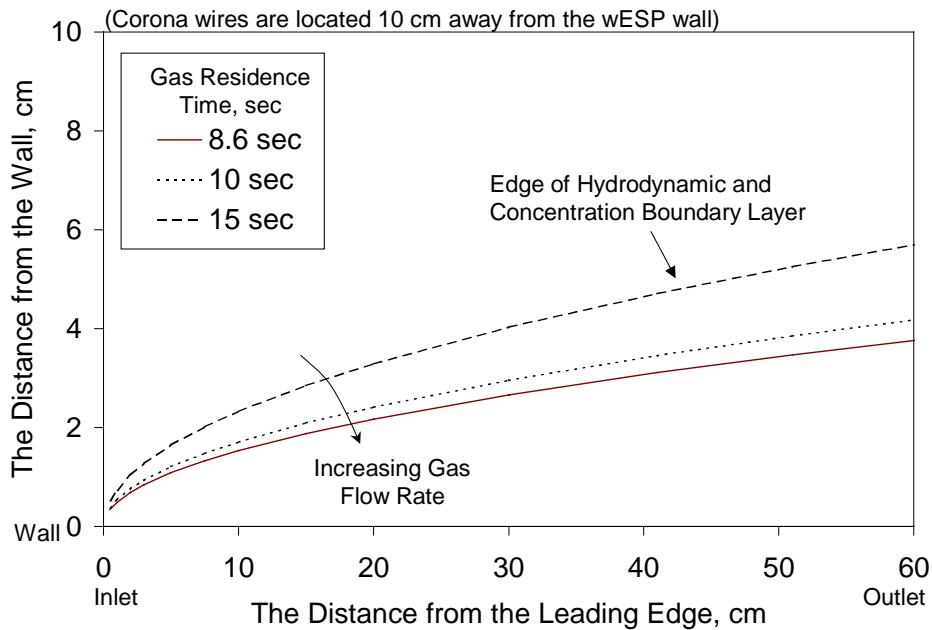


Figure 4.3 The Boundary Layer Profiles in the wESP

Wet ESP Conditions: In 20°C air, without corona discharge.

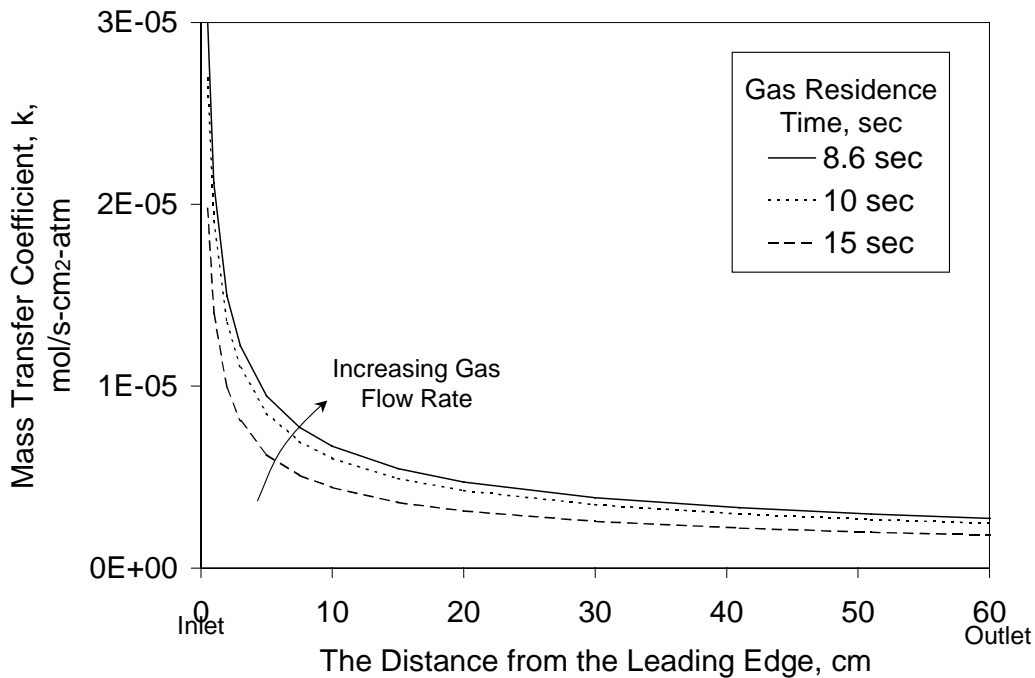


Figure 4.4 The Profiles of Mass Transfer Coefficient in the wESP

Wet ESP Conditions: In 20°C air, without corona discharge.

4.2 The Motion of Charged Particles and Ions in ESPs

The motion of charged particles or ions in ESPs was studied. It is assumed that particle motion is in the Stokes region ($Re < 1$), the terminal electrostatic velocity is obtained by balancing the electrostatic force and the Stokes drag force [10].

The electrostatic force:

$$F_e = N e E \quad \text{Eq. 4-5}$$

where

N : Number of charges on a particle

e : 1.6021×10^{-19} , coul

E : Electric field, kV/cm

The Stokes drag force:

$$F_d = \frac{C_d}{C_c} \frac{\pi}{8} \rho v_t^2 d^2 \quad \text{Eq. 4-6}$$

where

v_t : Terminal electrostatic velocity, cm/sec

d : Particle diameter, cm

ρ : Gas density, g/cm³

C_d : Drag coefficient; $C_d = 24 / Re$

Re : Reynolds number

C_c : Cunningham correction factor for particles less than 1 μm in dia. [10]

Balance the electrostatic force and the Stokes drag force to determine the terminal electrostatic velocity (drift velocity):

$$v_t = \frac{1}{d} \sqrt{\frac{8NeE}{\pi\rho C_d}} = \frac{NeEC_c}{3\pi\eta d} \quad \text{Eq. 4-7}$$

It is convenient to express the ability of a particle to move in an electric field in terms of *electrical mobility*, Z ($\text{cm}^2/\text{V}\cdot\text{s}$), the velocity of a particle with a given charge in an electric field of unit strength.

$$Z \equiv \frac{neC_c}{3\pi\eta d} \quad \text{Eq. 4-8}$$

Therefore:

$$v_t = Z * E \quad \text{Eq. 4-9}$$

The typical values of electrical mobility of electrons, ions, and aerosol particles at standard conditions are listed in Table 4.1.

Table 4.1 Electrical Mobility of Electrons, Ions, and Aerosol Particles at Standard Conditions

Particles diameter	Electrical mobility Z		Drift velocity in a typical ESP v_t
μm	$\text{cm}^2/\text{V}\cdot\text{s}$		cm/s
	Singly charged	Maximum charged	
Electron	666.67		
Negative air ion	1.57		3050
Positive air ion	1.40		3050
0.01	0.021	7.33	
0.1	2.70E-04	9.33	
1	1.10E-05		7400 *
10	9.67E-07		20000 *
100	9.33E-08		32000 *

* v_t (cm/s) in an unit electric field when the particles are with max charges. Because $Re > 1$, $v_t = Z * E$ does not hold [10].

In order to estimate the removal efficiency of a charged ion, the Deutsch-Anderson equation, the most widely used equation for estimating the efficiency of an ESP, is used here:

$$\eta = 1 - \exp\left(-\frac{A}{Q} v_t\right) \quad \text{Eq. 4-10}$$

where A is the cross section area, and Q is the gas flow rate.

According to the typical electrical mobilities in Table 4.1, an negative/positive gas ion will be 100% removed from the bulk gas to the gas/liquid interface within 0.002 sec (Stokes region) ~ 0.358 sec (non-Stokes region) after it receives a single charge in this wESP. Therefore, the performance of the gaseous pollutant removal depends on either the efficiency of gas charging, or the mass transfer into the liquid phase.

4.3 Chemistry of SO₂

4.3.1 Henry's Law

Henry's law describes the equilibrium of SO₂/water system: [59, 67, 68, 69]

$$P_{\text{SO}_2} = H_{\text{SO}_2} C_{\text{SO}_2} \quad \text{Eq. 4-11}$$

where

P_{SO_2} : the partial pressure of SO₂ , atm

C_{SO_2} : [SO_{2(aq)}] = [H₂SO₃] , mol/L

H_{SO_2} : Henry's law constant of SO₂ ; $\log H_{\text{SO}_2} = 7.521 - 1376.1/T$, atm-cm³/mol [59]

T : Temperature, K

4.3.2 Oxidation of SO₂

The thermodynamic properties of SO_x indicate that SO₂ has a strong tendency to react with O₂ in the air at normal conditions.



Thus, $[\text{SO}_3]/[\text{SO}_2] = 8 \times 10^{11}$ at equilibrium in air at 1 atm and 25°C [70]. However, the above reaction is very slow under catalyst-free conditions in the gas phase. SO_2 will be converted largely to H_2SO_4 at equilibrium.



4.3.3 Dissociation of SO_2

Sulfite species (H_2SO_3 , HSO_3^- , SO_3^{2-}) are the original form of sulfur species when SO_2 gas is absorbed into water. The dissolution of sulfite species includes the following reactions:



Equilibrium constant: $K_{a1} = 10^{(853/T - 4.74)}$ mol/L [59]



Equilibrium constant: $K_{a2} = 10^{(621.9/T - 9.278)}$ mol/L [59]

Sulfate (SO_4^{2-}) is the oxidized form of sulfite species when sulfite is oxidized by oxygen either in air or in water phase. The dissolution of sulfate species includes the following reactions:



Equilibrium constant: $K_{a1} = -3$ mol/L @298K [71]



Equilibrium constant: $K_{a2} = 1.99$ mol/L @298K [71]

The total sulfite concentration indicated in this paper includes the concentrations of three Sulfur-IV species: H_2SO_3 and anions HSO_3^- and SO_3^{2-} .

$$C_{\text{sulfite}} = [\text{H}_2\text{SO}_3] + [\text{HSO}_3^-] + [\text{SO}_3^{2-}] \quad \text{Eq. 4-20}$$

where C_{sulfite} is the total sulfite concentration (the total dissolved sulfur in solution in oxidation state 4).

Each species can be expressed as a function of total sulfite concentration.

$$[\text{H}_2\text{SO}_3] = \alpha_0 * C_{\text{sulfite}}; \alpha_0 = \left(1 + \frac{K_{a1}}{[\text{H}^+]} + \frac{K_{a1}K_{a2}}{[\text{H}^+]^2} \right)^{-1} \quad \text{Eq. 4-21}$$

$$[\text{HSO}_3^-] = \alpha_1 * C_{\text{sulfite}}; \alpha_1 = \left(\frac{[\text{H}^+]}{K_{a1}} + 1 + \frac{K_{a2}}{[\text{H}^+]} \right)^{-1} = \alpha_0 \frac{K_{a1}}{[\text{H}^+]} \quad \text{Eq. 4-22}$$

$$[\text{SO}_3^{2-}] = \alpha_2 * C_{\text{sulfite}}; \alpha_2 = \left(\frac{[\text{H}^+]^2}{K_{a1}K_{a2}} + \frac{[\text{H}^+]}{K_{a2}} + 1 \right)^{-1} = \alpha_1 \frac{K_{a2}}{[\text{H}^+]} \quad \text{Eq. 4-23}$$

The electro-neutrality equation is:

$$([\text{H}^+] - [\text{H}^+]_{\text{initial}}) = ([\text{OH}^-] - [\text{OH}^-]_{\text{initial}}) + [\text{HSO}_3^-] + 2[\text{SO}_3^{2-}] \quad \text{Eq. 4-24}$$

$$[\text{H}^+] - [\text{H}^+]_{\text{initial}} = \left(\frac{K_w}{[\text{H}^+]} - \frac{K_w}{[\text{H}^+]_{\text{initial}}} \right) + \alpha_1 C_{\text{sulfite}} + 2\alpha_2 C_{\text{sulfite}} \quad \text{Eq. 4-25}$$

$$[\text{H}^+] - [\text{H}^+]_{\text{initial}} = \left(\frac{K_w}{[\text{H}^+]} - \frac{K_w}{[\text{H}^+]_{\text{initial}}} \right) + \left(\frac{[\text{H}^+]}{K_{a1}} + 1 + \frac{K_{a2}}{[\text{H}^+]} \right)^{-1} C_{\text{sulfite}} + 2 \left(\frac{[\text{H}^+]^2}{K_{a1}K_{a2}} + \frac{[\text{H}^+]}{K_{a2}} + 1 \right)^{-1} C_{\text{sulfite}}$$

Eq. 4-26

where

$$K_w = 10^{(-4471/T + 6.0875 - 0.01706 * T)} = 1.00061 * 10^{-14} \quad @298\text{K} [71]$$

T = water temperature, K

The pH value of liquid can be found by solving $[H^+]$ from the above equation. On the other hand, by measuring the pH of water, total sulfite concentration can be found.

$$C_{\text{sulfite}} = \frac{\left([H^+] - [H^+]_{\text{initial}} \right) - \left(\frac{K_w}{[H^+]} - \frac{K_w}{[H^+]_{\text{initial}}} \right)}{\alpha_1 + 2\alpha_2} \quad \text{Eq. 4-27}$$

With the present of H_2SO_4 , The electro-neutrality equation is:

$$\left([H^+] - [H^+]_{\text{initial}} \right) = \left([OH^-] - [OH^-]_{\text{initial}} \right) + [HSO_3^-] + 2[SO_3^{2-}] + 2[SO_4^{2-}] \quad \text{Eq. 4-28}$$

$$[H^+] - [H^+]_{\text{initial}} = \left(\frac{K_w}{[H^+]} - \frac{K_w}{[H^+]_{\text{initial}}} \right) + \alpha_1 C_{\text{sulfite}} + 2\alpha_2 C_{\text{sulfite}} + 2C_{\text{sulfate}} \quad \text{Eq. 4-29}$$

4.4 Chemistry of NOx

4.4.1 Henry's law

Henry's law describes the equilibrium of NO_x /water system:

$$P_{NOx} = H [NO_x (aq)] \quad \text{Eq. 4-30}$$

where H is the Henry's law constant for NO or NO_2 (cm^3 -atm/mol).

The Henry's law constant of NO and NO_2 to water are 525,000 and 100,000 cm^3 -atm/mol, respectively, at room temperature [59]. The solubility of NO and NO_2 in water are 0.063 g/L and 1.26 g/L, respectively [3].

4.4.2 Gas Phase Reactions of Nitrogen Oxides

The oxidation of NO to NO₂ in the gas phase occurs in the presence of O₂.



Reaction rate constant: $\log k = 652.1/T - 0.7356 \text{ kN/m}^2$ [28,57,73]; $k = 1.4 \cdot 10^{-38} \text{ cm}^6/\text{sec}$ @298K [36]

Reverse reaction rate constant: $\log k = 12.6 - 5878/T = 0.17 \text{ cm}^3/\text{mol-sec}$ @300K [35]



Reaction rate constant: $\log k = 12.23 - (1018/T) = 8.83 \text{ cm}^3/\text{mol-sec}$ @300K [35]

Without the presence of water vapor, several NO₂ reactions may occur in the gas phase.



Equilibrium constant: $\log K = 2993/T - 9.226$; $K = 6.57 \text{ kN/m}^2$ @298K [57]

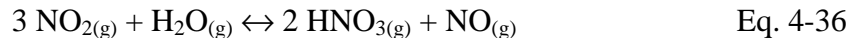


Equilibrium constant: $\log K = 2072/T - 7.234$; $K = 0.52 \text{ kN/m}^2$ @298K [57]

With the presence of water vapor or oxygen, the formation reaction of nitric acid in the gas phase might take place in the gas phase.



Equilibrium constant: $\log K = 2051.17/T - 6.7328$; $K = 1.41 \text{ kN/m}^2$ @298K [57]



Equilibrium constant: $\log K = 2003.8/T - 8.757$; $K = 9.272 \cdot 10^{-3} \text{ kN/m}^2$ @298K [57]



[28]

Some reactions lead to the formation of NO₃ gas and the following formation of N₂O₅ gas in the gas phase. Both NO₃ and N₂O₅ gases are very soluble.



[35]



Where M: particle [29]

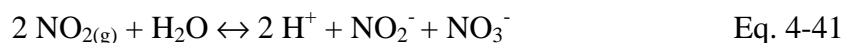
Reaction rate constant: $k = 6.6 \cdot 10^{11} \text{ cm}^3/\text{mol}\cdot\text{sec}$ @298K [36] ;
 Reverse reaction rate constant: $k = 73 \text{ sec}^{-1}$ @298K [36]



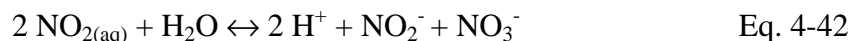
Reaction rate constant $k = 5 \cdot 10^{-21} \text{ cm}^3/\text{sec}$ @298K [36, 74]

4.4.3 Removal of Nitrogen Oxides

NO_2 forms nitrite and nitrate ions when absorbed in water. The equivalent amounts of NO_2^- and NO_3^- ions exist in the solution due to the dissolution of NO_2 [57].

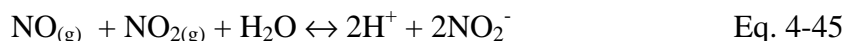
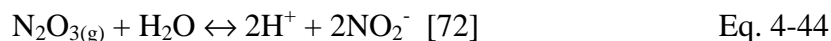


Equilibrium constant: $K = 244 \text{ M}^4/\text{atm}^2$ @298K [20, 28, 59, 72]



Equilibrium constant: $K = 2.44 \cdot 10^6 \text{ M}^2$ @298K

Other forms of NO_x are easily dissolved into water as well, especially into a basic solution [57, 72].



Equilibrium constant: $K = 3.28 \cdot 10^{-5} \text{ M}^4/\text{atm}^2$ @298K [59]



Equilibrium constant $\log K = -3.15$ @298K [28, 57, 71, 72]



Equilibrium constant $\log K = 1$ @298K [57, 71, 72]

However, HNO_2 is a weak acid and easily to decompose to NO and NO_2 gases if there is no basic species in the solution [57].



Combining the most possible reactions Eq. 4-41 and Eq. 4-48, the net reaction of NO_2 removal is:



This most possible reaction paths of NO_x removal are illustrated in Figure 4.5. When NO_2 dissolves into water, it is possible for one-third of the nitric oxide to separate and return to the gas phase, somewhat impairing the efficiency of NO_x removal [28].

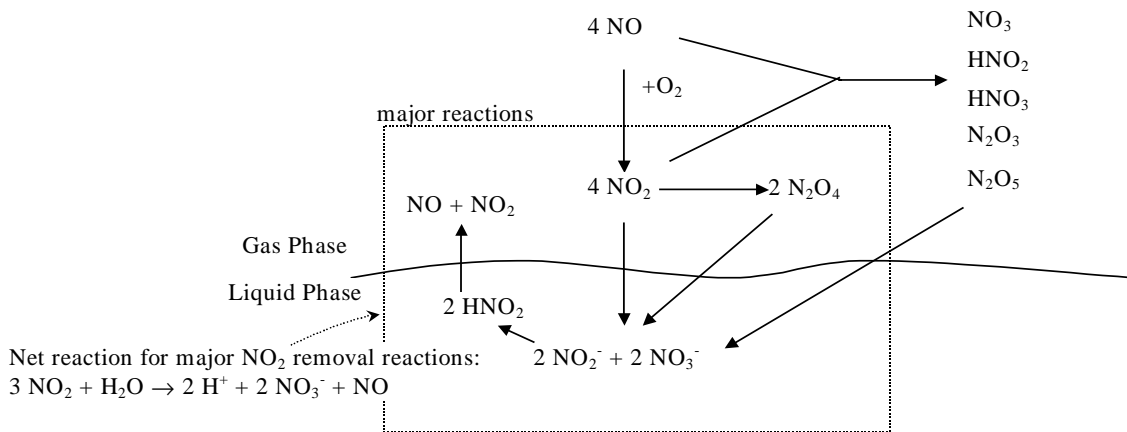


Figure 4.5 Most Possible Reaction Paths of NO_x Removal

4.5 Equilibrium State N-CSTR Model of wESP

The absorption of SO_2 into water involves physical absorption and hydrolysis reactions. In every SO_2 -water application, there is an equilibrium that dictates the maximum (saturated) amount of SO_2 that may be displaced from the gas into the water due to absorption. Henry's law describes the equilibrium concentrations at the gas-liquid interface. A major research goal was

to determine whether the SO₂-water equilibrium could be reached in the short gas-liquid contact time (< 5 sec) available in the wESP, and whether the electrostatic field had any effect on the equilibrium level.

The Equilibrium State N-CSTR model estimates the maximum natural SO₂ removal after the simple physical absorption and hydrolysis reactions by assuming that wESP system is at the SO₂-water equilibrium state. In the n-CSTR model, it is assumed that the system acts as several completely stirred tank reactors (CSTR) in series.

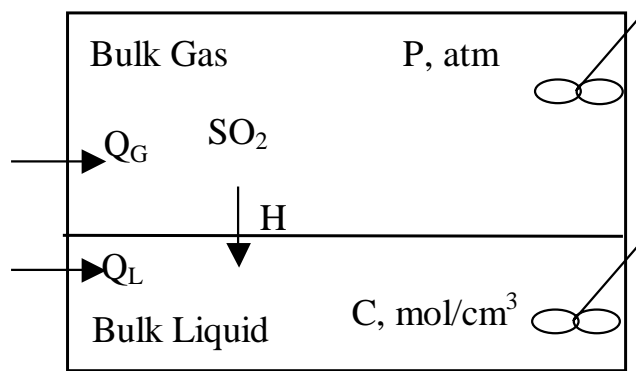


Figure 4.6 The Equilibrium State N-CSTR model

It is assumed that the SO₂ and water are at equilibrium, the mass balance of SO₂ can be derived for completely mixed gas and liquid phases:

SO₂ Mass balance: initial SO₂ (liquid phase SO₂ + gas phase SO₂) = Total SO₂ after reaching equilibrium

$$0 + \frac{\rho_{\text{SO}_2} \left(Q_G \frac{P_{\text{in}}}{P_T} \right)}{M_{\text{W}_{\text{SO}_2}}} = Q_L C_{\text{Sulfite}} + \frac{\rho_{\text{SO}_2} \left(Q_G \frac{P}{P_T} \right)}{M_{\text{W}_{\text{SO}_2}}} \quad \text{Eq. 4-50}$$

with equilibrium condition between gas/liquid phases

$$P = H C_{\text{H}_2\text{SO}_3} \quad \text{Eq. 4-51}$$

where:

H = Henry's law constant

C = H₂SO₃ or sulfite concentration in the liquid phase, mol/cm³

ρ_{SO₂} = density of SO₂ = 2.811*10⁻³ g/cm³ @ 25°C

P_{in} = inlet SO₂ gas partial pressure, atm

P = reactor and outlet SO₂ gas partial pressure, atm

P_T = inlet total gas pressure = 1 atm

Q_G = gas volumetric flow rate, cm³/sec

Q_L = water volumetric flow rate, cm³/sec

M_{w SO₂} = molecular weight of SO₂, g/mole

$$C_{\text{sulfite}} = \alpha_0^{-1} C_{\text{H}_2\text{SO}_3} \quad \text{where } \alpha_0 = \left(1 + \frac{K_{a1}}{[\text{H}^+]} + \frac{K_{a1}K_{a2}}{[\text{H}^+]^2} \right)^{-1}$$

SO₂ gas partial pressure is solved as:

$$P = \left(\frac{H \rho_{\text{SO}_2} Q_G}{\alpha_0^{-1} Q_L M_{w \text{SO}_2} P_T + H \rho_{\text{SO}_2} Q_G} \right) P_{\text{in}} \quad \text{Eq. 4-52}$$

Therefore, the SO₂ removal efficiency at the equilibrium state, η_{EQ}, for one CSTR is:

$$\eta_{\text{EQ}} = \frac{P_{\text{in}} - P}{P_{\text{in}}} = \left(1 + \frac{\alpha_0 H \cdot \rho_{\text{SO}_2} Q_G}{Q_L M_{w \text{SO}_2} P_T} \right)^{-1} = (1 - a)^{-1} \quad \text{Eq. 4-53}$$

$$\text{where } a = \frac{\alpha_0 H \cdot \rho_{\text{SO}_2} Q_G}{Q_L M_{w \text{SO}_2} P_T}$$

An actual wESP system acts somewhere between an ideal CSTR and a plug flow reactor (PFR). The overall removal efficiency at equilibrium can be expressed as a series of several CSTRs by replacing Q_L with Q_L/n as follows:

$$\begin{aligned}\eta_{\text{overall}} &= 1 - (1 - \eta_{\text{EQ}})^n \\ &= 1 - \left(1 - \frac{1}{1 + na}\right)^n\end{aligned}\tag{Eq. 4-54}$$

where n is the number of CSTR tanks in series.

From this equilibrium model, the maximum overall SO_2 removal efficiency at the equilibrium state can be predicted and compared to the experimental removal efficiency. The number of tanks, n , is between 1 and infinity. As number n approaches infinity, the wESP system acts like a PFR.

Since this removal efficiency is due to water absorption only, which is the primary removal mechanism in the traditional wet scrubbing systems, it takes very long time for system to reach the equilibrium state, and the system does not approach this predicted removal under general scrubbing conditions without any other enhancement such as high voltage corona. All the electrostatic experimental results of wESP tests were compared with the equilibrium removal efficiency to evaluate the electrostatic effect. Both CSTR and PFR modeling results of SO_2 removal are presented in the figures of this research.

4.6 Electrostatics Enhanced Mass Transfer N-CSTR Model of wESP

Electrostatics Enhanced Mass Transfer model estimates the actual SO_2 removal in a wESP by using mass transfer coefficient (K_{OG}). In this model, wESP system is considered as several complete mixed tanks in series (n -CSTR) with the SO_2 mass transfer from the gas phase

into the liquid phase. Electrostatic enhancement factors are used to account for the influence of electrostatics on the mass transfer coefficients.

The actual flux of SO_2 mass transfer across gas-liquid interface at steady state in a wESP can be predicted in terms of the overall mass transfer coefficient (K_{OG}) as shown in Figure 4.7.

$$N_{\text{SO}_2} = K_{OG} (P_{\text{SO}_2,b} - H_{\text{SO}_2} C_{\text{H}_2\text{SO}_3,b}) \quad \text{Eq. 4-55}$$

where

N = Flux through the gas-liquid interface, $\text{mol}/\text{sec}\cdot\text{cm}^2$

P = SO_2 partial pressure in the bulk gas, atm

C = H_2SO_3 or $\text{SO}_{2(\text{aq})}$ concentration in the bulk liquid, mol/cm^3

K_{OG} = The overall gas side mass transfer coefficient, $\text{mol}/\text{sec}\cdot\text{cm}^2\cdot\text{atm}$; K_{OG} is a function of operational conditions (power, polarity, ..)

H_{SO_2} = The Henry's Law Constant for $\text{SO}_2/\text{H}_2\text{SO}_3$ system. $H_{\text{SO}_2} = 0.80 \text{ atm}/\text{M}$ at 25°C [59]

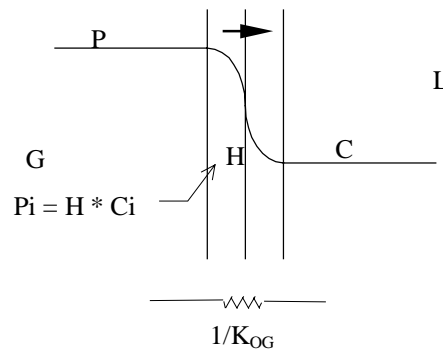


Figure 4.7 Gas-liquid Interface Mass Transfer

It is assumed that both gas and liquid phases are well mixed. No oxidation of SO_2 occurs. Ideal gas law is applicable. Consider the mass balance of SO_2 in the gas and the liquid phases in one continuous stirred tank reactor (CSTR) as shown in Figure 4.8.

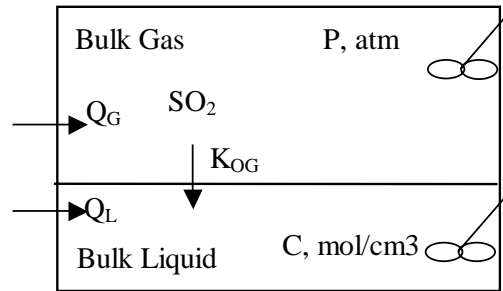


Figure 4.8 One CSTR in Electrostatics Enhanced Mass Transfer N-CSTR Model

The gas phase: SO_2 in (mole/sec) = SO_2 transferred to liquid + SO_2 out

$$Q_G \frac{P_{\text{in}}}{RT} = A \cdot K_{\text{OG}} (P - H C_{\text{H}_2\text{SO}_3}) + Q_G \frac{P}{RT} \quad \text{Eq. 4-56}$$

The liquid phase: SO_2 transferred to liquid = total sulfite compounds out, input sulfite is always zero since fresh water is used.

$$A \cdot K_{\text{OG}} (P - H C_{\text{H}_2\text{SO}_3}) = Q_L C_{\text{sulfite}} \quad \text{Eq. 4-57}$$

where:

P_{in} = Inlet SO_2 gas partial pressure, atm

P_T = Inlet gas total pressure = 1 atm

Q_G = Gas volumetric flow rate, cm^3/sec

Q_L = Water volumetric flow rate, cm^3/sec

A = Gas-liquid interface area, cm^2

R = Universal gas constant = $82.054 \text{ cm}^3\text{-atm/mol-K}$

$$C_{\text{sulfite}} = \alpha_0^{-1} C_{\text{H}_2\text{SO}_3} \quad \text{where } \alpha_0 = \left(1 + \frac{K_{a1}}{[\text{H}^+]} + \frac{K_{a1}K_{a2}}{[\text{H}^+]^2} \right)^{-1}$$

SO_2 partial pressure "P" in gas and sulfite concentration "C" in water are solved.

$$P = \frac{Q_G (AHK_{OG} + \alpha_0^{-1} Q_L) P_{in}}{AK_{OG} \alpha_0^{-1} Q_L RT + Q_G (AHK_{OG} + \alpha_0^{-1} Q_L)} = \frac{P_{in}}{1 + \frac{RT}{Q_G \left(\frac{\alpha_0 H}{Q_L} + \frac{1}{AK_{OG}} \right)}} \quad \text{Eq. 4-58}$$

$$C = \frac{Q_G AK_{OG} P_{in}}{AK_{OG} \alpha_0^{-1} Q_L RT + Q_G (AHK_{OG} + \alpha_0^{-1} Q_L)} = \frac{P_{in}}{H + \alpha_0^{-1} Q_L \left(\frac{RT}{Q_G} + \frac{1}{AK_{OG}} \right)} \quad \text{Eq. 4-59}$$

The removal efficiency is determined by the inlet and outlet SO₂ partial pressures.

$$\eta = 1 - \frac{P}{P_{in}} = \frac{AK_{OG} \alpha_0^{-1} Q_L RT}{AK_{OG} \alpha_0^{-1} Q_L RT + Q_G (AHK_{OG} + \alpha_0^{-1} Q_L)} \quad \text{Eq. 4-60}$$

After simplification:

$$\eta = \left[1 + \frac{Q_G}{RT} \left(\frac{\alpha_0 H}{Q_L} + \frac{1}{AK_{OG}} \right) \right]^{-1} = \frac{1}{1 + a} \quad \text{Eq. 4-61}$$

where

$$a \equiv \frac{Q_G}{RT} \left(\frac{\alpha_0 H}{Q_L} + \frac{1}{AK_{OG}} \right)$$

In n-CSTR model, the system behaves as n CSTRs in series. By replacing A and Q_L with A/n and Q_L/n, the overall removal efficiency is:

$$\begin{aligned} \eta_{\text{overall}} &= 1 - (1 - \eta)^n \\ &= 1 - \left(1 - \frac{1}{1 + na} \right)^n \end{aligned} \quad \text{Eq. 4-62}$$

This model establishes the relationship between the overall removal efficiency of the wESP and the overall mass transfer coefficient. The modeling results are shown in section 5.1.2.

4.7 Thin Film Mass Transfer Theory of SO₂ Absorption

The enhancements of SO₂ absorption by chemical reactions and electrostatic effects are modeled in the batch reactor by using the two thin films mass transfer theory. Mass transfer coefficients as well as the electrostatic enhancement factors are studied to describe the SO₂ mass transfer under corona discharge.

4.7.1 Determination of Overall Mass Transfer Coefficient K_{OG}

Consider the mass transfer of SO₂ from the gas to the liquid phase at unsteady state in the batch reactor as shown in the following figure.

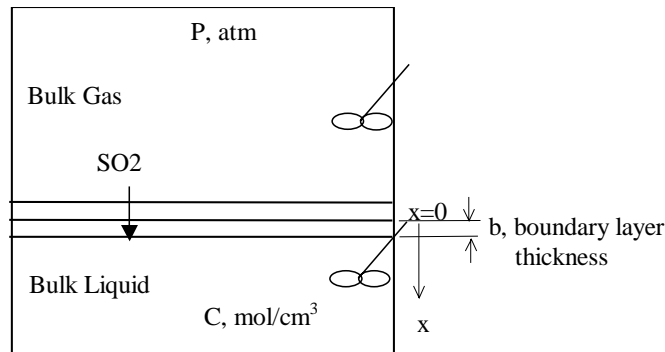


Figure 4.9 Thin Film Mass Transfer Theory in the Batch Reactor

The SO₂ flux at certain time can be expressed by the overall gas-side mass transfer coefficient K_{OG}:

$$N_{SO_2} = K_{OG} (P_{SO_2,b} - H_{SO_2} C_{H_2SO_3,b}) \quad \text{Eq. 4-63}$$

where

$N =$ Flux through the gas-liquid interface, mol/sec-cm²

$P_b =$ SO₂ partial pressure in the bulk gas, atm

$C_b =$ H₂SO₃ or SO_{2(aq)} concentration in the bulk liquid, mol/cm³

$K_{OG} =$ The overall gas side mass transfer coefficient, mol/sec-cm²-atm;

K_{OG} is system specific and vary with electrostatic conditions (power, polarity, ..)

$H_{SO_2} =$ The Henry's law constant for SO₂/H₂SO₃ system. $H_{SO_2} = 0.8$ atm/M at 25°C [59]

SO₂ partial pressure is continuously measured during a test. In order to solve mass transfer coefficient, K_{OG} , SO₂ flux and H₂SO₃ concentration has to be calculated. SO₂ flux, N , is obtained experimentally from the slope in Figure 4.10:

$$N_{SO_2} = \frac{dP}{RTdt} \frac{V_G}{A} \quad \text{Eq. 4-64}$$

where

$R =$ Universal gas constant = 82.054 cm³-atm/mol-K

$T =$ Temperature, K

$V_G =$ Volume of gas chamber, cm³

$A =$ Gas-liquid interface area, cm²

The flux at any time within the initial 10 minutes is almost unchanged. Therefore, an average flux is obtained between 3 and 9 minutes and represents the flux within the first 10 minutes.

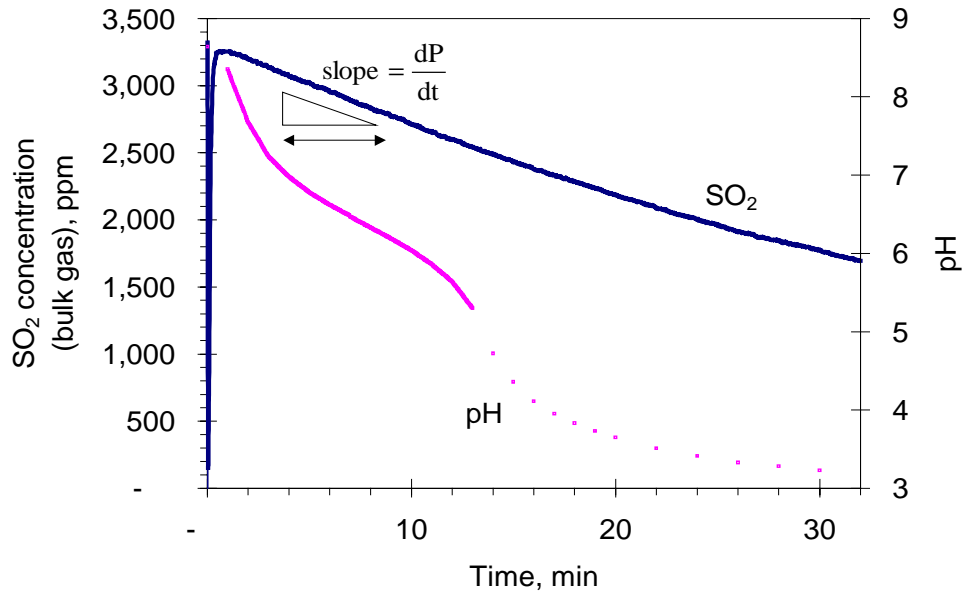


Figure 4.10 Typical Result of a Batch Reactor Test

Batch reactor test condition: 3320 ppm SO₂ in pure N₂, tap water, no corona discharge, room temp.

Following assumptions are made in order to get the bulk H₂SO₃ concentration: the bulk gas and bulk liquid are well mixed except in the two thin films near the gas-liquid interface. No oxidation of SO₂ occurs. By assuming the mass of sulfur in the two thin films is negligible, the total mass of sulfur removed from the bulk gas is completely mixed in the bulk liquid. Therefore, the total sulfite concentration in the bulk liquid at certain time is:

$$[\text{sulfite}]_b = \frac{(P_b - P_{0,b})V_G}{RTV_L} \quad \text{Eq. 4-65}$$

where

[sulfite]_b = Total sulfite concentration in the bulk liquid, mol/cm³

P_{0,b} = Initial SO₂ partial pressure in the bulk gas, atm

V_L = Volume of liquid chamber, cm³

From the discussion of SO₂ dissociation at section 4.3.3, the H₂SO₃ concentration, as well as other sulfite compounds in the bulk liquid, can be obtained from the total sulfite concentration by monitoring the bulk liquid pH:

$$[\text{H}_2\text{SO}_3]_b = \alpha_0 * [\text{sulfite}]_b \quad \text{Eq. 4-66}$$

where $\alpha_0 = \left(1 + \frac{K_{a1}}{[\text{H}^+]} + \frac{K_{a1}K_{a2}}{[\text{H}^+]^2} \right)^{-1}$; $C_{\text{sulfite}} = \alpha_0^{-1} C_{\text{H}_2\text{SO}_3}$

Thus, according to the definition at Eq. 4-63, the overall mass transfer coefficient, K_{OG}, can be obtained from the slope of (P_{SO₂,b} - H_{SO₂}C_{H₂SO₃,b}) vs. flux N. Results of overall mass transfer coefficient, K_{OG}, are summarized at Table 7.1 and Figure 7.7.

4.7.2 Mass Transfer Modeling at Gas Phase Boundary Layer

The SO₂ flux can be expressed by the gas-side mass transfer coefficient k_g:

$$N_{\text{SO}_2} = k_g (P_{\text{SO}_2,b} - P_{\text{SO}_2,i}) \quad \text{Eq. 4-67}$$

where

k_g = Gas side mass transfer coefficient (mol/sec-cm²-atm)

P_b = SO₂ partial pressure in the bulk gas (atm)

P_i = SO₂ partial pressure at the interface (atm)

By knowing k_g, the interface SO₂ partial pressure can be calculated:

$$P_{\text{SO}_2,i} = P_{\text{SO}_2,b} - \frac{N_{\text{SO}_2}}{k_g} \quad \text{Eq. 4-68}$$

as well as the interface H₂SO₃ (or SO_{2(aq)}) concentration:

$$[\text{H}_2\text{SO}_3]_i = \frac{P_{\text{SO}_2,i}}{H_{\text{SO}_2}} \quad \text{Eq. 4-69}$$

where H_{SO_2} is the Henry's Law Constant for $\text{SO}_2/\text{H}_2\text{SO}_3$ system.

4.7.3 Mass Transfer Modeling at Liquid Phase Boundary Layer

Considering SO_2 dissociation at the liquid boundary layer (Figure 4.9), the differential equations describing the diffusion of all species in the liquid phase, based on film theory and total material balance can be written as follows [75].

Material balance of all sulfite compounds:

$$D_{\text{H}_2\text{SO}_3} \frac{d^2[\text{H}_2\text{SO}_3]}{dx^2} + D_{\text{HSO}_3^-} \frac{d^2[\text{HSO}_3^-]}{dx^2} + D_{\text{SO}_3^{2-}} \frac{d^2[\text{SO}_3^{2-}]}{dx^2} = 0 \quad \text{Eq. 4-70}$$

where D_i is the diffusivity of compound i in water at 25°C (cm^2/sec) [Table 10.9, 75, 76]

Charge balance (electro-neutrality condition):

$$D_{\text{H}^+} \frac{d^2[\text{H}^+]}{dx^2} - D_{\text{HSO}_3^-} \frac{d^2[\text{HSO}_3^-]}{dx^2} - 2D_{\text{SO}_3^{2-}} \frac{d^2[\text{SO}_3^{2-}]}{dx^2} - D_{\text{OH}^-} \frac{d^2[\text{OH}^-]}{dx^2} = 0 \quad \text{Eq. 4-71}$$

By integrating the above two ordinary differential equations, the general solutions of the above film theory material balance equations are solved as follows:

$$D_{\text{H}_2\text{SO}_3} [\text{H}_2\text{SO}_3] + D_{\text{HSO}_3^-} [\text{HSO}_3^-] + D_{\text{SO}_3^{2-}} [\text{SO}_3^{2-}] = a_1 x + a_2 \quad \text{Eq. 4-72}$$

$$D_{\text{H}^+} [\text{H}^+] - D_{\text{HSO}_3^-} [\text{HSO}_3^-] - 2D_{\text{SO}_3^{2-}} [\text{SO}_3^{2-}] - D_{\text{OH}^-} [\text{OH}^-] = a_3 x + a_4 \quad \text{Eq. 4-73}$$

The boundary conditions for these equations are:

At the gas-liquid interface, $x = 0$,

$$[\text{H}_2\text{SO}_3] = [\text{H}_2\text{SO}_3]_i; [\text{HSO}_3^-] = [\text{HSO}_3^-]_i; [\text{SO}_3^{2-}] = [\text{SO}_3^{2-}]_i; [\text{H}^+] = [\text{H}^+]_i \quad \text{Eq. 4-74}$$

$$D_{\text{H}^+} \frac{d[\text{H}^+]}{dx} - D_{\text{HSO}_3^-} \frac{d[\text{HSO}_3^-]}{dx} - 2D_{\text{SO}_3^{2-}} \frac{d[\text{SO}_3^{2-}]}{dx} - D_{\text{OH}^-} \frac{d[\text{OH}^-]}{dx} = 0 \quad \text{Eq. 4-75}$$

At the liquid film-bulk phase boundary layer, $x = b$,

$$[\text{H}_2\text{SO}_3] = [\text{H}_2\text{SO}_3]_b; [\text{HSO}_3^-] = [\text{HSO}_3^-]_b; [\text{SO}_3^{2-}] = [\text{SO}_3^{2-}]_b; [\text{H}^+] = [\text{H}^+]_b \quad \text{Eq. 4-76}$$

where

b = Liquid boundary layer thickness (cm)

Enhancement Factor due to Chemical Dissociation

Put boundary conditions Eq. 4-74 and Eq. 4-76 into the first general solution Eq. 4-72:

at $x = 0$

$$D_{\text{H}_2\text{SO}_3} [\text{H}_2\text{SO}_3]_i + D_{\text{HSO}_3^-} [\text{HSO}_3^-]_i + D_{\text{SO}_3^{2-}} [\text{SO}_3^{2-}]_i = a_2 \quad \text{Eq. 4-77}$$

at $x = b$

$$D_{\text{H}_2\text{SO}_3} [\text{H}_2\text{SO}_3]_b + D_{\text{HSO}_3^-} [\text{HSO}_3^-]_b + D_{\text{SO}_3^{2-}} [\text{SO}_3^{2-}]_b = a_1 b + a_2 \quad \text{Eq. 4-78}$$

After solving coefficients a_1 and a_2 , Eq. 4-72 becomes:

$$\begin{aligned} & D_{\text{H}_2\text{SO}_3} [\text{H}_2\text{SO}_3] + D_{\text{HSO}_3^-} [\text{HSO}_3^-] + D_{\text{SO}_3^{2-}} [\text{SO}_3^{2-}] \\ &= \left(D_{\text{H}_2\text{SO}_3} [\text{H}_2\text{SO}_3]_b + D_{\text{HSO}_3^-} [\text{HSO}_3^-]_b + D_{\text{SO}_3^{2-}} [\text{SO}_3^{2-}]_b - D_{\text{H}_2\text{SO}_3} [\text{H}_2\text{SO}_3]_i - D_{\text{HSO}_3^-} [\text{HSO}_3^-]_i - D_{\text{SO}_3^{2-}} [\text{SO}_3^{2-}]_i \right) \frac{x}{b} \\ &+ \left(D_{\text{H}_2\text{SO}_3} [\text{H}_2\text{SO}_3]_b + D_{\text{HSO}_3^-} [\text{HSO}_3^-]_b + D_{\text{SO}_3^{2-}} [\text{SO}_3^{2-}]_b \right) \end{aligned} \quad \text{Eq. 4-79}$$

The flux of H_2SO_3 (excluding the chemical dissociation)[75, 77] is given by

$$N_{SO_2}^o = k_1^o ([H_2SO_3]_i - [H_2SO_3]_b)$$

$$k_1^o = \frac{D_{H_2SO_3}}{b}$$
Eq. 4-80

where

k_1^o = Liquid side mass transfer coefficient excluding the chemical dissociation

The rate of absorption of SO_2 including the chemical dissociation is given by

$$N_{SO_2} = \phi_c k_1^o ([H_2SO_3]_i - [H_2SO_3]_b)$$
Eq. 4-81

where

ϕ_c = Enhancement factor due to the chemical dissociation of H_2SO_3 (dimensionless)

The absorption rate, N_{SO_2} , is also equal to the first differential of negative Eq. 4-79:

$$N_{SO_2} = - \left(D_{H_2SO_3} \frac{d[H_2SO_3]}{dx} + D_{HSO_3^-} \frac{d[HSO_3^-]}{dx} + D_{SO_3^{2-}} \frac{d[SO_3^{2-}]}{dx} \right)$$

$$= \frac{1}{b} \left(D_{H_2SO_3} [H_2SO_3]_i + D_{HSO_3^-} [HSO_3^-]_i + D_{SO_3^{2-}} [SO_3^{2-}]_i - D_{H_2SO_3} [H_2SO_3]_b - D_{HSO_3^-} [HSO_3^-]_b - D_{SO_3^{2-}} [SO_3^{2-}]_b \right)$$

From Eq. 4-80 and Eq. 4-81, the dissociation enhancement factor, ϕ_c , of the film theory is

solved as:

$$\phi_c = \frac{N_{SO_2}}{N_{SO_2}^o}$$

$$= \frac{D_{H_2SO_3} [H_2SO_3]_i + D_{HSO_3^-} [HSO_3^-]_i + D_{SO_3^{2-}} [SO_3^{2-}]_i - D_{H_2SO_3} [H_2SO_3]_b - D_{HSO_3^-} [HSO_3^-]_b - D_{SO_3^{2-}} [SO_3^{2-}]_b}{D_{H_2SO_3} ([H_2SO_3]_i - [H_2SO_3]_b)}$$

$$\phi_c = 1 + \left(\frac{D_{HSO_3^-}}{D_{H_2SO_3}} \right) \left(\frac{[HSO_3^-]_i - [HSO_3^-]_b}{[H_2SO_3]_i - [H_2SO_3]_b} \right) + \left(\frac{D_{SO_3^{2-}}}{D_{H_2SO_3}} \right) \left(\frac{[SO_3^{2-}]_i - [SO_3^{2-}]_b}{[H_2SO_3]_i - [H_2SO_3]_b} \right)$$
Eq. 4-82

Proton Concentration at the Interface

Considering the second general solution Eq. 4-73 and the boundary condition Eq. 4-75, it is determined that:

$$a_3 = 0 \quad \text{Eq. 4-83}$$

and

$$\begin{aligned} & D_{\text{H}^+} [\text{H}^+]_i - D_{\text{HSO}_3^-} [\text{HSO}_3^-]_i - 2D_{\text{SO}_3^{2-}} [\text{SO}_3^{2-}]_i - D_{\text{OH}^-} [\text{OH}^-]_i \\ & = D_{\text{H}^+} [\text{H}^+]_b - D_{\text{HSO}_3^-} [\text{HSO}_3^-]_b - 2D_{\text{SO}_3^{2-}} [\text{SO}_3^{2-}]_b - D_{\text{OH}^-} [\text{OH}^-]_b \end{aligned} \quad \text{Eq. 4-84}$$

The concentrations of other sulfite compounds can be expressed in terms of H_2SO_3 and H^+ concentrations at the interface.

$$\begin{aligned} [\text{HSO}_3^-]_i &= K_{a1} \frac{[\text{H}_2\text{SO}_3]_i}{[\text{H}^+]_i} \\ [\text{SO}_3^{2-}]_i &= K_{a1} K_{a2} \frac{[\text{H}_2\text{SO}_3]_i}{[\text{H}^+]_i^2} \end{aligned} \quad \text{Eq. 4-85}$$

Replace the concentrations of Eq. 4-84 with Eq. 4-85 and rearrange the equation with respect to $[\text{H}^+]_i$:

$$\begin{aligned} & D_{\text{H}^+} [\text{H}^+]_i^3 + \left(D_{\text{HSO}_3^-} [\text{HSO}_3^-]_b - D_{\text{H}^+} [\text{H}^+]_b + 2D_{\text{SO}_3^{2-}} [\text{SO}_3^{2-}]_b + D_{\text{OH}^-} [\text{OH}^-]_b \right) [\text{H}^+]_i^2 \\ & - \left(D_{\text{HSO}_3^-} K_{a1} [\text{H}_2\text{SO}_3]_i + D_{\text{OH}^-} K_w \right) [\text{H}^+]_i - 2D_{\text{SO}_3^{2-}} K_{a1} K_{a2} [\text{H}_2\text{SO}_3]_i = 0 \end{aligned} \quad \text{Eq. 4-86}$$

Therefore, the value $[\text{H}^+]_i$, can be obtained by knowing the bulk phase concentrations and $[\text{H}_2\text{SO}_3]_i$.

4.7.4 Determination of Local Mass Transfer Coefficients and Dissociation Enhancement Factor

The K_{OG} are consisted of the local mass transfer coefficients in both the gas phase and the liquid phase.

$$\frac{1}{K_{OG}} = \frac{1}{k_g} + \frac{H}{k_l} \quad \text{Eq. 4-87}$$

$$k_l = \phi_c k_l^o \quad \text{Eq. 4-88}$$

where

k_g = Gas side mass transfer coefficient (mol/sec-cm²-atm)

k_l = Liquid side mass transfer coefficient (cm/sec)

k_l^o = Liquid side mass transfer coefficient excluding the chemical dissociation (cm/sec)

ϕ_c = Enhancement factor due to chemical dissociation (dimensionless), defined by Eq. 4-81

In order to determine the value of k_l and ϕ_c experimentally, SO₂ absorption was studied into pure water and into high-pH (NaOH) solution. These trials were conducted under the same experimental condition as the non-alkalinity tests that were compared to.

In the tests with NaOH solution, dissolved SO₂ reacts instantaneously and irreversibly with a large excess of reactant at the gas-liquid interface. The pH value remained around 13.4 throughout the testing period. Therefore, the any mass transfer resistance in the liquid phase is considered to be negligible ($H/k_l = 0$) as illustrated in Figure 4.11 [75, 77]. The overall mass transfer coefficient calculated from the NaOH tests is equal to the gas side mass transfer coefficient.

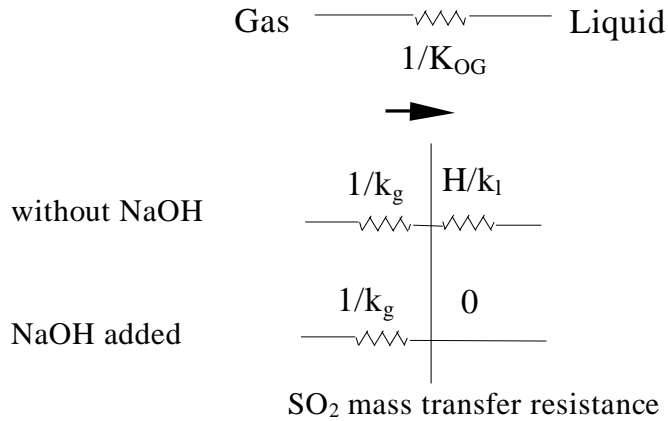


Figure 4.11 Removal of the Liquid Side Mass Transfer Resistance

Each set of non-corona batch tests consists of two tests at the same conditions except one in pure water and the other in NaOH solution. Determination is based on the liquid side mass transfer coefficient excluding the dissociation, k_1^o , is the same for both tests because all the effect of chemical dissociation is included in enhancement factor ϕ_c . The calculation procedures are listed as the following steps and summarized at Table 4.2:

1. Calculate the SO₂ absorption flux of both tests by Eq. 4-64.
2. Calculate the total sulfite concentration in the bulk liquid of both tests by Eq. 4-65.
3. Calculate the concentrations of all sulfite compounds of both tests by Eq. 4-66.
4. Determine the K_{OG} of both tests by using the method in section 4.7.1.
5. Assume that the k_g of pure water test is equal to the K_{OG} of NaOH test.
6. Obtain the k_1 of pure water test from Eq. 4-87.
7. Calculate the interface SO₂ partial pressure of pure water test from k_g by Eq. 4-68.
8. Calculate the interface H₂SO₃ concentration of pure water test by Eq. 4-69.
9. Solve the interface $[H^+]_i$ concentration of pure water test by Eq. 4-86.

10. Solve the interface $[\text{HSO}_3^-]_i$ and $[\text{SO}_3^{2-}]_i$ concentrations of pure water test by Eq. 4-85.
Then the total sulfite concentration in the bulk liquid of pure water test can be obtained.
11. Solve the chemical dissociation enhancement factor, ϕ_c , of pure water test from Eq. 4-82.
12. Calculate the k_l^o of pure water test by Eq. 4-88.
13. This k_l^o is the same as of NaOH test because all the effect of chemical dissociation is included in enhancement factor ϕ_c .
14. Since the liquid side mass transfer resistance is negligible, assume the k_g of NaOH test is equal to the K_{OG} of NaOH test as a starting value.
15. Repeat step 7 to 13 of NaOH test and solve all the bulk and interface concentrations to obtain enhancement factor ϕ_c of NaOH test.
16. Calculate the k_l of NaOH test by Eq. 4-88.
17. Calculate the new k_g value of NaOH test by Eq. 4-87. Check this value with the previous assumed k_g value at step 14. If the difference is unacceptable ($> 0.1\%$), go back to step 14. Replace the previous assumed k_g value with the new k_g value and repeat step 15 to 17. If the difference is acceptable ($< 0.1\%$), go to next step.
18. Check the newly solved k_g value of NaOH test with the previous assumed k_g of pure water test. They should be the same because the gas conditions are the same. If the difference is unacceptable ($> 0.1\%$), go back to step 5. Replace the previous assumed k_g value with the new k_g value and repeat step 6 to 18. If the difference is acceptable ($< 0.1\%$), this process ends.

Table 4.2 Summary of the Calculation of Thin Film Mass Transfer Theory

Test	N_{SO_2}	K_{OG}	kg	k_l	k_l^o	ϕ_c
Pure water	1, Eq. 4-64	4, Sec. 4.7.1	5, 18	6, Eq. 4-87	12, Eq. 4-88	11, Eq. 4-82
NaOH solution	1, Eq. 4-64	4, Sec. 4.7.1	14, 17	16, Eq. 4-88	13	15, Eq. 4-82
	$P_{SO_2,b}$	$[H^+]_b$	[sulfite] _b	$[H_2SO_3]_b$	$[HSO_3^-]_b$	$[SO_3^{2-}]_b$
Pure water	Measured	Measured	2, Eq. 4-65	3, Eq. 4-66	3, Eq. 4-66	3, Eq. 4-66
NaOH solution	Measured	Measured	2, Eq. 4-65	3, Eq. 4-66	3, Eq. 4-66	3, Eq. 4-66
	$P_{SO_2,i}$	$[H^+]_i$	[sulfite] _i	$[H_2SO_3]_i$	$[HSO_3^-]_i$	$[SO_3^{2-}]_i$
Pure water	7, Eq. 4-68	9, Eq. 4-86	10	8, Eq. 4-69	10, Eq. 4-85	10, Eq. 4-85
NaOH solution	15, Eq. 4-68	15, Eq. 4-86	15	15, Eq. 4-69	15, Eq. 4-85	15, Eq. 4-85

1, 2, 3 represent the value is solved at calculation step 1, step 2, or step 3.

The results of mass transfer coefficients and resistances and chemical dissociation enhancement factor for non-corona tests are shown in Table 7.3.

4.8 Electrostatic Enhancement Factors

From the results of overall mass transfer coefficient, K_{OG} , in Table 7.1, the corona-reduced total mass transfer resistance (form test #225a to #328) could be greater than the gas mass transfer resistance (which is equal to the K_{OG} of test #302). This experiment results showed that the corona discharge not only reduced the gas side mass transfer resistance, but also reduced the liquid side resistance. Therefore, the electrostatic enhancement of the mass transfer on both sides should be studied.

In order to compare the mass transfer in the system with/without corona discharge, electrostatic enhancement factors $\phi_{e,g}$ and $\phi_{e,l}$ are introduced to the mass transfer coefficients on the both sides as illustrated in Figure 4.12. It is assumed that all the electrostatics affects are

included in the factors $\phi_{e,g}$ and $\phi_{e,l}$, so the mass transfer coefficients k_g and k_l ($k_l = \phi_c * k_l^o$) remain the same in all the trials.

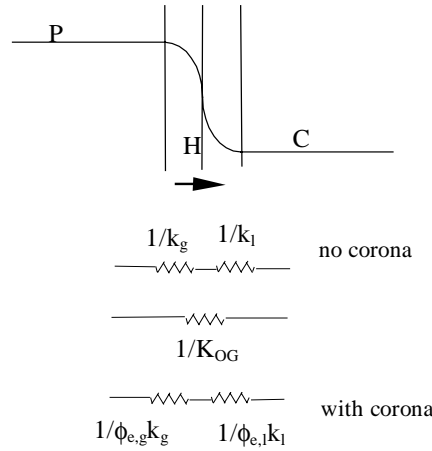


Figure 4.12 Electrostatic Enhancement Factors of Mass Transfer Coefficients

The following equation includes all the electrostatics effects in an electrostatic enhancement factor ϕ_e .

$$\frac{1}{K_{OG}} = \frac{1}{\phi_{e,g}k_g} + \frac{H}{\phi_{e,l}k_l} \quad \text{Eq. 4-89}$$

where

ϕ_e : electrostatic enhancement factor, $\phi_e = 1$ for non-powered tests

The mass transfer coefficients have been solved for systems without corona discharge ($\phi_e = 1$) at Table 7.2. The K_{OG} of the non-corona test was compared to the K_{OG} of the corona tests. Any increase in the mass transfer rate in the tests with power was accounted for with ϕ_e .

4.8.1 Determination of Electrostatic enhancement Factors

Similar to the process at Section 4.7.4, each set of corona batch tests consists of two tests at the same conditions except one in pure water and the other in NaOH solution. Determination

is based on that the liquid side mass transfer coefficient excluding the dissociation, k_1^0 , and the gas side electrostatic enhancement factors $\phi_{e,g}$ and $\phi_{e,l}$ are the same for both tests. The calculation procedures are listed as the following steps (continued from section 4.7.4) and summarized at Table 4.3:

19. Determine the K_{OG} of both tests by steps 1 ~ 4.
20. Assume that the total k_g (total $k_g = \phi_{e,g} * k_g$) of pure water test is equal to the K_{OG} of NaOH test.
21. Obtain the total k_1 ($\phi_{e,l} * k_1$) of pure water test from Eq. 4-87.
22. Solve the chemical dissociation enhancement factor, ϕ_c , of pure water test by steps 7 ~ 11.
23. The k_1^0 is the same as of non-corona tests because all the effect of electrostatics is included in enhancement factor ϕ_e .
24. Solve the liquid side electrostatic enhancement factors $\phi_{e,l}$ from ϕ_c , k_1^0 and total k_1 .
25. The $\phi_{e,l}$ of NaOH test is equal to the value of pure water test.
26. Since the liquid side mass transfer resistance is negligible, assume the total k_g of NaOH test is equal to the K_{OG} of NaOH test as a starting value.
27. Solve the chemical dissociation enhancement factor, ϕ_c , of NaOH test by steps 7 ~ 11.
28. Calculate the total k_1 of NaOH test by multiplying k_1^0 , ϕ_c and $\phi_{e,l}$.
29. Calculate the new total k_g value of NaOH test by Eq. 4-87. Check this value with the previous assumed total k_g value at step 26. If the difference is unacceptable ($> 0.1\%$), go back to step 26. Replace the previous assumed total k_g value with the new total k_g value and repeat step 27 to 29. If the difference is acceptable ($< 0.1\%$), go to next step.

30. Check the newly solved k_g value of NaOH test with the previous assumed k_g of pure water test. They should be the same because the gas conditions are the same. If the difference is unacceptable ($> 0.1\%$), go back to step 20. Replace the previous assumed total k_g value with the new total k_g value and repeat step 21 to 30. If the difference is acceptable ($< 0.1\%$), go to next step.
31. Calculate the $\phi_{e,g}$ of both tests by comparing the total k_g with the k_g of non-corona tests.

Table 4.3 Summary of the Calculation of Electrostatic Enhancement Factors

Test	K_{OG}		$\phi_{e,g}$	total k_g $= \phi_{e,g} * k_g$
Pure water	19, (1 ~ 4)		31	20, 30
NaOH solution	19, (1 ~ 4)		31	26, 29
	k_l^o	ϕ_c	$\phi_{e,l}$	total k_l $= \phi_{e,l} * k_l$
Pure water	23	22, (7 ~ 11)	24	21, Eq. 4-87
NaOH solution	23	27, (7 ~ 11)	25	28

*1, 2, 3 represent the value is solved at calculation step 1, step 2, or step 3.

The results of electrostatic enhancement factors are shown in Table 7.3, Figure 7.8 and Figure 7.9.

5. SO₂ REMOVAL IN WESP

This chapter will discuss the results of gaseous pollutant removal vs. various electrical, physical, and chemical factors in the wESP. Each of these factors will be discussed in detail below.

5.1 Removal vs. Electrical Properties

Initially tests were conducted without water to determine the effect of the corona discharge on SO₂ removal under dry conditions. Figure 5.1 shows that the pulsed corona discharge caused a momentary drop in the outlet SO₂ concentration that returned to its original value after a few minutes.

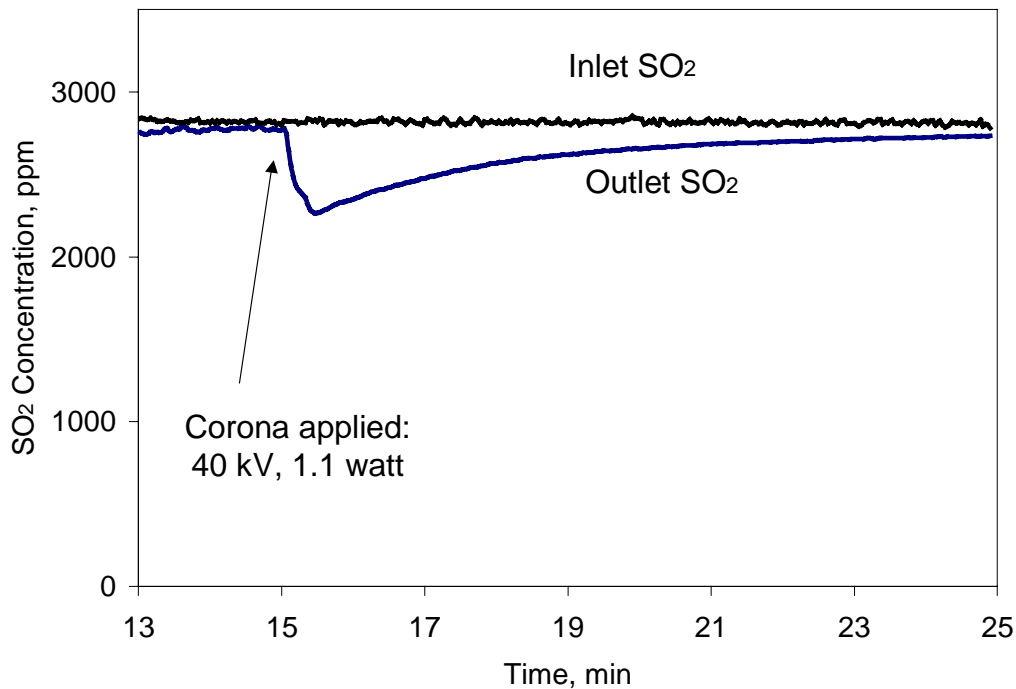


Figure 5.1 SO₂ Concentration in ESP under Dry Condition

Wet ESP Experimental Conditions: In 20°C dry air, 10 sec gas residence time, without water; with a negative corona.

This momentary drop demonstrated that SO₂ could be charged and moved to the collection plate where it was absorbed. In this dry system, the charge was quickly dissipated and the SO₂ molecules re-entered the gas stream. After equilibrium was established between the attraction and re-entrainment of SO₂, no more net removal of SO₂ was measured.

The introduction of water caused the drop of SO₂ concentration because of the absorption of water, even if there was not a corona discharge. And the corona power can drive the SO₂ further into the water.

5.1.1 Removal Efficiency vs. Corona Voltage and Power

Figure 5.2 and Figure 5.3 show the results of tests conducted to measure SO₂ removal when the power and input SO₂ concentration were adjusted under wet condition. Theoretically, equilibrium would be reached when approximately 66.9% of the SO₂ is absorbed into the water under the same operational conditions as those in Figure 5.2. However, it can be seen from the "no power" data that the system does not approach that degree of removal by itself without applying the corona discharge. The application of power clearly drove the SO₂ removal level to the SO₂/water equilibrium state, even beyond the equilibrium level for those runs that had a higher input SO₂ concentration. This is explained by the formation of a large gas concentration gradient at the gas-side boundary layer that results in a new, higher equilibrium level that is not based on the bulk gas concentration. This phenomenon can be considered as a pseudo equilibrium based on the electron attachment effect. When the SO₂ concentration was over 2000 ppm, equilibrium was obtained by using a 35 watts corona discharge.

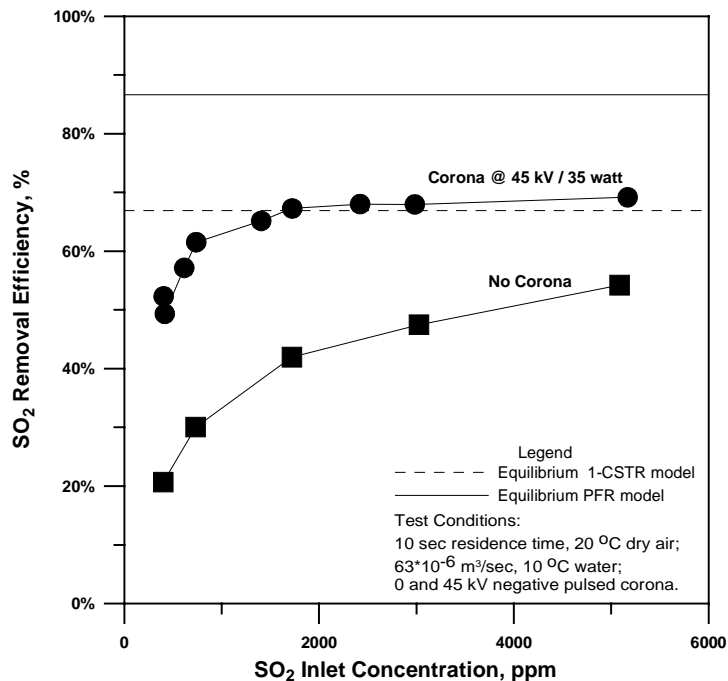


Figure 5.2 SO₂ Removal Efficiency vs. Inlet SO₂ Concentration in wESP

Wet ESP Experimental Conditions: In 20°C 43%RH air; 10 sec gas residence time, 3.8 L/min 10°C water, with 0 and 45 kV negative pulsed corona.

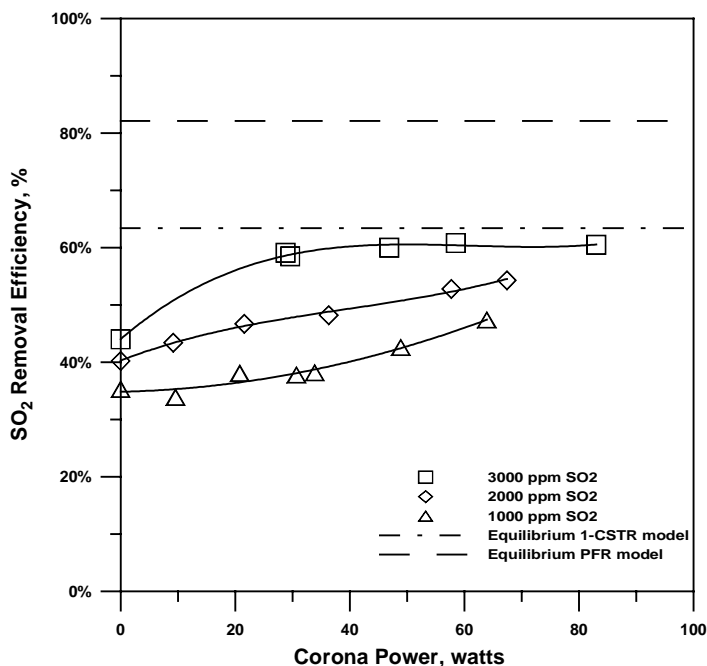


Figure 5.3 SO₂ Removal Efficiency vs. Corona Power in wESP

Wet ESP Experimental Conditions: In 20°C 70% humidified air, 8.5 sec gas residence time, 3.8 L/min 10°C water; with a negative pulsed corona.

Figure 5.3 also shows clearly that the corona power drove the SO₂ removal level to approach the SO₂/water equilibrium value. The SO₂/water system should theoretically come to equilibrium when approximately 63.4% of the SO₂ is removed through water absorption based on the conditions shown in Figure 5.3. When the power was less than 40 watts, the system did not approach this equilibrium state. When the corona power and SO₂ concentration were sufficient, equilibrium was reached, which represents the maximum level of physical absorption.

5.1.2 Modeling Results of Electrostatics Enhanced Mass Transfer N-CSTR Model in wESP

Figure 5.4 and Figure 5.5 show the overall mass transfer coefficients of the wESP with respect to corona power and inlet SO₂ concentration.

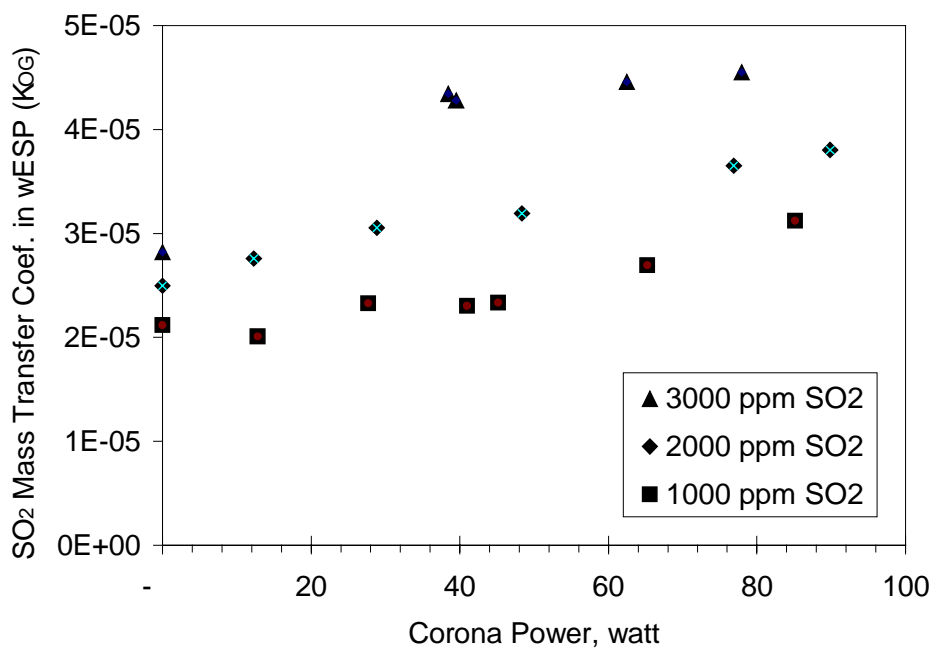


Figure 5.4 Overall Mass Transfer Coefficient vs. Corona Power in wESP

Wet ESP Experimental Conditions: In 20°C, 70% humidified air, 8.5 sec gas residence time, 3.8 L/min 10°C water; with a negative pulsed corona.

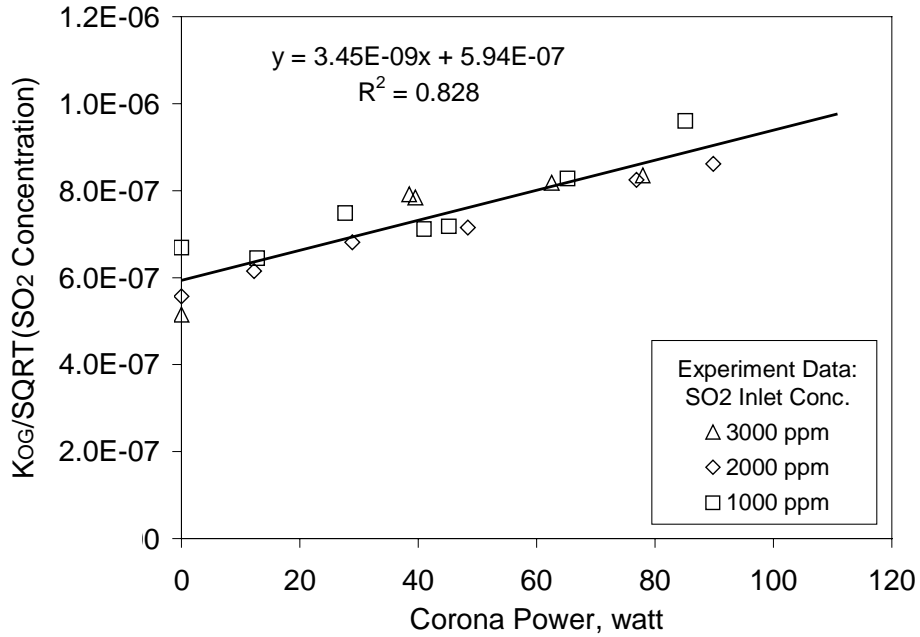


Figure 5.5 Mass Transfer Coefficient vs. Corona Power and Inlet SO₂ concentration in wESP

Wet ESP Experimental Conditions: In 20°C, 70% humidified air, 8.5 sec gas residence time, 3.8 L/min 10°C water, with a negative pulsed corona.

The Electrostatics Enhanced Mass Transfer N-CSTR model describes the relationship between the removal efficiency and the mass transfer coefficient of the wESP with the known system parameters such as the gas and liquid flow rates, collection area, pH value of the bulk liquid, and system temperature. The overall mass transfer coefficient K_{OG} was determined from the overall removal efficiency as a function of inlet SO₂ concentration and corona power (Figure 5.4). By combining the mass transfer coefficient and the inlet SO₂ concentration, it is possible to derive the following empirical formula as shown in Figure 5.5:

$$K_{OG} = \left(3.45 \times 10^{-9} P_{wr} + 5.94 \times 10^{-7} \right) \sqrt{P_{SO_2, in}} \quad \text{Eq. 5-1}$$

where

K_{OG} = The overall gas side mass transfer coefficient, mol/sec-cm²-atm

$P_{\text{SO}_2, \text{in}}$ = Inlet SO₂ gas concentration, ppm

P_{wr} = Corona discharge power, watt

Using Eq. 5-1, it is possible to determine the mass transfer coefficient by knowing the corona power and inlet SO₂ concentration. Combining Eq. 5-1 with the Electrostatics Enhanced Mass Transfer N-CSTR model developed in section 4.6, it is also possible to predict the overall SO₂ removal efficiency of the wESP.

5.2 Pollutant Concentration and Flow Conditions

5.2.1 SO₂ Concentration

In Figure 5.2 and Figure 5.3, we can see that the higher the input SO₂ concentration, the higher the removal efficiency. This relationship held even for the trials without corona power. The higher SO₂ concentration provides a higher driving force for mass transfer that translated into higher removal efficiency. It is reasonable to assume that as more SO₂ molecules are present, larger clusters are more readily formed[26]. The electrons and ions needed to remove these clusters are readily available when the corona power is applied.

When SO₂ concentration was 1000 ppm, the removal efficiency approximately doubled by 47 watts of applied power at 10-second residence time (Figure 5.2). This enhancement became smaller at higher SO₂ concentrations. When the removal exceeds the equilibrium level (based on bulk concentrations), further removal enhancement decreases and removal efficiency tends to approach a maximum level. These results demonstrate that when the input SO₂ concentration and power are sufficient, the mass transfer of SO₂ into the water is limited more by the liquid chemistry than by the corona power or SO₂ concentration.

5.2.2 Gas and Liquid Flow Rate

Figure 5.6 and Figure 5.7 show the effect of gas residence time and the liquid/gas volumetric flow rate on SO₂ removal. It was found that the SO₂ removal efficiency increased as the gas residence time and the liquid/gas volumetric flow rate increased.

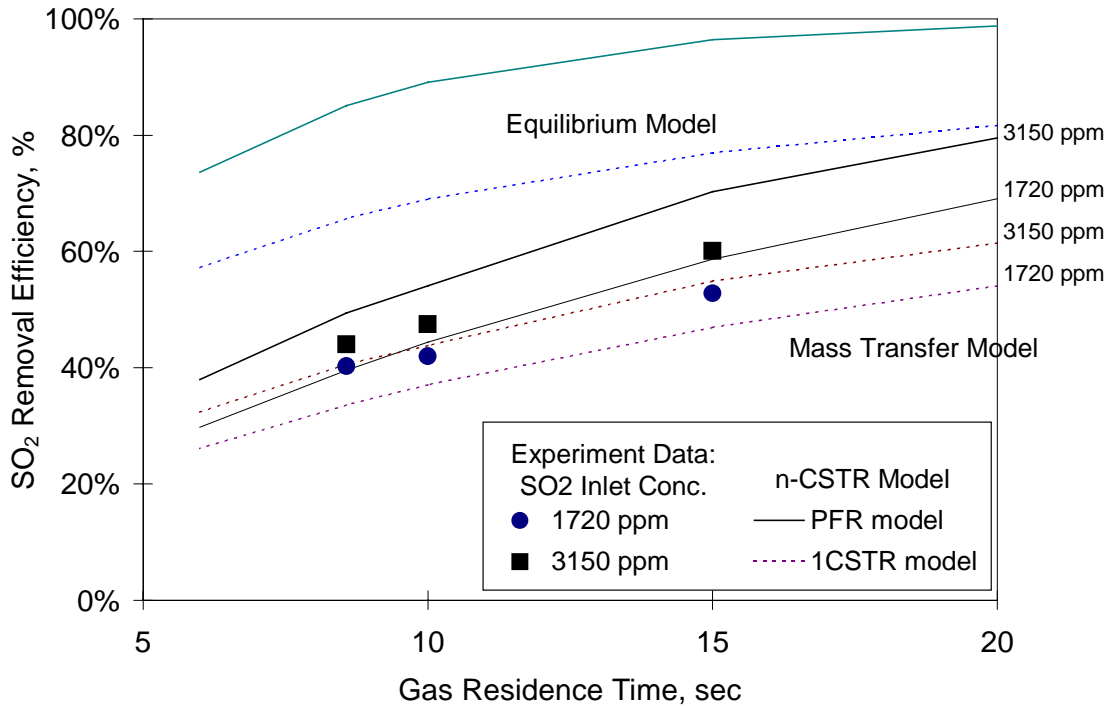


Figure 5.6 SO₂ Removal vs. Gas Residence Time in wESP

Wet ESP Experimental Conditions: In 20°C 43%RH air, 3.8 L/min 10°C water, without corona discharge.

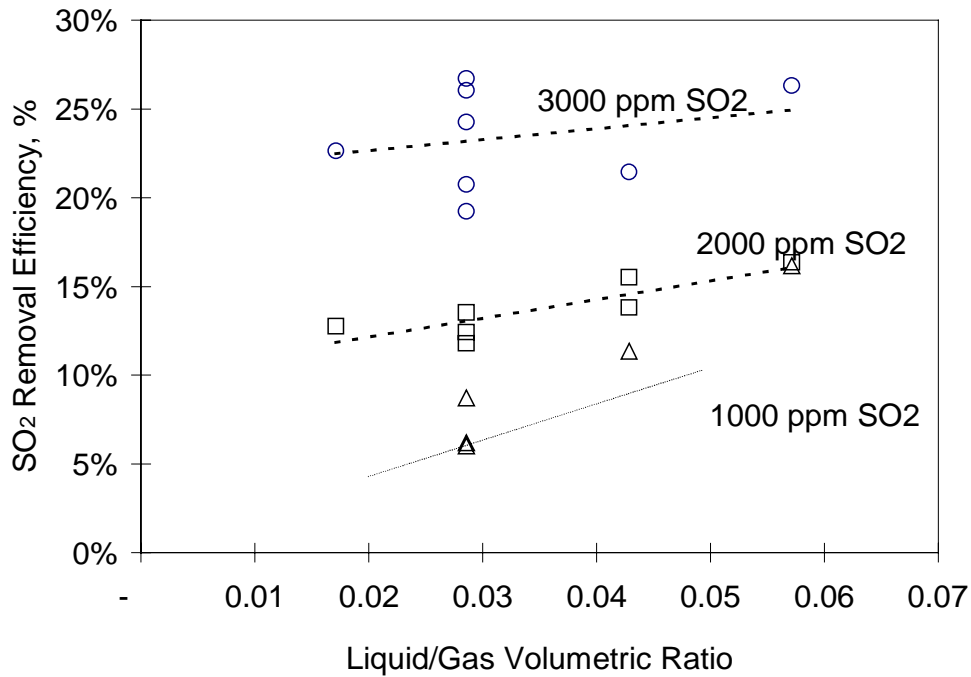


Figure 5.7 SO₂ Removal vs. Gas/Liquid Volumetric Flow Ratio in wESP

Wet ESP Experimental Conditions: In 20°C, 70% humidified air, 8.6 sec gas residence time, 10°C water, without corona discharge.

5.3 Ozone Injection

5.3.1 In-Situ Ozone

One explanation for the separation of SO₂ could be the formation of ozone (O₃) in the wESP and the subsequent possible oxidation of SO₂ to SO₃, even though this reaction has been reported to be slow at these temperatures [15]. SO₃ is very soluble in water and easily reacts with water to form sulfuric acid. Therefore, the effect of in-situ ozone formation on SO₂ oxidation was studied. The maximum power the system could achieve without sparks was ~ 80 W (60 kV). The amount of in-situ O₃ formation was determined by passing clean air (i.e., without SO₂) through the wESP at the same flow rates as used in the SO₂ removal experiments. The O₃ concentration was then sampled internally in the wESP at the end of the collection plates. Figure 5.8 shows the relationship between ozone concentration and corona power.

It was observed that the in-situ ozone concentration increased as the corona power increased, even when SO₂ was present in the system. This situation implies that the oxidation reaction, as originally envisioned, was too slow to account for the high levels of removal reported here. It was also found experimentally that the concentration of O₃ produced in-situ varied directly with the power level, but did not exceed 7 ppm at the 60 kV voltage level. A relationship between in-situ ozone concentration, corona power, and gas residence time can be seen in Figure 5.9. The maximum ozone concentration of 3.5 ppm was achieved at the corona intensity of 7.5 kV/cm, which was close to the reported ozone yield of 0.18 ppm at corona intensity of 8 kV/cm [33].

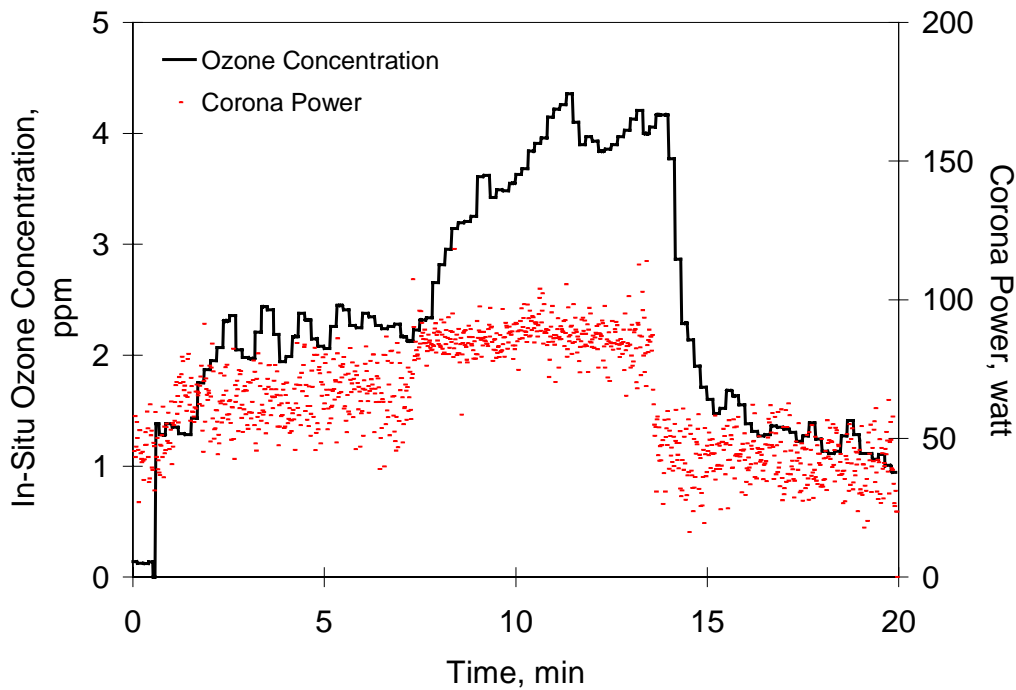


Figure 5.8 Relationship between In-situ Ozone and Power in wESP

Wet ESP Experimental Conditions: In 20°C 70% humidified air, 8.6 sec gas residence time, 3.8 L/min water 10°C, with a negative pulsed corona.

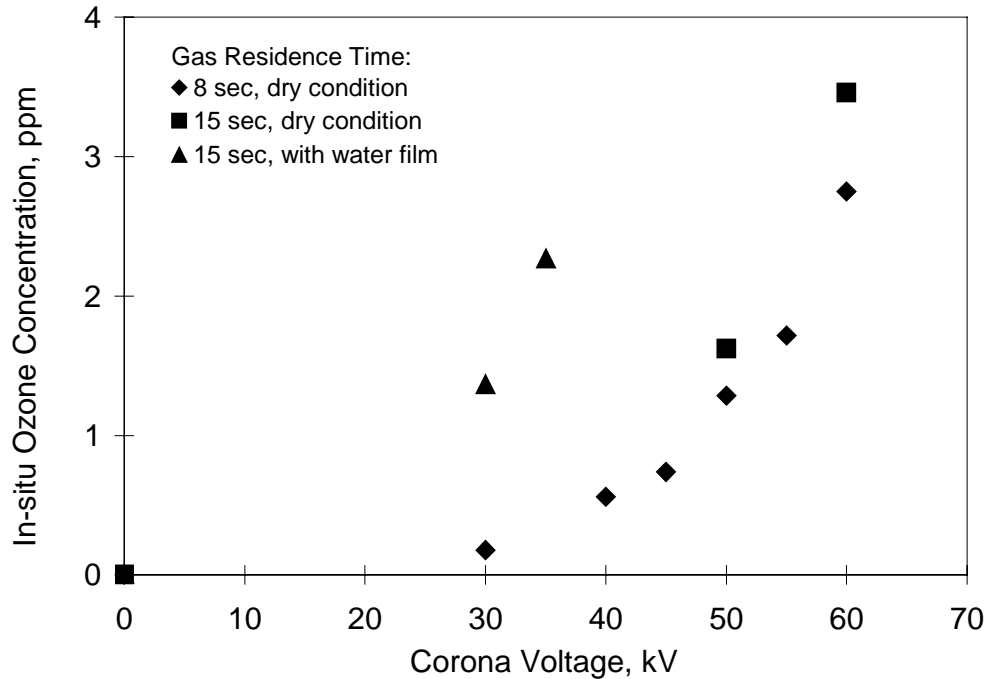


Figure 5.9 Relationship between In-situ Ozone, Gas Residence Time and Corona Power

Wet ESP Experimental Conditions: In 20°C 43%RH air, 3.8 L/min water 10°C, with a negative pulsed corona.

Since the reaction between ozone and NO_x or SO₂ is a one-to-one molar ratio, there is not enough in-situ ozone present to remove a significant amount of NO_x or SO₂. Therefore, it was concluded that the amount of in-situ ozone formed was not sufficient to be considered a major removal mechanism.

5.3.2 Ozone Injection

In the experiments reported in this section, ozone was generated externally and introduced into the gas phase in the wESP to study the effects of ozone on the removal of SO₂. The in-situ ozone concentration generated by the positive corona discharge was 0.23 ppm under the same wESP conditions, which confirms that the amount of in-situ ozone at such a low corona power level was very small.

The results of SO₂ removal with ozone injection into the SO₂/air stream are shown in Figure 5.10 and Figure 5.11. These results show that the presence of ozone slightly enhanced SO₂ removal in the case of non-corona-discharge. However, in the case of corona discharge, the presence of ozone inhibited SO₂ removal if SO₂ was the only gaseous pollutant in the gas stream. This inhibition was greater with a higher corona discharge. One possible explanation is that electrons were consumed by ozone rather than by SO₂. The ozone could compete with the SO₂ for free radicals or electrons from the corona discharge because ozone is much more reactive than SO₂. Fewer amounts of electrons were available for SO₂, resulting in less SO₂ removal.

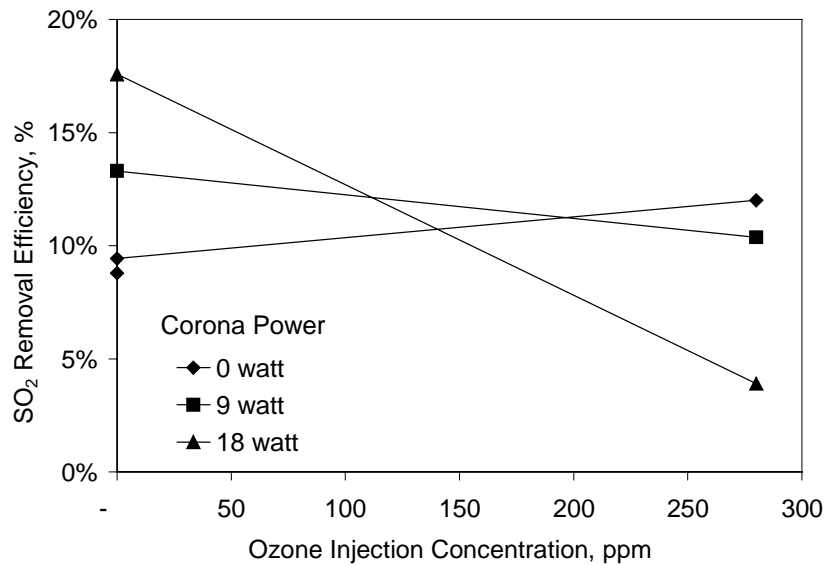


Figure 5.10 SO₂ Removal vs. Ozone Injection in the SO₂/Air Stream

Wet ESP Experimental Conditions: In dry air, 2000 ppm SO₂, 10 sec gas residence time, room temperature, 3.8 L/min 10°C water, with a positive pulsed corona.

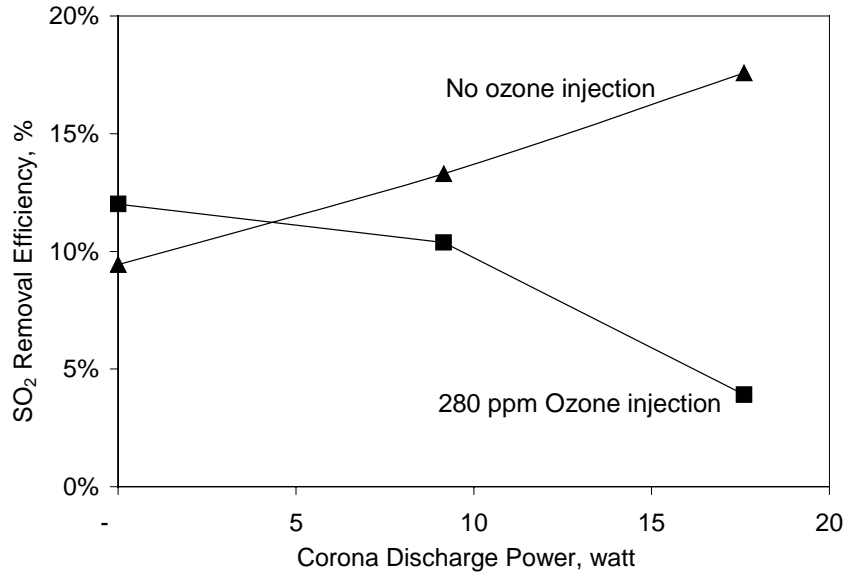


Figure 5.11 SO₂ Removal vs. Corona Discharge in the SO₂/Air Stream

Wet ESP Experimental Conditions: In dry air, 2000 ppm SO₂, 10 sec gas residence time, room temperature, 3.8 L/min 10°C water, with a positive pulsed corona.

The SO₂ removal results from ozone injection in SO₂/NO_x/air stream are shown in Figure 5.12 and Figure 5.13. The results demonstrate that in the presence of NO_x, ozone improved the SO₂ removal in both with and without the corona cases. It is believed that most of the ozone immediately reacted with NO, because the reaction rate of ozone to NO is ten orders of magnitude higher than the reaction rate of ozone to SO₂. Therefore, when NO was present, less ozone competed with the SO₂ for radicals or electrons and the SO₂ removal efficiency increased as the corona power and ozone levels increased. Moreover, the NO₂ from the oxidation of NO might oxidize SO₂ as well [35].



Reaction rate constant: $\log k = 14.4 - 5789/T$ at 434~504K [35]

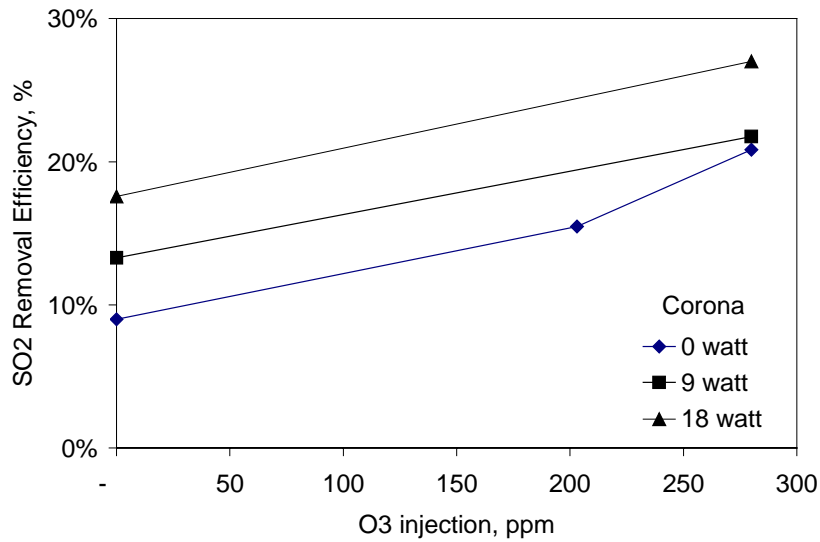


Figure 5.12 SO₂ Removal vs. Ozone Injection in SO₂/NO_x/Air Stream

Wet ESP Experimental Conditions: In dry air, 2000 ppm SO₂, 1100 ppm NO_x, 10 sec gas residence time, room temperature, 3.8 L/min 10°C water, with a positive pulsed corona.

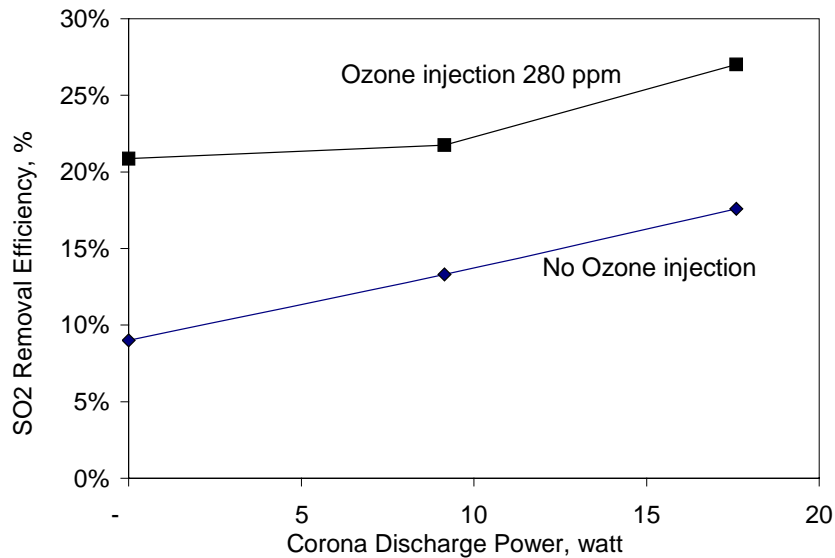


Figure 5.13 SO₂ Removal vs. Corona Discharge in SO₂/NO_x/Air Stream

Wet ESP Experimental Conditions: In dry air, 2000 ppm SO₂, 1100 ppm NO_x, 10 sec gas residence time, room temperature, 3.8 L/min 10°C water, with a positive pulsed corona.

5.4 Ammonia Injection

With ammonia injection, SO₂ removal quickly reached ~100%. White ammonium salt aerosols were instantly formed in cases with and without O₂ and/or NO_x. Ammonia is supplied in a stoichiometric quantity with respect to the SO₂ and/or NO_x to be removed. The stoichiometric ratio is defined as the following:

$$\text{stoichiometric ratio} = \frac{\text{mole of NH}_3}{(\text{mole of NO}_x) + 2(\text{mole of SO}_2)} \quad \text{Eq. 5-3}$$

The SO₂ removal results of ammonia injection into the SO₂/air stream are shown in Figure 5.14 and Figure 5.15.

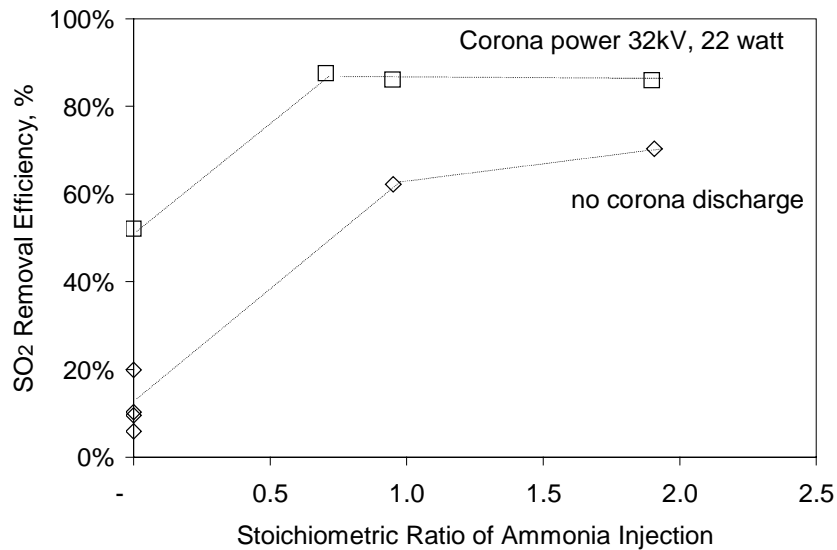


Figure 5.14 SO₂ removal vs. Ammonia Injection in SO₂/Air Stream

Wet ESP Experimental Conditions: In dry air, with 2100 ppm SO₂, 10 sec gas residence time, room temperature, 3.8 L/min 10°C water, with a positive pulsed corona.

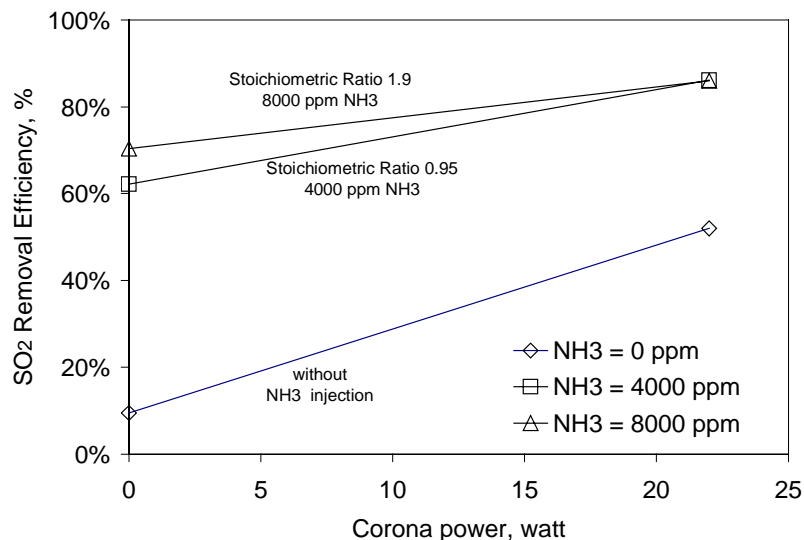


Figure 5.15 SO₂ removal vs. Ammonia Injection and Corona Discharge in SO₂/Air Stream

Wet ESP Experimental Conditions: In dry air, with 2100 ppm SO₂, 10 sec gas residence time, room temperature, 3.8 L/min 10°C water, with a positive pulsed corona.

This result shows that ammonia improved the SO₂ removal in both corona and non-corona-discharge cases. The maximum SO₂ removal was approximately 87% under a 22 watts corona discharge. In non-corona tests, the maximum SO₂ removal with ammonia injection was approximately 70% because the aerosols could not be removed efficiently. However, this improvement approached an upper limit as the ammonia increased. The maximum removal of 2100 ppm inlet SO₂ could be achieved with less than a 4000 ppm NH₃ injection, or with a 0.7 stoichiometric ratio of NH₃ with respect to the SO₂. This result implies that some byproducts were in the form of ammonium bi-sulfite (NH₄HSO₃), bi-sulfate (NH₄HSO₄), or a combination of these two compounds.

In the experiments of simulated flue gas, some NH₃ was consumed by CO₂ in the flue gas and formed ammonia bicarbonate. Carbon content was found in the collected aerosols (section 6.4.1). This decreases SO₂ removal because less NH₃ was available for SO₂.

5.5 Fates of Sulfur

5.5.1 pH in the Water of wESP

The pH values were sampled in the six water collection chambers, each chamber representing a sequential SO₂ removal occurring in the wESP. For each set of tests, the n-CSTR equilibrium model was used to estimate the maximum natural SO₂ removal due to physical absorption and hydrolysis reactions. The results of the pH measurements and equilibrium modeling of the six chambers along the direction of the gas flow are given in Table 5.1 and shown in Figure 5.16.

Table 5.1 Experimental and Equilibrium Modeling Results of pH Value in Six Phases

Test Number	Corona Power	Inlet SO ₂ Conc.	SO ₂ Removal Eff.	pH Values					
	kW			ppm	%	Section 1	Section 2	Section 3	Section 4
Exp. #4	17.3	3,346	73.9	3.19	3.18	3.17	3.48	3.29	3.86
Equilibrium model of test #4		3,346		1.92	2.12	2.31	2.50	2.70	2.89
Exp. #5	10.7	1,554	52.8	5.23	6.00	6.30	6.32	6.15	5.95
Equilibrium model of test #5		1,554		2.26	2.45	2.64	2.84	3.03	3.22
Exp. #6	39.4	1,657	74.6	4.30	4.60	5.63	6.20	6.25	5.98
Equilibrium model of test #6		1,657		2.23	2.42	2.61	2.81	3.00	3.19
Exp. #7	78.4	1,682	74.1	4.45	4.20	5.56	6.19	6.26	6.00
Equilibrium model of test #7		1,682		2.22	2.41	2.61	2.80	2.99	3.19

Wet ESP Experimental Conditions: In 70%RH air, 15 sec gas residence time, room temperature, 3.8 L/min 10°C water, with a negative pulsed corona

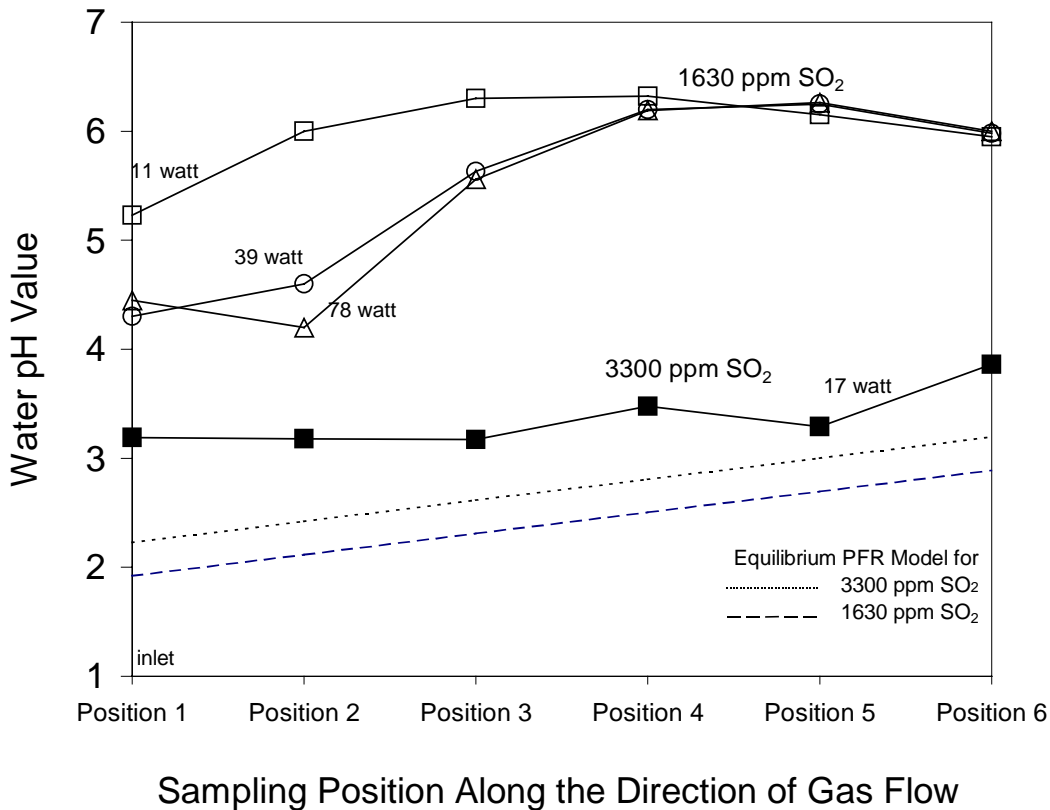


Figure 5.16 pH in Phases of wESP at Low and High SO₂ Inlet Concentration

Wet ESP Experimental Conditions: In 70%RH air, 15 sec gas residence time, room temperature, 3.8 L/min 10°C water, with a negative pulsed corona

In Figure 5.16, water was more acidic in the first two sections for a SO₂ concentration of 1630 ppm, indicating that most of the SO₂ removal took place in the first one-third of the wESP. Higher SO₂ concentrations resulted in more SO₂ removal and lower water pH level. At a SO₂ concentration of 3300 ppm, the water pH approached the pH levels predicted by the Equilibrium State model. These results indicate that by applying the corona, it drove SO₂ into the water phase, and the SO₂ removal increased as the corona power increased. In the cases of 1630 ppm inlet SO₂, the pH values at various power levels indicate that corona discharge drove the removal efficiency toward the equilibrium level. The pH values also approached to model values as overall system efficiency approached to the equilibrium removal efficiency.

5.5.2 Concentrations of Sulfite and Sulfate

The concentration of sulfite and sulfate for water samples of six phases are shown in Figure 5.17. The sulfite concentrations were greater than the increased sulfate concentrations in the middle phases (positions 2 to 5), which is contradictory to the cases in the gas inlet and outlet phases (positions 1 and 6) where the sulfate concentrations were greater than the sulfite concentrations. Since the corona discharge wires were located in the middle sections, these results suggest that the sulfur removed by the corona in the liquid is more likely to be sulfite (the original form of gas absorption) instead of sulfate (the oxidization form). This difference was measured not only for the non-corona case where sulfite resulted from SO_2 absorption, but also for the corona cases where electron attachment might be the primary removal mechanism rather than oxidizing SO_2 to SO_3 .

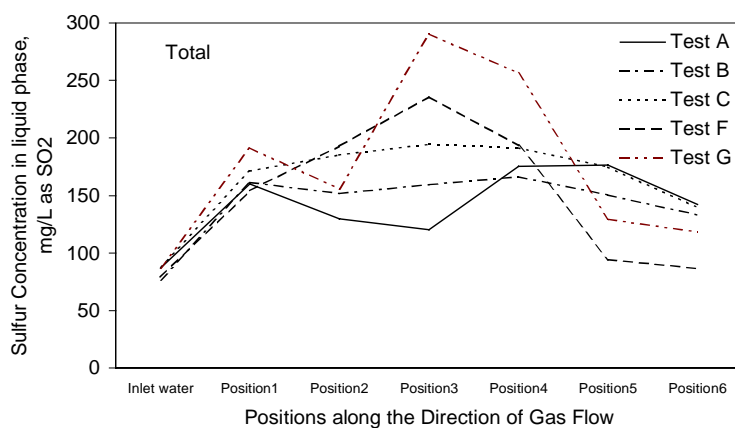
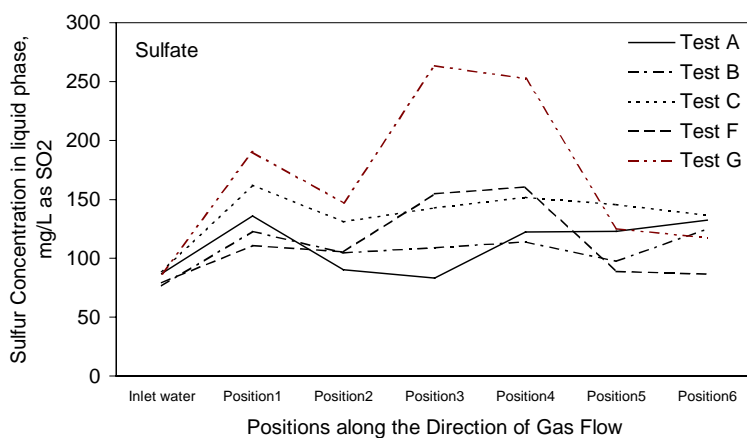
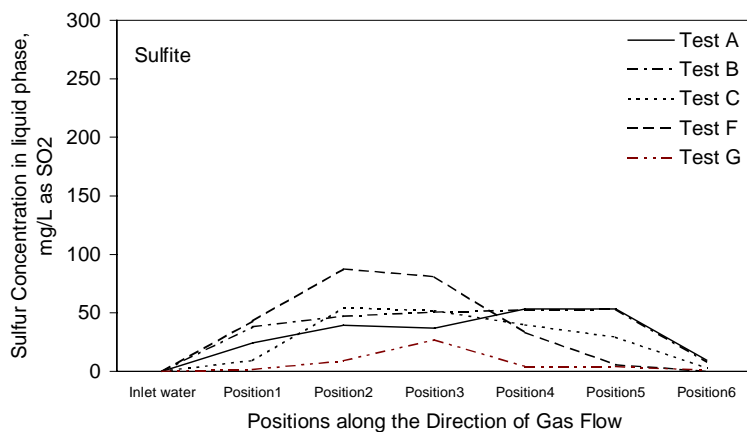


Figure 5.17 Sulfite and Sulfate Concentrations of Water Samples in Six Positions

Wet ESP Experimental Conditions: Tests A, B, C: In air (25°C), 1000 ppm NO_x, 2000 ppm SO₂. Tests F, G: In humidified 5.8% O₂, 11% CO₂ simulated flue gas (25°C), 770 ppm NO_x, 2000~3000 ppm SO₂. All Tests: 10 sec gas residence time, 3.8 L/min water (12°C). Test A no corona, Test B +65 kV, Test C +68 kV, Test F -32 kV, Test G -30 kV pulsed corona.

5.5.3 Sulfur Mass Balance

The mass balance of sulfur in both the gas and liquid phases was conducted to verify the results of the gas phase removal. The sulfur balance results from iodometric sulfite analysis and gravimetric sulfate analysis are shown in Table 5.2. The difference in sulfur uptake shows that wet chemistry methods were easy to overestimate the anion concentrations, especially sulfate concentrations. It was shown experimentally that if samples were not tested immediately, the measured sulfate concentrations went up quickly. The wet chemistry methods took 3 hours to analysis one sample, while the Ion Chromatograph method only took 20 minutes.

Table 5.2 Sulfur Mass Balance of Iodometric Sulfite Tests and Gravimetric Sulfate Tests Results

	Gas Phase						Liquid Phase			Difference in Sulfur Uptake*
	Power	SO ₂ Input	SO ₂ Removal Eff.	NO _x Input	SO ₂ Removed	Total Sulfur Removed	SO ₃ ²⁻ Conc.	SO ₄ ²⁻ Conc.	Total Sulfur Increased	
	Watt	ppm	ppm	ppm	cm ³ /sec as SO ₂	mg/sec as SO ₂	mg/L as SO ₂	mg/L as SO ₂	mg/sec as SO ₂	
#1	45.0	1,986	36.4%	0	1.36	3.80	13.06	88.80	6.43	69%
#2	14.0	2,000	33.3%	0	1.26	3.50	18.13	57.00	4.74	36%
#3	37.0	1,984	29.5%	1,000	1.11	3.07	20.53	76.60	6.13	99%
#4	11.0	1,991	26.0%	1,000	0.98	2.72	26.93	111.78	8.75	222%

Wet ESP Experimental Conditions: In dry air, 10 sec gas residence time, room temperature, 3.8 L/min 10°C water, with a positive pulsed corona.

* Difference in sulfur uptake: Difference of liquid phase total sulfur increase mg/sec and gas phase total sulfur removed (mg/sec)

The sulfur balance results from ion chromatograph analysis are shown in Table 5.3 for three wESP tests for various operational conditions. For each wESP test, the sulfate concentration of raw tap water was sampled and subtracted from the results. Comparing with the

traditional gravimetric and iodometric methods, ion chromatograph analysis provides more accurate results than wet chemistry methods.

Table 5.3 Mass balance of Sulfur by Ion Chromatograph Method

Test#	Removed from the Gas Phase			Increased at the Liquid Phase			Difference in sulfur uptake*
	SO ₂ Inlet	SO ₂ outlet	Total S Removed	Sulfite SO ₃ ²⁻	Sulfate SO ₄ ²⁻	Total S Increased	
	ppm	ppm	mg/sec as SO ₂	mg/L as SO ₂	mg/L as SO ₂	mg/sec as SO ₂	%
A	3164	2534	3.31	35.88	30.14	4.17	26%
B	3187	2323	4.54	41.64	29.78	4.51	0.7%
C	1945	801	6.01	31.22	52.14	5.26	12%

Wet ESP Experiment Conditions: 240 CFH, 10 sec gas residence time, 3.8 L/min 10°C water, Test A: no corona, B: 47.5 watt, C: 40.8 watt positive pulsed corona. Sulfite and sulfate concentrations have been converted to the mass of sulfur dioxide gas (mg as SO₂).

* Difference in sulfur uptake: Difference of liquid phase total sulfur increase and gas phase total sulfur removed

6. NO_x REMOVAL IN WESP

Previous results showed that without the NH₃ injection, SO₂ could be easily removed up to 70% by applying the water film and 45 kV (40 watt) corona in the wESP. De-SO_x is much easier than De-NO_x and is relatively irrelevant to the O₂ level of the flue gas in the wESP. The success of NO_x removal is the key to the combined SO₂ and NO_x removal in the wESP process.

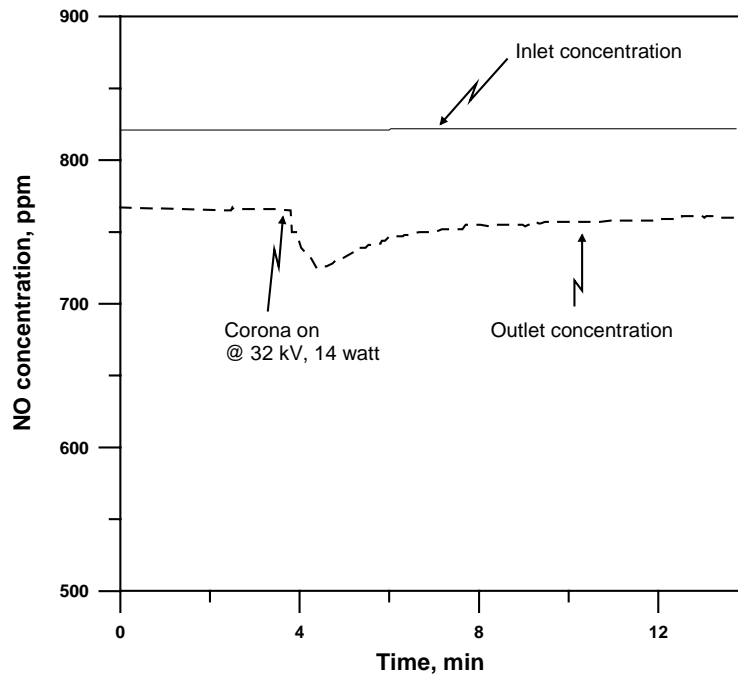


Figure 6.1 NO Removal in Dry ESP

Wet ESP Experimental Conditions: In 3% O₂ 20°C 70%RH humidified simulated flue gas, 800 ppm NO, 11.4 sec gas residence time, without water, with a positive pulsed corona.

Initial test was conducted to determine the effect of the electrostatic field on NO removal in dry condition. Figure 6.1 shows that as in the case of SO₂, the corona discharge caused a momentary drop in the outlet NO concentration, which returned to its original value after a few minutes. This momentary drop demonstrated that NO molecules could be charged and moved to the collection plate. In the dry system, the charge was quickly dissipated and the NO molecules

re-entered into the gas stream. After the equilibrium between the attraction and re-entrainment of NO was established, the system reached a steady state and no more net removal of NO was measured.

6.1 In Nitrogen

Tests were conducted in the air stream and in the nitrogen stream to determine the effect of oxidation on NO removal. In a pure N₂ stream (Tests #1, 2, and 3 of Table 6.1), less than 4% of NO is removed, even though both corona discharge and water film were applied. These results suggest that NO has to be oxidized into NO₂ (or other more soluble nitrogen oxides) before any significant removal could take place. The water vapor from the evaporation in the wESP (41.8 ~ 43.2% relative humidity for 3.8 L/min water flow) oxidizes or absorbs only 0.8% of NO. A corona level of 31 kV (12 watts) increased NO removal very little in a nitrogen stream. Therefore, NO_x removal can only be initiated after NO was oxidized either by O₂ or the oxidizing radicals developed from O₂ under the corona discharge.

Table 6.1 Test Removal of Nitrate Oxide in a Nitrogen Stream and in Air

Test Number	#1	#2	#3	#4	#5	#6
Carrier Gas	N ₂			Air		
Residence Time, sec	11.5			10.5		
Water Flow Rate, L/min	3.8		9.5	3.8		
Voltage Applied, kV	None	31	31	None	N.A.	N.A.
Power Applied, watt	None	12	12	None	30	22.5
Inlet NO conc., ppm	782	748	722	1100	1100	764
Outlet NO conc., ppm	773	728	699	913	896	657
NO Removal Efficiency	1.2%	2.7%	3.2%	17%	19%	14%

Wet ESP Experimental Conditions: In 25 °C air or nitrogen, 12 °C water, with a positive pulsed corona.

N.A.: Not available. Data is missing.

6.2 In Air

6.2.1 Without Ozone or Ammonia Injections

In air (Tests #4, 5, and 6 of Table 6.1), approximately one tenth of the NO is oxidized to NO₂ in 10 seconds at room temperature. There was 17% removal of NO in the air stream without corona discharge, which is attributed to the oxidation of NO by air and ultimately NO₂ removal by water. The corona discharge increased the removal.

In Figure 6.2 and Figure 6.3, tests were conducted to measure the NO_x removal when the power, gas residence time, and input NO_x concentration were adjusted. In non-corona tests, NO was oxidized to NO₂ by O₂ and absorbed by water in the wESP. That resulted in 6~8% removal efficiency. In Figure 6.2, the application of power increased the NO removal level by another 10%. However, 20% seems to be the limit of NO removal efficiency when the residence time is less than 10 seconds.

In Figure 6.3, higher inlet NO concentrations led to higher removal efficiencies, which are consistent with SO₂ removal in the wESP. This is explained by the formation of a large gas concentration gradient at the gas-side boundary layer that results in a new, higher equilibrium level not based on the bulk gas concentration. Longer residence times also lead to higher removal efficiencies.

In conclusion, the maximum NO_x removal efficiency was less than 20% in an air stream when the gas residence time was less than 8.5 seconds.

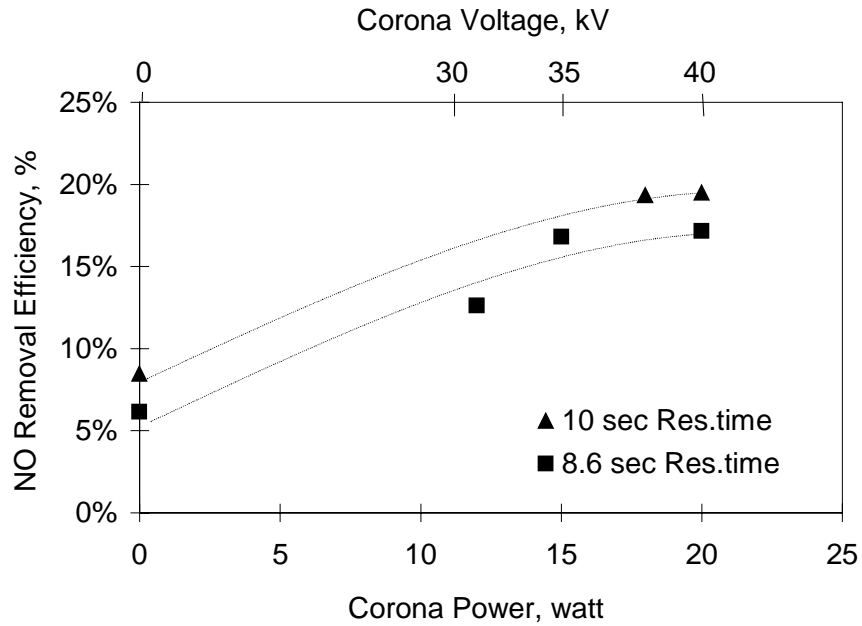


Figure 6.2 NO Removal Efficiency vs. Corona Power in Air

Wet ESP Experimental Conditions: In 25°C 43%RH air, 1000 ppm NO, 3.8 L/min 10°C water, with a positive pulsed corona.

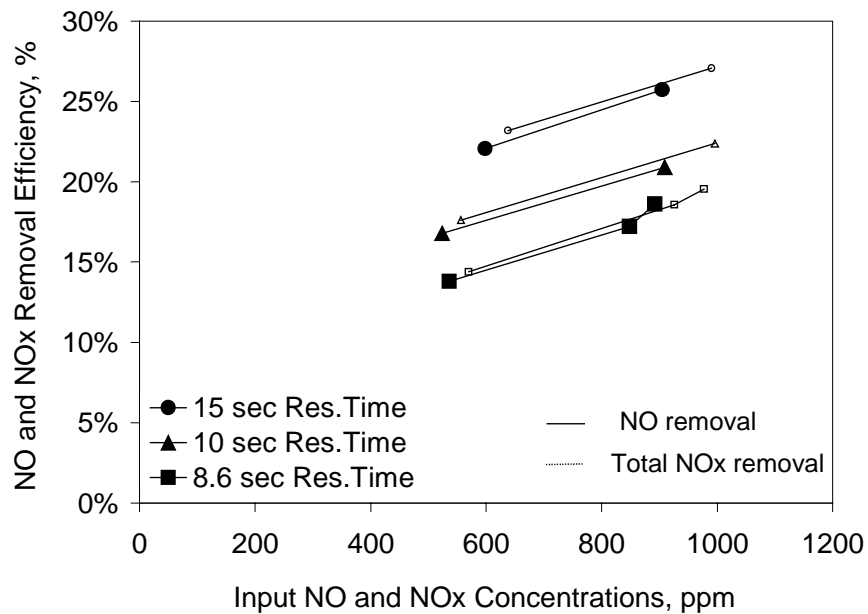


Figure 6.3 NO and NO_x Removal vs. Input NO_x Concentration and Gas Residence Time in Air

Wet ESP Experimental Conditions: In 25°C, 43%RH air, 3.8 L/min 12°C water, with a positive pulsed corona.

6.2.2 With Ozone Injection

The ozone concentration generated by the positive corona discharge was 0.23 ppm for the same experimental conditions in the wESP. Since the reaction between ozone and NO_x is at a one-to-one molar ratio, the amount of in-situ ozone would not be enough to be considered a primary removal mechanism in this process. Therefore, ozone was generated externally and introduced into the gas phase in the wESP to study the effects of ozone on the removal of NO_x .

The NO_x removal results of ozone injection in air- NO_x stream under a positive corona are shown in Figure 6.4. NO_x removal efficiency was lower than NO removal efficiency because the NO_2 level increased at the wESP outlet. The NO_2 increase resulted from the oxidation of NO by ozone. These results show that the presence of 300 ppm ozone improved both NO removal (from ~18% to ~50%) and NO_x removal (from ~10% to ~25%) in both the corona and non-corona discharge cases. Ozone has little effect on the efficiency of total NO_x removal.

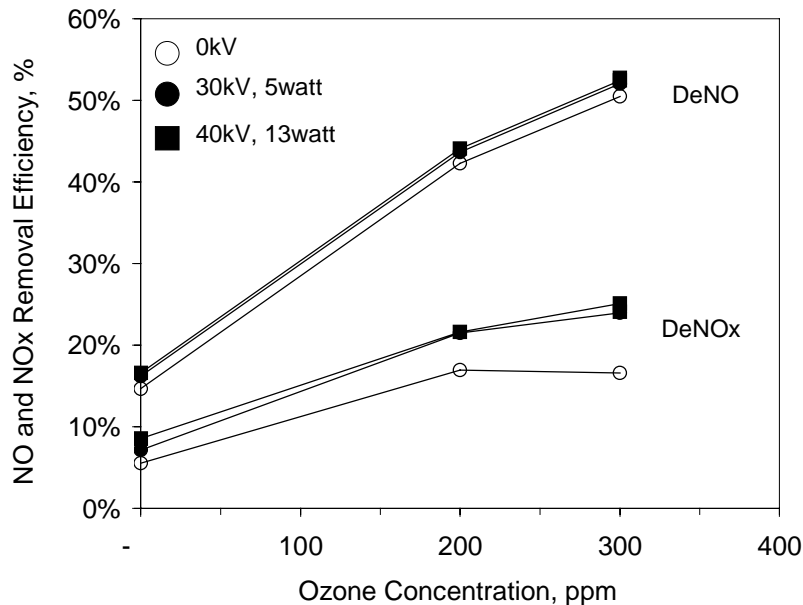


Figure 6.4 The NO and NO_x Removal vs. Ozone Injection in Air-NO_x Stream

Wet ESP Experimental Conditions: In 25°C 43%RH air, 717~776 ppm NO (797~878 ppm NO_x), 8.6 sec gas residence time, 3.8 L/min 12°C water, with a positive pulsed corona.

The NO_x removal results of ozone injection in SO₂/NO_x/air stream are shown in Figure 6.5 and Figure 6.6. Ozone improved NO and total NO_x removal from ~22% to ~40% in the conditions with and without a corona discharge, for both the NO_x/air and SO₂/NO_x/air streams. Ozone injection almost doubled the De-NO_x efficiency, yet still was lower than the practical level. Moreover, lower NO removal, but higher total NO_x removal, was obtained with the presence of SO₂ in the SO₂/NO_x/air stream. Therefore, the presence of SO₂ may slightly improve the NO₂ and total NO_x removal.

The presence of ozone improved the NO and NO_x removal; however, this improvement slightly decreased as the corona power increased. Experiments were conducted using positive corona discharge with ozone injection into the corona discharge region. These results show that ozone suppressed the corona effect and NO_x removal did not increase by applying or increasing corona.

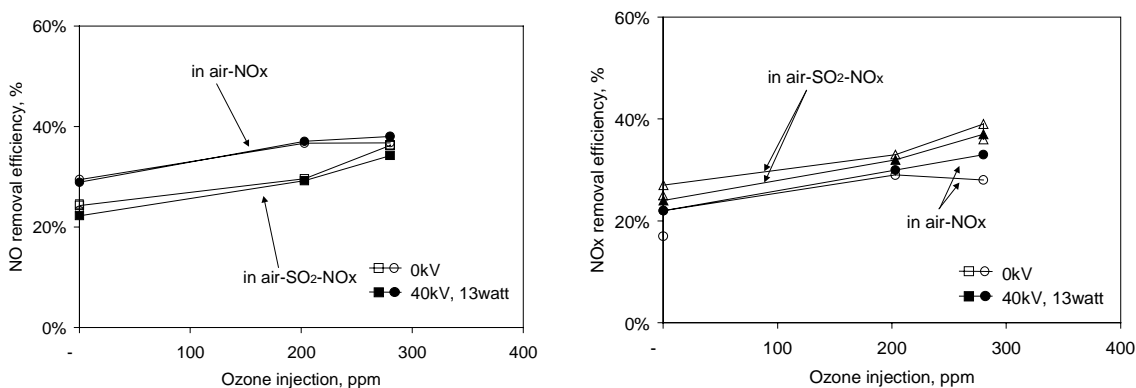


Figure 6.5 The NO and NO_x Removal vs. Ozone Injection in NO_x/Air and SO₂/NO_x/Air Streams

Wet ESP Experimental Conditions: In 25 °C 43%RH NO_x/air or SO₂/NO_x/air streams, with ~1100 ppm NO (~1230 ppm NO_x), 10 sec gas residence time, 3.8 L/min water 12 °C, with a positive pulsed corona.

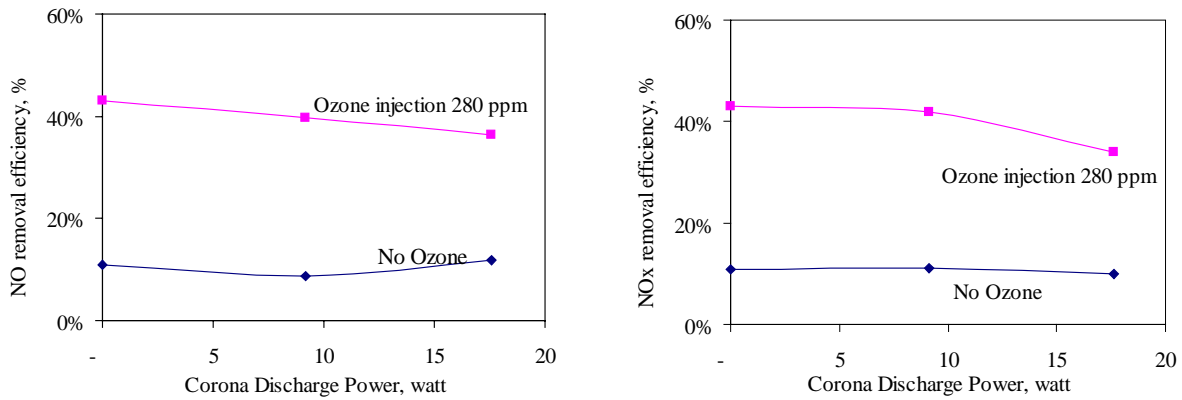


Figure 6.6 The NO_x Removal in SO₂/NO_x/Air Stream

Wet ESP Experimental Conditions: In 25°C 43%RH SO₂/NO_x/air stream, with ~1100 ppm NO (~1230 ppm NO_x), ozone injection into corona discharge region, 10 sec gas residence time, 3.8 L/min 12°C water, with a positive pulsed corona.

6.2.3 With Ammonia Injection Only (without Ammonium-Sulfur Aerosol)

In order to separate the effect of the in-situ ammonium sulfur aerosol, experiments in this section were conducted in the absence of SO₂ except in Figure 6.7b. The NO_x removal results of ammonia injection in NO_x-air stream show that NO removal was not improved in either corona or non-corona cases (Figure 6.7a). Corona power enhanced the SO₂ removal, but was not so helpful for NO_x removal. When a corona discharge was applied to a simulated flue gas, the improvement of NO_x removal efficiency was usually less than 2% before the voltage reached the operation limit. In a few cases, NO_x removal was decreased after the power was turned on, meaning that sometimes the generation of NO_x could be more than the removal of NO_x in corona discharge. When SO₂ was present (Figure 6.7b), however, the in-situ ammonium salt aerosols improved the NO removal efficiency by 10% and the total NO_x removal efficiency by almost 20%. This enhanced effect will be discussed in detail in the following section.

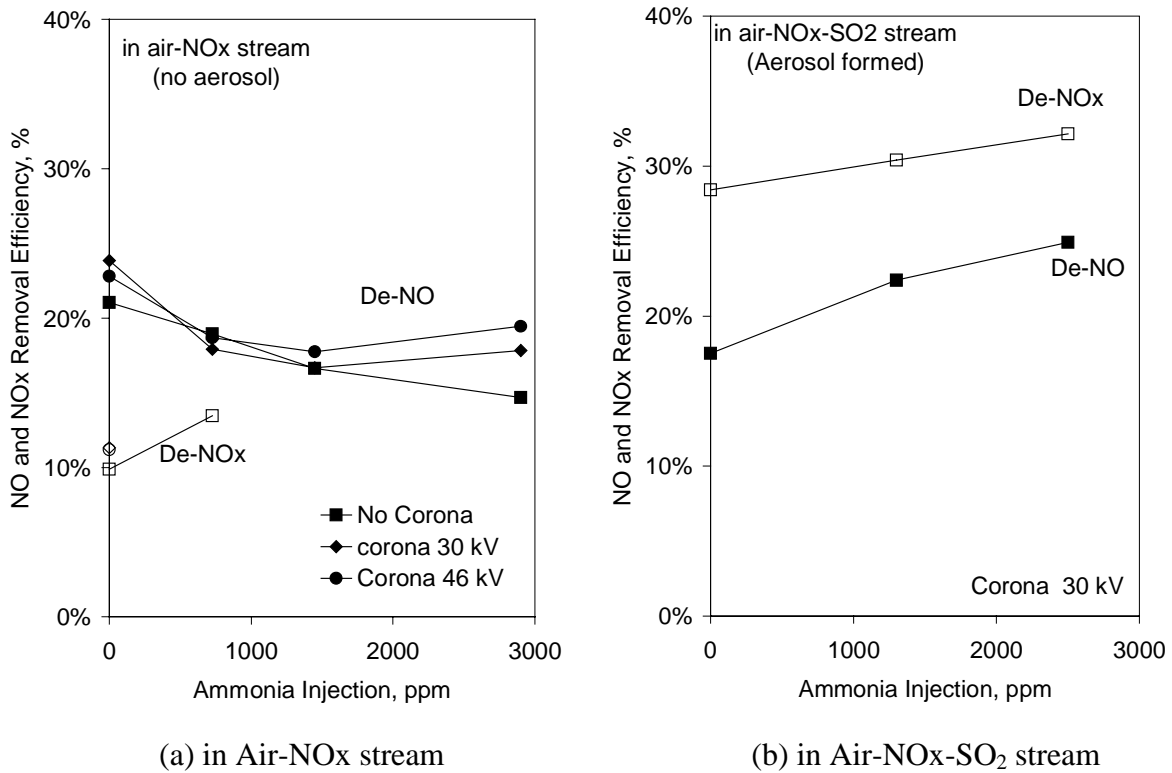


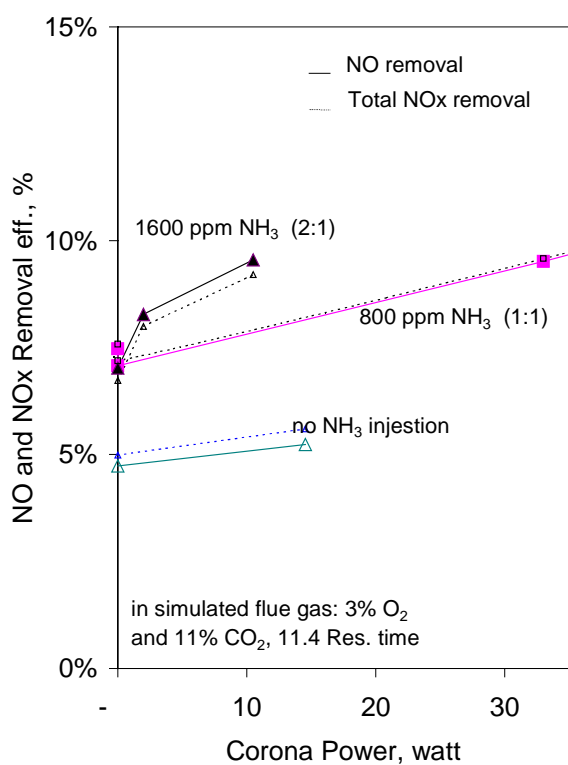
Figure 6.7 NO and NO_x Removal vs. Ammonia Injection in Air

Wet ESP Experimental Conditions: In 25°C 80%RH air, 714~776 ppm NO (762~878 ppm NO_x), 8.6 sec gas residence time, 3.8 L/min 12°C water, with a positive pulsed corona.

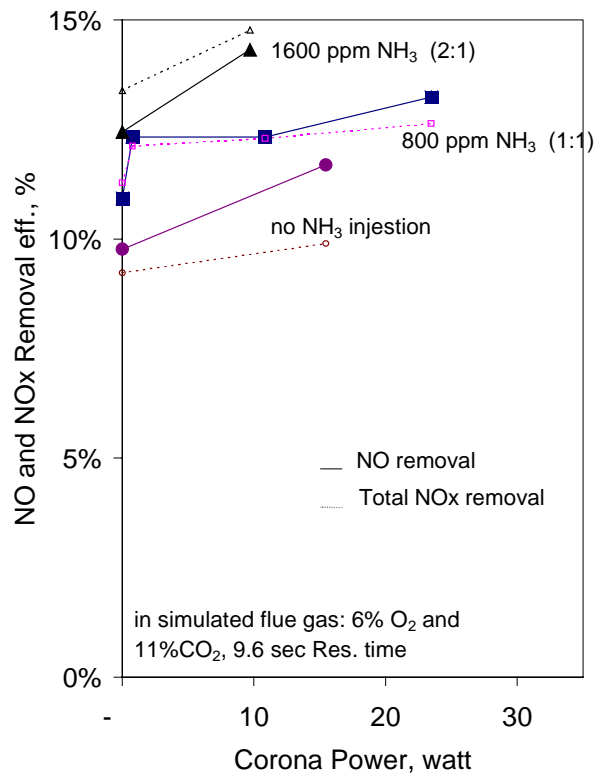
6.3 In Simulated Flue Gas

6.3.1 With Ammonia Injection Only

Ammonia was injected upstream of the wESP with a reaction time of 16.5 seconds before entering the corona discharge region. The NO removal results from ammonia injection in simulated 3%-O₂ and 6%-O₂ flue gases are summarized in Figure 6.8.



(a) 3%-O₂ Flue Gas



(b) 6%-O₂ Flue Gas

Figure 6.8 NO_x Removal with Ammonia Injection in Simulated Flue Gases

Wet ESP Experimental Conditions: In 25°C 3%-O₂ and 6%-O₂, 11% CO₂ humidified simulated flue gas, 800 ppm NO, no SO₂, 11.4 sec gas residence time, 3.8 L/min 12°C water, with a positive pulsed corona.

Before the injection of NH₃, the removal efficiency of 800 ppm NO_x was reduced from 20 ~ 30% (in air) to 5% (in 3%-O₂ flue gas) and 12% (in 6%-O₂ flue gas) because of the low oxygen levels. In non-corona cases, NH₃ increased NO removal by only 2% at a NH₃-NO_x stoichiometric injection ratio 1:1. When the ammonia injection was doubled, no significant increase of De-NO or De-NO_x efficiency was observed because no additional NO₂ was generated. Ammonia only helps the removal of NO₂, not NO [16, 20, 21].

In cases of corona discharge, removal efficiency increased with ammonia concentration because corona discharge oxidized additional NO to NO₂, although the amount of oxidation was

very small (~2%). These results indicate that oxygen sources are critical to the oxidation of NO, which leads to the NO_x removal in wESPs.

6.3.2 With Ozone Injection Only

The low oxygen content in the flue gas could not oxidize NO sufficiently to achieve a significant level of NO_x removal. Moreover, the corona power in the wESP was not enough to drive a significant chemical reaction to NO. Therefore, ozone was injected into a simulated 3%-O₂ flue gas as an oxidizer. Without ammonia injection, 200 ppm ozone injection increased the NO removal efficiency from 6% to 36% by oxidizing NO to NO₂ (Table 6.3). However, total NO_x removal increased only from 5% to 17%, which indicated that NO₂ cannot be removed efficiently in the wESP.

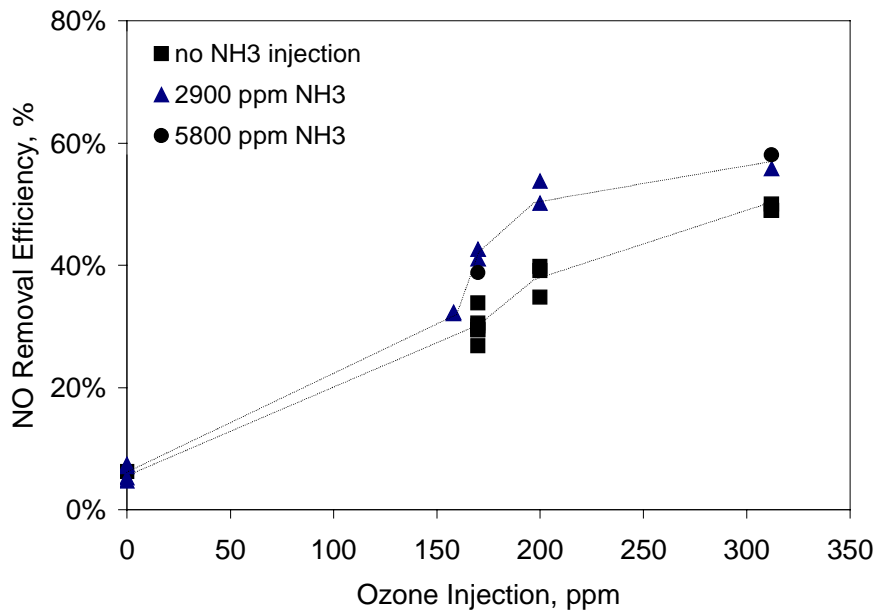
6.3.3 With Ammonia and Ozone Co-Injection (without Ammonium Sulfur Aerosol)

The effect of co-injection of ammonium and ozone were studied in a simulated flue gas (Figure 6.9). In order to separate out the effect of the in-situ ammonium sulfur aerosol, experiments in this section were conducted in the absence of SO₂.

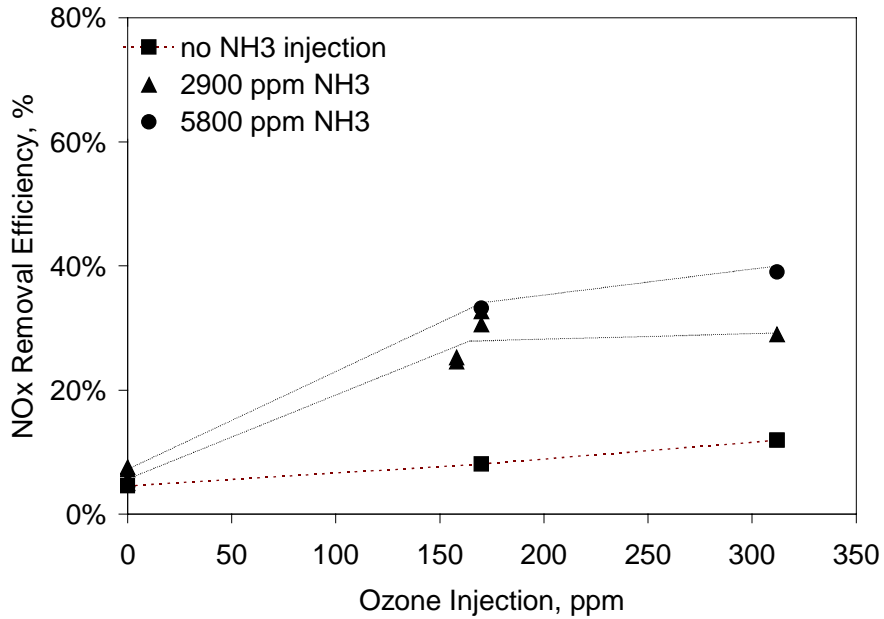
Applying NH₃ improved only little of the NO removal (Figure 6.9a), and no further improvement was measured from 2900 ppm to 5800 ppm of NH₃ injection. Most of the NO removal was done by ozone oxidation. 60% of NO was oxidized by 312 ppm ozone as reported in the previous results (Figure 6.4). Then the NO₂ reacted with NH₃ to form NH₄NO₃ aerosols. The absorption ability of NO₂ (Henry's constant 0.01 mol/L-atm) is higher than NO (0.0019 mol/L-atm), but still lower than SO₂ (1.24 mol/L-atm). Within the short gas residence time of wESP, the formation of ammonium salts helps to remove NO₂. Higher NH₃ concentration

produced more NH_4NO_3 aerosols, which resulted in more total NO_x removal. The maximum NO_x removal was 40% due to the formation of NH_4NO_3 aerosols, with the injection of 312 ppm O_3 and 5800 ppm NH_3 .

However, not all of NO_2 was converted to NH_4NO_3 aerosols. When 312 ppm O_3 and 5800 ppm NH_3 were injected, 60% of NO (419 ppm) was oxidized to NO_2 , but only 300 ppm of NO_x was removed. This means that 166 ppm NO_2 (including the 47 ppm of inlet NO_2) was not absorbed in water or converted to aerosols. In other words, 36% of the NO_2 could not be converted to aerosols within 8.6 seconds, even with abundant NH_3 . This is the reason why the total NO_x removal efficiency was less than the NO removal efficiency. The next section will show that the presence of ammonium sulfur aerosols not only converted this 36% of NO_2 to NH_4NO_3 aerosols, but also enhanced another 20% of NO_x removal.



(a) **NO Removal**



(b) NO_x Removal

Figure 6.9 The NO_x Removal vs. Ammonium and Ozone in Simulated Flue Gas

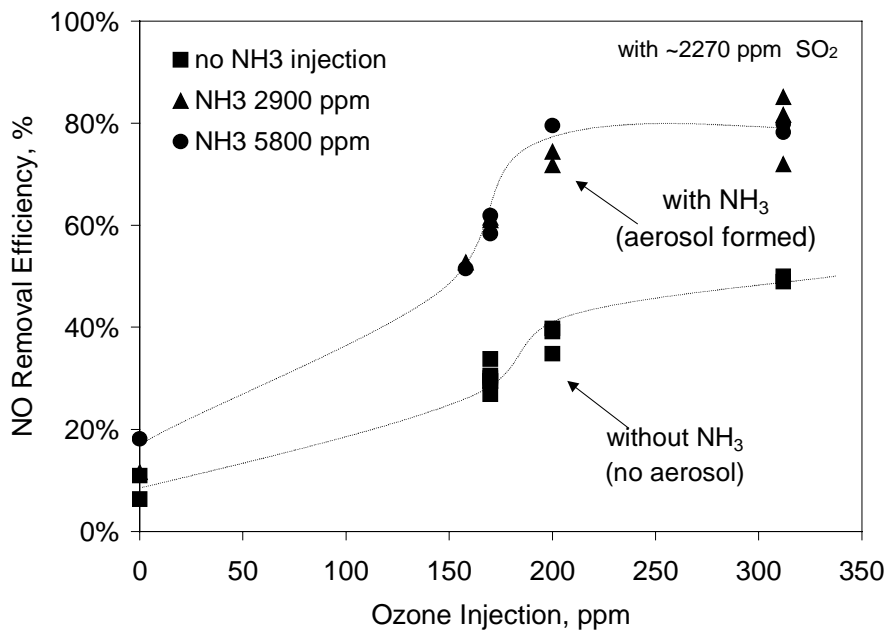
Wet ESP Experimental Conditions: In 25°C 3% O₂, 8~11% CO₂ humidified simulated flue gas, with 700~800 ppm NO (750~850 ppm NO_x), without SO₂, 8.6 sec gas residence time, 3.8 L/min 12°C water, with 30~40 kV negative pulsed corona.

6.4 Enhanced Effect of In-situ Ammonium Sulfur Aerosols

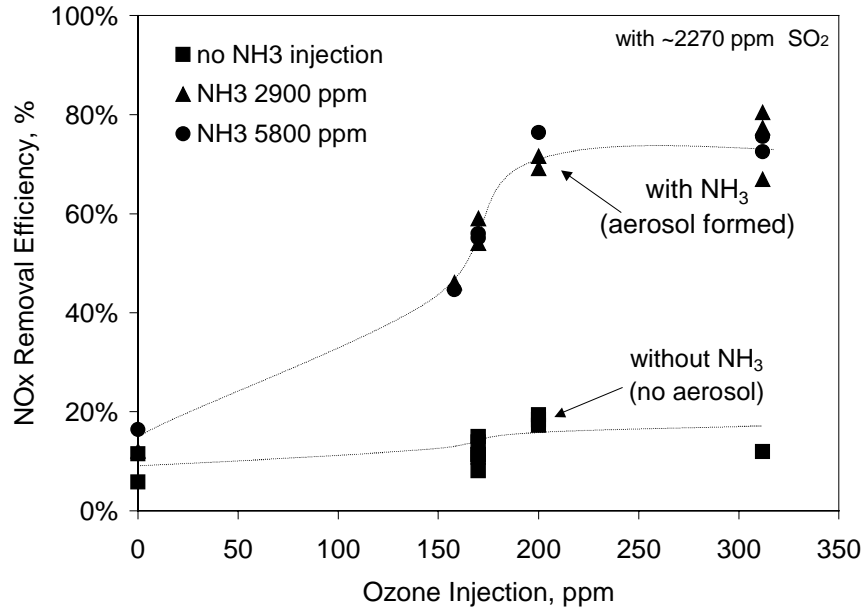
Very high NO_x removals were measured when the in-situ ammonium sulfur aerosols were formed in a simulated flue gas that contained ammonia, sulfur dioxide, and ozone (Table 6.3). The high collection efficiency of aerosols in the wESP was visually confirmed. With the co-presence of 2500 ppm SO₂ and 2500 ppm NH₃ (ammonia to pollutants stoichiometric ratio 0.44), without ozone, total NO_x removal increased from 18% to 32% (Figure 6.7a and b). With 200 ppm ozone injection, total NO_x removal increased to 72% (Figure 6.11). Further increasing the additives to 312 ppm O₃ and 2900 ppm NH₃ (stoichiometric ratio 0.53), total NO_x removal increased to 80% (Figure 6.10).

Figure 6.10 clearly shows the enhanced effect of in-situ aerosols. Without aerosols, ozone improved the total NO_x removal very little (Figure 6.10b). When the aerosols were formed, 200 ppm of ozone resulted in the maximum total NO_x removal (~80%). Ozone input higher than 200 ppm did not further improve the removal. Doubling NH₃ also did not further increase the amount of aerosols or NO_x removal.

The significance of this enhanced effect by the in-situ ammonium salt aerosols was verified by adjusting the amount of in-situ aerosols as shown in Figure 6.11. With a 2500 ppm ammonia injection, more SO₂ resulted in more in-situ aerosols because excess NH₃ was present. Aerosols increased both the NO and NO₂ removal efficiency.



(a) NO Removal



(b) NO_x Removal

Figure 6.10 The Improved NO_x Removal vs. Ammonium and Ozone in Simulated Flue Gas

Wet ESP Experimental Conditions: In 25°C 3% O₂, 8~11% CO₂ humidified simulated flue gas, with 700~800 ppm NO (750~850 ppm NO_x), 2200~2500 ppm SO₂, 8.6 sec gas residence time, 3.8 L/min 12°C water, with 30~40 kV negative pulsed corona.

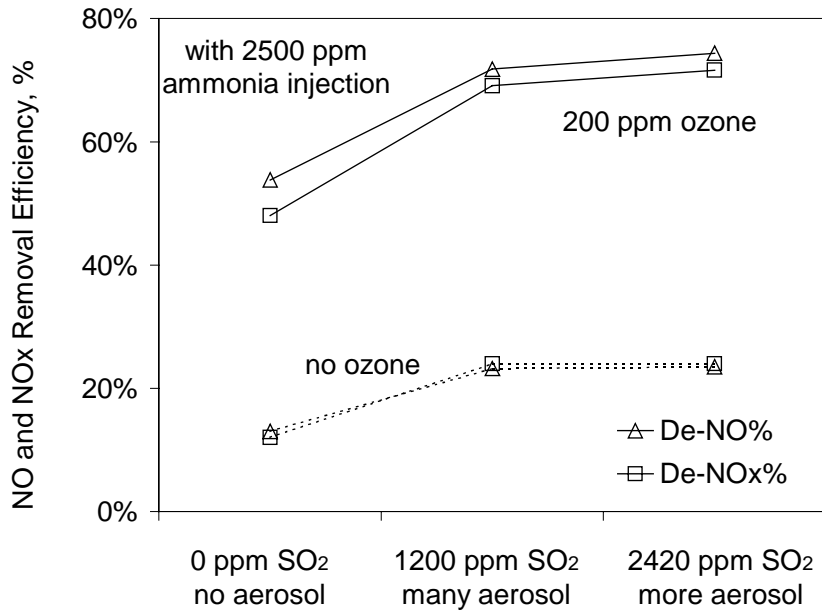


Figure 6.11 The Improved NO_x removal Efficiency vs. Ammonium Sulfur Aerosols

Wet ESP Experimental Conditions: 200 ppm O₃ tests: in 4.3%-O₂ simulated flue gas; Without O₃ tests in 6%-O₂ simulated flue gas; All tests: in 25°C 8% CO₂ humidified simulated flue gas, 700 ppm NO, 8.6 sec gas residence time, 3.8 L/min 12°C water, with a positive pulsed corona.

Summarizing the results in Figure 6.10 and Figure 6.11, aerosols enhanced both the NO and NO₂ removal efficiency. When ozone was injected, aerosols increased NO removal by 30 ~ 40%, and total NO_x removal by 50 ~ 68% (depending on the ozone concentration). And the agreement between NO and NO_x removal efficiencies indicated that most of the NO₂ was removed. Ozone played an important role as well. Without ozone, ammonium sulfur aerosols enhanced NO and NO_x removal by only 10% because little NO₂ was available to remove. With 200 ppm ozone injection, the formation of NH₄NO₃ increased 30 ~ 36% of total NO_x removal, even without ammonium sulfur aerosols (Figure 6.9 and Figure 6.11). And ammonium sulfur aerosols enhanced the NO_x removal efficiency by another 24% (Figure 6.11). Therefore, the oxidation of NO has to be enhanced by introducing strong oxidizers, such as ozone, or by increasing the corona discharge power.

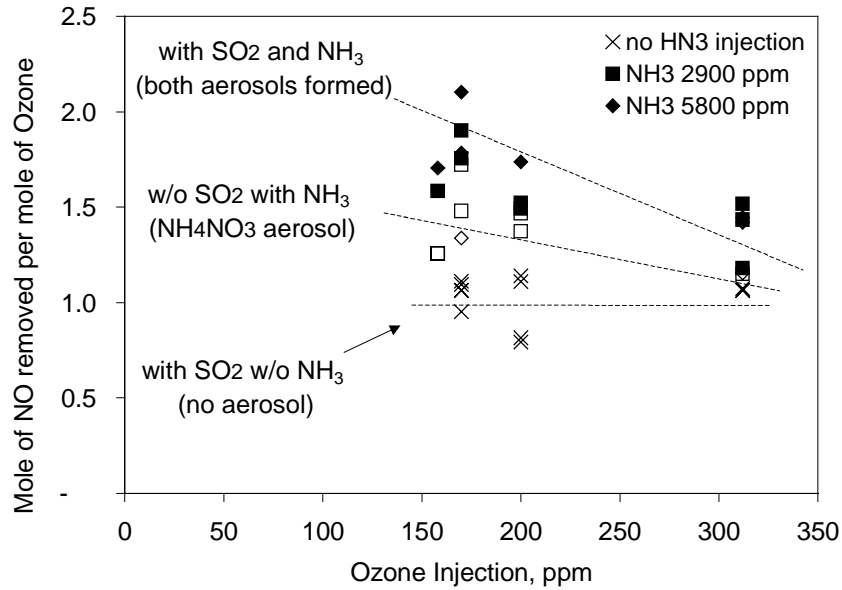
It has been reported that particles could enhance the removal of SO₂, as discussed in section 2.6.4 [5, 63]. The NO_x removal results presented here shows that the in-situ ammonium salt aerosols produced from the reaction of NH₃ and SO₂ substantially enhanced NO_x removal. The in-situ aerosols were well spread in the flue gas and enhanced the oxidation of NO, as well as the formation of NH₄NO₃. It is believed that these aerosols served as highly efficient adsorbents and provided tremendous surface area to enhance the De-NO_x chemical reactions. O₃, NO, H₂O, and NH₃ were adsorbed on the surface of aerosols. First the aerosols enhanced the NO oxidation, and then enhanced the reaction between NO₂, H₂O, and NH₃. This explains why both NO₂ removal and NO removal were improved when the aerosols were present.

The aerosol formation itself is a SO₂ removal process that improved SO₂ removal to ~100%. Once the SO₂ and NO_x were separated from the gas, all the pollutants and byproducts

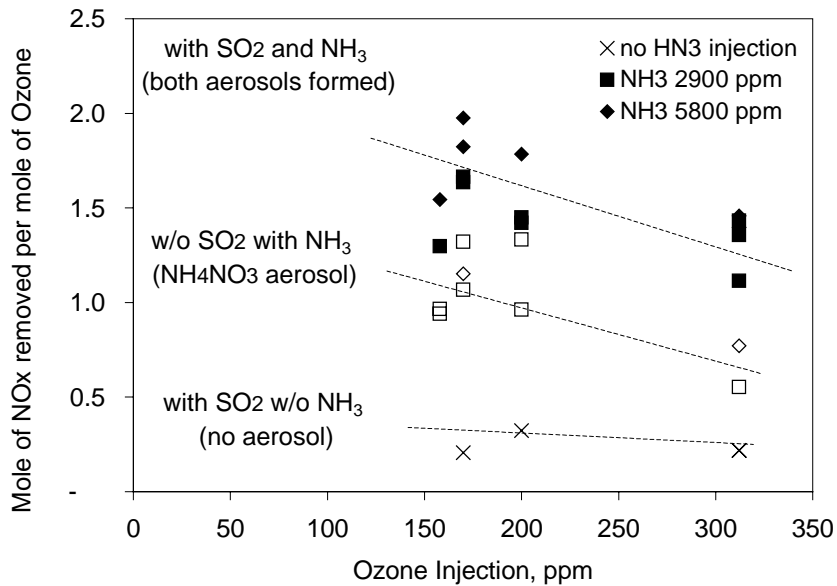
are trapped on the aerosol surface and reverse reactions are greatly hampered [5]. These aerosols can be easily removed from gas phase into water in a wESP. Any un-reacted gas pollutants absorbed on the surface are removed with the aerosols.

6.4.1 Molecules of NO Removed per Molecule of Ozone

Ozone generation requires considerable power. So it is important to know how many molecules of NO can be removed per molecule of O₃ injected. Figure 6.12a shows that without the formation of salt aerosols, one molecule of O₃ removed (oxidized) one molecule of NO. But only less than half molecule of NO_x was removed by one molecule of O₃ because the NO₂ could not be removed effectively in the wESP. However, with the formation of ammonium nitrate aerosol, approximately one molecule of NO_x was removed by one molecule of O₃. Furthermore, with the enhanced effect of ammonium sulfur aerosols, one molecule of O₃ removed 2 to 2.5 molecules of NO and NO_x. The effectiveness of ozone decreased as more ozone was injected. Therefore, there is a compromise between the NO_x removal and the amount of ozone injection.



(a) Molecules of NO Removed per Molecule of Ozone



(b) Molecules of NO_x Removed per Molecule of Ozone

Figure 6.12 Molecules of NO Removed per Molecule of Ozone

Wet ESP Experimental Conditions: In 25°C 3% O₂, 8~11% CO₂ humidified simulated flue gas with 700~800 ppm NO (750~850 ppm NO_x), 2200~2500 ppm SO₂, 8.6 sec gas residence time, 3.8 L/min 12°C water, with 30~40 kV negative pulsed corona.

6.4.2 Ammonia Slippage

Ammonia slippage is always an environmental concern. Although high amounts of NH_3 were injected into the system, the outlet NH_3 concentration is below the detection limit (100 ppm) of our ammonia analyzer whenever ammonium salt aerosols were formed. The actual emission concentration should be determined by an ammonia analyzer with a lower detection limit. Low NH_3 emissions can be expected because of the following three reasons: (1). NH_3 with equal or less than the stoichiometric (NH_3 to SO_2 and NO_x) ratio was added into the system, (2). NH_3 is soluble and un-reacted NH_3 dissolves in the water in the wESP. Dissolved NH_3 will not release back to the air if the solution is maintained at high pH level before treatment, and (3). Corona discharge further enhances the NH_3 absorption rate as the absorption of SO_2 in the wESP.

6.5 Ultimate Analysis of the Ammonium Salt Aerosols

In the experiments of SO_2 and NO_x removals shown in Figure 6.10, the 2900 ppm of input NH_3 was approximately the sum of the concentrations of removed SO_2 (98% of 2400 ppm) and NO_x (72% of 700 ppm). Therefore, the formed ammonium salt aerosols were more likely to be ammonium bi-sulfite (NH_4HSO_3) or bisulfate (NH_4HSO_4), along with ammonium nitrate (NH_4NO_3). This estimation is further confirmed by the ultimate contents analysis of collected aerosols.

The byproducts were collected and analyzed by a CHNS analyzer for C, H, and N contents and by a total sulfur analyzer for the sulfur content. The oxygen content was estimated by assuming that the remaining content is oxygen. The analysis results of two aerosol samples are listed in Table 6.2. These samples were collected from the wESP tests with 98% removal of

2400 ppm SO₂ and 74% removal of 700 ppm NO_x. The constitution of byproducts was estimated by minimizing the square differences between the analysis results of C, H, N, S, and O values and the combination of all the possible compounds (ammonium sulfite, bisulfite, sulfate and bisulfate). The most possible combination of byproducts is 12.4% NH₄NO₃, 81.1% (NH₄)HSO₄, 1.5% (NH₄)HCO₃, and 5% H₂O. The ultimate contents of this estimated byproduct mixture are close to the analysis results (Table 6.2).

Table 6.2 Ultimate Analysis of the Ammonium Salt Aerosols Collected at wESP

	C	H	N	S	O
Experimental Results					
Analysis #1	0.11%	1.65%	15.5%	26.2%	56.5%
Analysis #2	0.33%	1.46%	18.1%	17.5%	62.7%
Average of #1 & #2	0.22%	1.56%	16.8%	21.9%	59.6%
Theoretical Calculation					
NH ₄ NO ₃	0%	5.00%	35.0%	0%	60.0%
(NH ₄) ₂ SO ₃	0%	6.9%	24.1%	27.6%	41.4%
(NH ₄) ₂ SO ₄	0%	6.1%	21.2%	24.2%	48.5%
(NH ₄)HSO ₃	0%	5.1%	14.1%	32.3%	48.5%
(NH ₄)HSO ₄	0%	4.35%	12.2%	27.8%	55.7%
(NH ₄)HCO ₃	15.2%	6.33%	17.7%	0%	60.8%
H ₂ O	0%	11.11%	0%	0%	88.9%
Best Fitting Result: 12.4% NH₄NO₃ and 81.1% (NH₄)HSO₄ with 1.5% (NH₄)HCO₃ and 5% H₂O	0.22%	4.80%	14.5%	22.6%	57.9%

6.6 Summary of wESP Performance

The summary of the maximum removal efficiency in air and simulated flue gas in the wESP are listed in Table 6.3. The removal mechanisms of NO and NO_x in air and the 3%-O₂ simulated flue gas are summarized and illustrated in Figure 6.13 to Figure 6.15.

Table 6.3 Summary of Maximum Removal Efficiency in the wESP

	No In-Situ Ammonium Sulfur Aerosols Formed				In-Situ Ammonium Sulfur Aerosols Formed			
	Pulsed Wet-ESP	With Ammonia Injection		With Ozone Injection	With Ammonia and Ozone Co-Injection		With Ammonia and Ozone Co-Injection	
Corona Discharge	30 kV	30 kV	30 kV	30 kV	30 kV	30 kV	40 kV	40 kV
Ammonia	0	2500 ppm	5800 ppm	0	2500 ppm	5800 ppm	2900 ppm	5800 ppm
Ozone	0	0	0	200 ppm	200 ppm	200 ppm	312 ppm	312 ppm
Maximum SO ₂ Removal	50~55%	88~95%	98~100%	76~79%	~98%	~99%	~100%	~100%
Maximum NO Removal (3%-O ₂ flue gas)	6%	n.a.	14%	36%	74%	80%	82%	78~80%
Maximum NO _x Removal (3%-O ₂ flue gas)	5%	n.a.	13%	17%	72%	79%	77%	72~76%
Maximum NO Removal (in Air)	28%	32%	n.a.	57~59%	64~67%	n.a.	n.a.	n.a.
Maximum NO _x Removal (in Air)	18%	25%	n.a.	39~43%	51~57%	n.a.	n.a.	n.a.

n.a.: not available.

Experiments were conducted in air or in 3% O₂, 11% CO₂ humidified simulated flue gas at 25°C, with ~700 ppm NO, ~2400 ppm SO₂, 8.6 sec gas residence time, 3.8 L/min 12 °C water, with pulsed coronas.

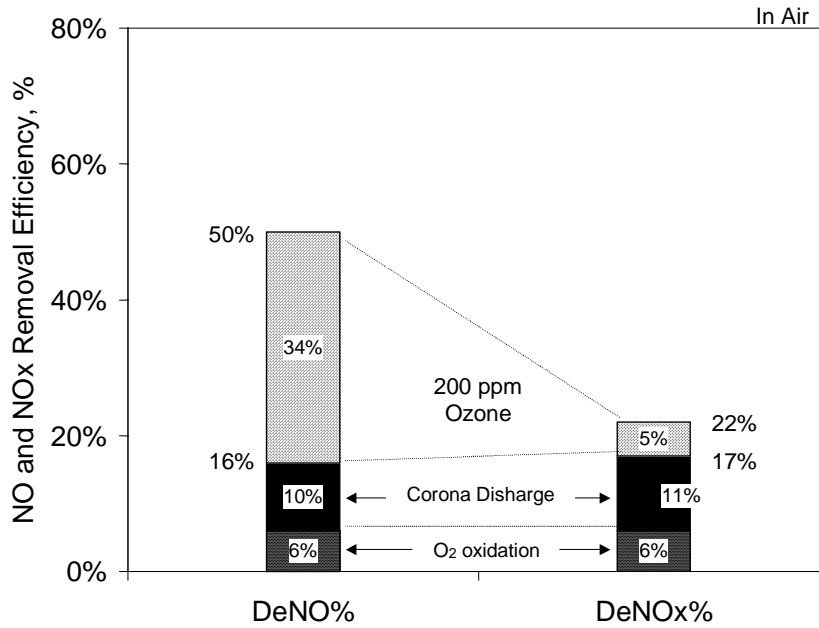


Figure 6.13 Removal Mechanisms of NO and NO_x in Air

Wet ESP Experimental Conditions: In 25°C 43%RH air, 800~1000 ppm NO, 8.6~10 sec gas residence time, 3.8 L/min 10°C water, with a positive pulsed corona.

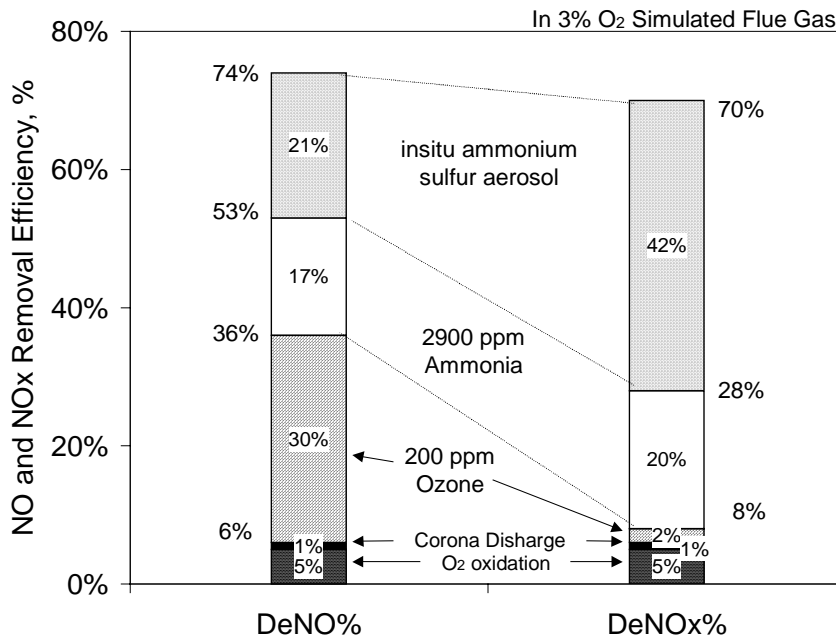


Figure 6.14 Removal Mechanisms of NO and NO_x in 3%-O₂ Simulated Flue Gas

Wet ESP Experimental Conditions: In 25°C 3%-O₂ 8~11% CO₂ humidified simulated flue gas, 800~1000 ppm NO, 2500 ppm SO₂, 10 sec gas residence time, 3.8 L/min 10°C water, with pulsed coronas.

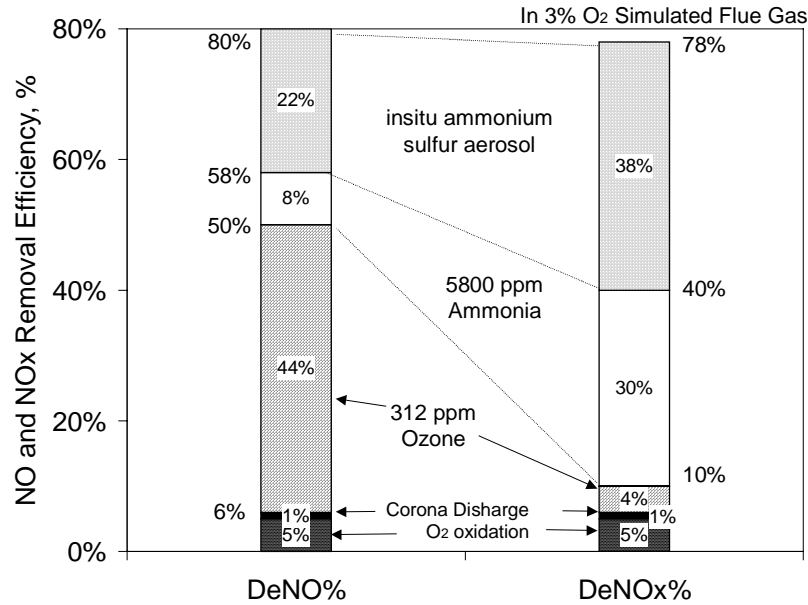


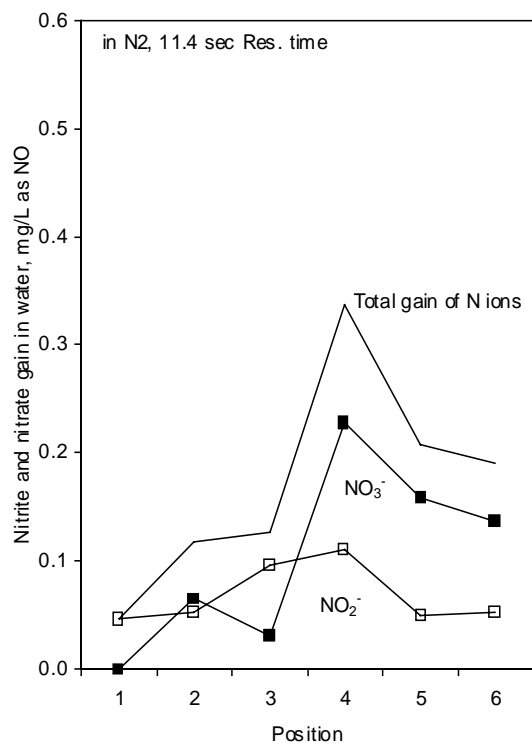
Figure 6.15 Removal Mechanisms of NO and NOx with More Additives in 3%-O₂ Simulated Flue Gas

Wet ESP Experimental Conditions: In 25°C 3%-O₂ 8~11% CO₂ humidified simulated flue gas, 800~1000 ppm NO, 2500 ppm SO₂, 10 sec gas residence time, 3.8 L/min 10°C water, with pulsed coronas.

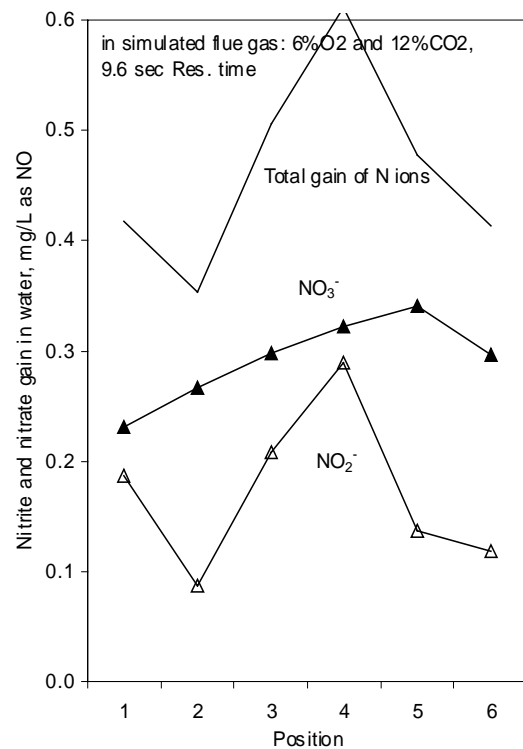
6.7 Fates of Nitrogen

6.7.1 Concentrations of Nitrite and Nitrate in Water

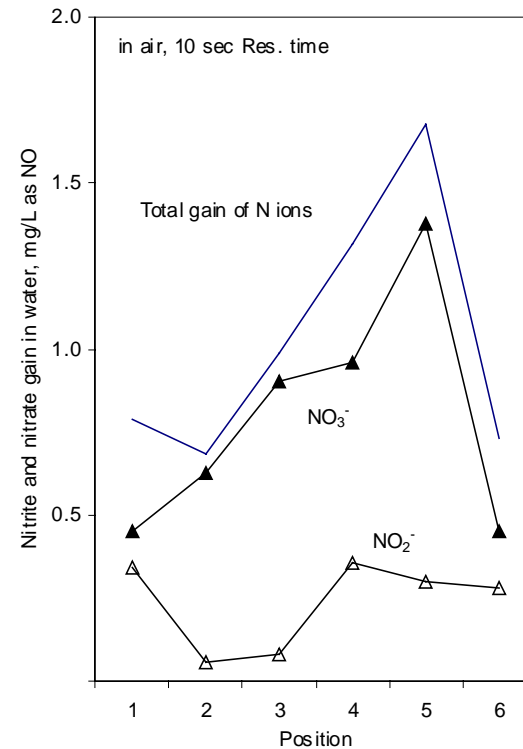
Wet ESP tests were conducted in nitrogen, in air and in simulated flue gas. Nitrite and nitrate concentrations were measured at six wESP positions and converted to the mass of nitric oxides gas (mg/L as NO) for comparison. Raw tap water was sampled to measure the original nitrate content in each test. The concentrations of nitrite and nitrate for water samples of the six compartments are shown in Figure 6.16. The results show that most of the removal occurred at the corona discharge region (position 2~5). The removal increased as the oxygen level of the gas stream increased, which shows the NO_x removal was very sensitive to the oxidation of NO. The results of another 5 samples are shown in Figure 6.17. Nitrite concentrations in the middle phases were generally greater than the cases in the gas inlet and outlet phases.



(a)



(b)



(c)

Figure 6.16 Increased Nitrite and Nitrate Concentrations of wESP tests in Air, N₂ and Simulated Flue Gas

Wet ESP Experimental Conditions: In air, N₂ and humidified 6% O₂, 11% CO₂ simulated flue gas stream (25°C), 770 ppm NO, no SO₂, 3.8 L/min water (12°C), with 35 kV positive pulsed corona. The nitrate concentration in this figure has been subtracted by the nitrate content of raw tap water.

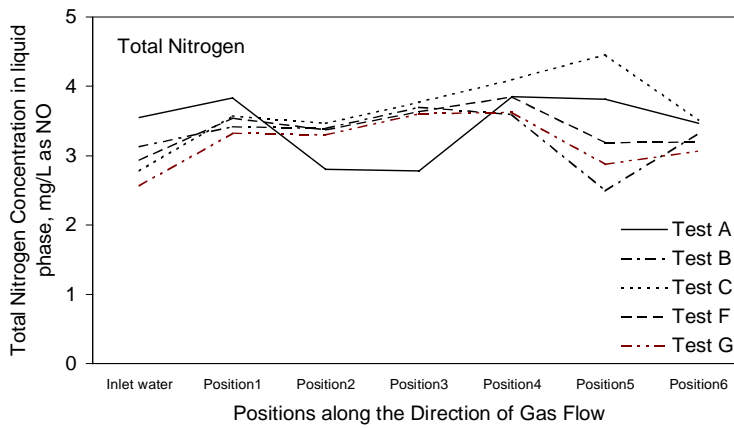
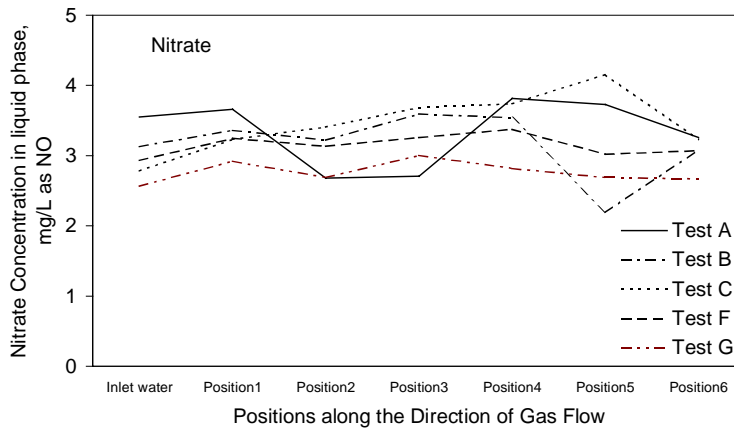
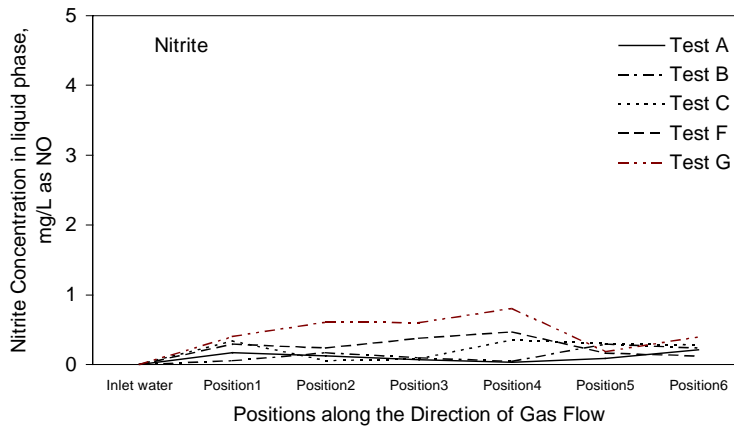


Figure 6.17 Nitrite and Nitrate Concentrations of Water Samples of Six Positions

Wet ESP Experimental Conditions: Tests A, B, C: In air (25°C), 1000 ppm NO_x, 2000 ppm SO₂. Tests F, G: In humidified 5.8% O₂, 11% CO₂ simulated flue gas (25°C), 770 ppm NO_x, 2000~3000 ppm SO₂. All Tests: 10 sec gas residence time, 3.8 L/min water (12°C). Test A no corona, Test B +65 kV, Test C +68 kV, Test F -32 kV, Test G -30 kV pulsed corona.

6.7.2 Mass Balance of Nitrogen

The mass balance of nitrogen in both gas and liquid phases was conducted to verify the results of gas phase removal. As shown in Table 6.4, three wESP tests were conducted for various operational conditions. For each wESP test, the nitrate concentration of raw tap water was sampled and subtracted from the results. Results show that approximately half of the removed nitrogen was not sampled in the liquid phase.

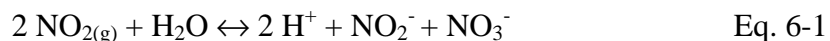
Table 6.4 Mass balance of Nitrogen by Ion Chromatograph Method

Test#	Removed from the Gas Phase			Increased in the Liquid Phase			Difference in nitrogen uptake*
	NO _x Inlet	NO _x Outlet	Total N Removed	Nitrite NO ₂ ⁻	Nitrate NO ₃ ⁻	Total N Increased	
	ppm	ppm	mg/sec as NO	mg/L as NO	mg/L as NO	mg/sec as NO	%
A	1,000	800	0.50	0.50	3.26	0.22	57%
B	1,000	790	0.53	0.66	3.16	0.19	63%
C	899	710	0.47	1.03	3.57	0.25	46%

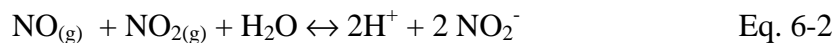
Wet ESP Experiment Conditions: In 20°C 43%RH air, 10 sec gas residence time, 3.8 L/min 10°C water, Test A: no corona, B: 47.5 watt, C: 40.8 watt positive pulsed corona. Nitrite and nitrate concentrations have been converted to the mass of nitric oxides gas (mg as NO)

* Difference in nitrogen uptake: Difference of liquid phase total nitrogen increase and gas phase total nitrogen removed.

According to the NO_x removal theory in section 4.4.3, when one mole of NO₂ dissolves in water, the equivalent amounts of NO₂⁻ and NO₃⁻ ions exist in the solution. However, HNO₂ is a weak acid and easily to decompose back to NO and NO₂ gases at room temperature if NO₂⁻ ion is not fixed by basic species [57]. The equilibrium constants of two major nitrogen oxides reactions between aqueous and gas phases are listed below [59]. However, the reaction rate constants for these reactions are not available.



Equilibrium constant: $K_1 = 2.44 \cdot 10^2 \text{ M}^4/\text{atm}^2$ @298K [59]



Equilibrium constant: $K_2 = 3.28 \cdot 10^{-5} \text{ M}^4/\text{atm}^2$ @298K [59]

By combining the above two reactions, the ratio of nitrate to nitrite ions at equilibrium in the system is given by:

$$\frac{[\text{NO}_3^-]}{[\text{NO}_2^-]} = \frac{P_{\text{NO}_2}}{P_{\text{NO}}} \frac{K_1}{K_2} \quad \text{Eq. 6-3}$$

where $K_1/K_2 = 7.4 \times 10^6$ at 298K.

As long as the partial pressure of NO_2 is greater than 1/1000 of the partial pressure of NO , $[\text{NO}_3^-]$ is 7400 times greater than $[\text{NO}_2^-]$ at equilibrium. Since the water samples were stayed at room temperature for couple hours before being analyzed, the nitrite concentrations were expected much less than the nitrate concentrations. This is the reason that the mass concentrations of nitrite in the liquid phase were much less than those of nitrate as shown in Table 6.4, which made the total mass of nitrogen in the liquid phase was less than that in the gas phase.

7. SO₂ REMOVAL RESULTS OF BATCH TESTS

SO₂ mass transfer rates are compared for various experimental conditions. The method to determine the overall mass transfer coefficient, K_{OG} , is addressed in detail in the theory discussion of section 4.7.1.

7.1 Gas Mixing

The effect of SO₂ absorption rates of gas phase mechanical mixing was studied in the batch reactor as shown in Figure 7.1 and Figure 7.2. A variable speed gas-mixing fan was used in the first plexi-glass batch reactor. A CPU fan controlled by input electrical power was used in the new glass batch reactor. The relationship of fan speed and power input is determined by:

$$P = F_D v_m = n \left(C_D A_p \rho \frac{v_m^2}{2} \right) v_m \quad \text{Eq. 7-1}$$

where:

F_D = Drag force on fan paddles, dyne

v_m = Mean velocity of fan paddles, cm/sec

n = Number of fan paddles

C_D = Drag coefficient, 1.2

A_p = Surface area of fan paddles, 5.25 cm²

ρ = Density of air, 0.001205 g/cm³

The results showed that removal efficiency increased as the degree of gas mixing increased. The trends indicate that the value of the mass transfer coefficient increases as mixing was increased until it approaches an upper limit. The maximum mass-transfer enhancement by gas-phase mechanical mixing is around 1.60 times with less than 0.8 watt (power density: 27.4 watt/m³) input of mixing power for the tests of both reactors. The fan input power was set at 0.872 watt for all other tests to avoid the incomplete gas mixing.

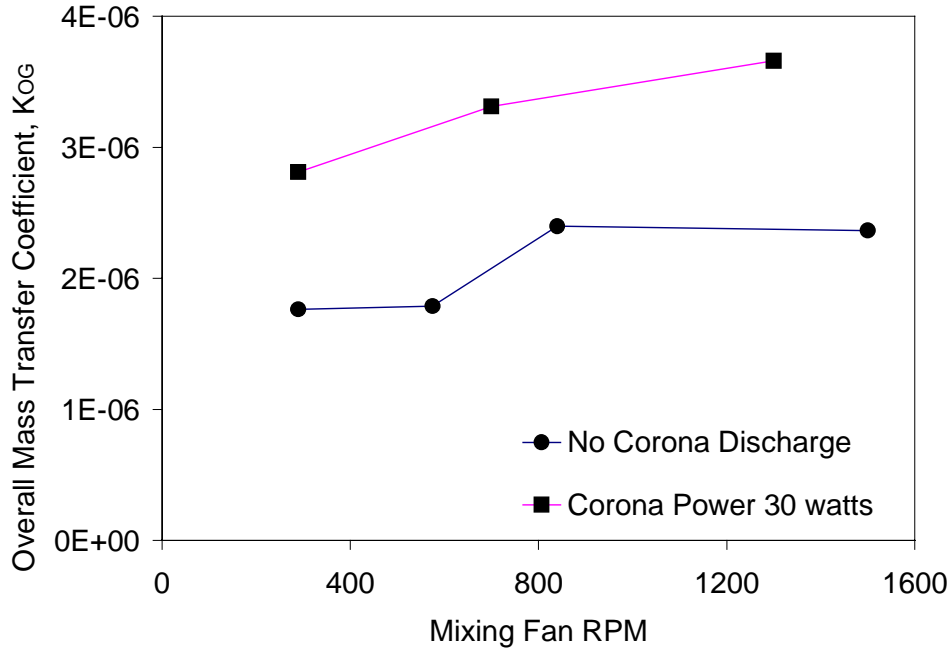


Figure 7.1 Overall Mass Transfer Coefficient vs. Gas Mixing Fan Speed

Batch Reactor Test Condition: 5200 ppm SO₂ in plexi-glass reactor, in pure N₂ and boiled de-ionized water. Total volume of gas chamber: 29247 cm³, without corona discharge, room temp.

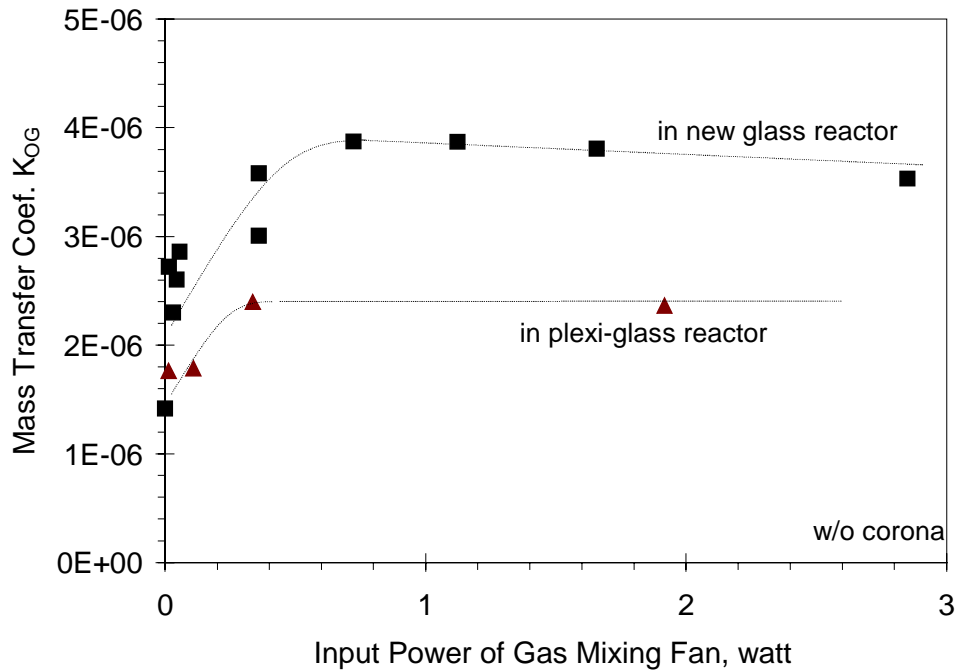


Figure 7.2 Overall Mass Transfer Coefficient vs. Gas Phase Mixing

Batch Reactor Test Condition:: 3100 ppm SO₂ in new glass reactor, 5200 ppm SO₂ in plexi-glass reactor, in pure N₂ and boiled de-ionized water. Total volume of gas chamber: 29247 cm³, without corona discharge, room temp.

7.2 Liquid Mixing

The SO₂ absorption rates are affected by the liquid phase mechanical mixing as shown in Figure

7.3.

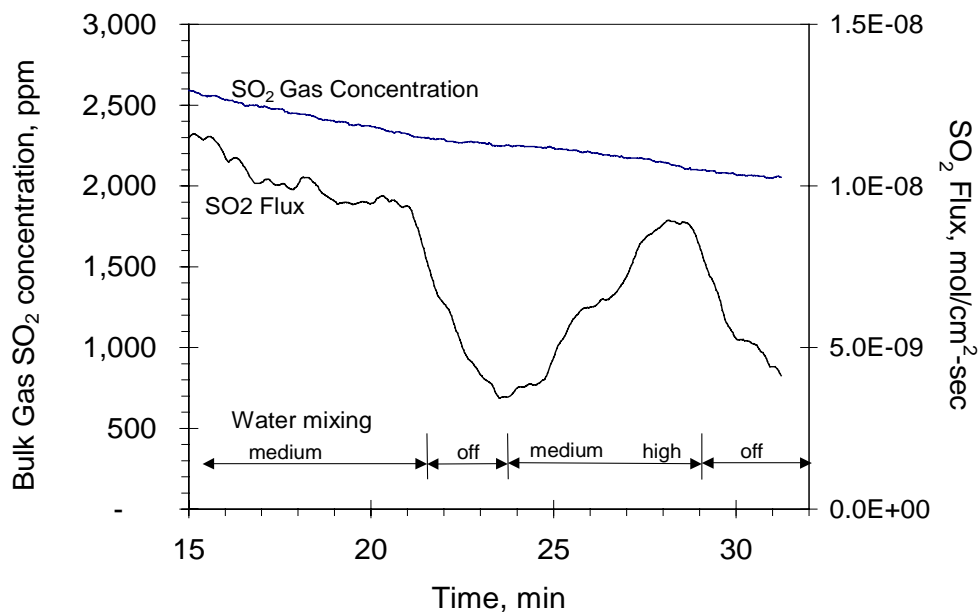


Figure 7.3 Overall Mass Transfer Coefficient vs. Liquid Phase Mixing

Batch Reactor Test Condition: 3340 ppm SO₂ in pure N₂, de-ionized water, at room temperature, no corona discharge.

7.3 Pulsing

Both polarities have the ability to spark to the grounded plate if the power is too high. The highest achievable voltages were 70 kV and 55 kV in the wESP system and the batch reactor used in experiments, respectively. The high power level could be achieved only when the voltage was pulsed, because pulsing increased the spark voltage.

It is found experimentally that pulsing not only raise the spark limit, but also provide more a energetic corona at the same corona voltage level. Pulsing corona resulted in better mass transfer of SO₂ than DC corona as shown in the Figure 7.4, which was also reported in other researches [5, 15, 16].

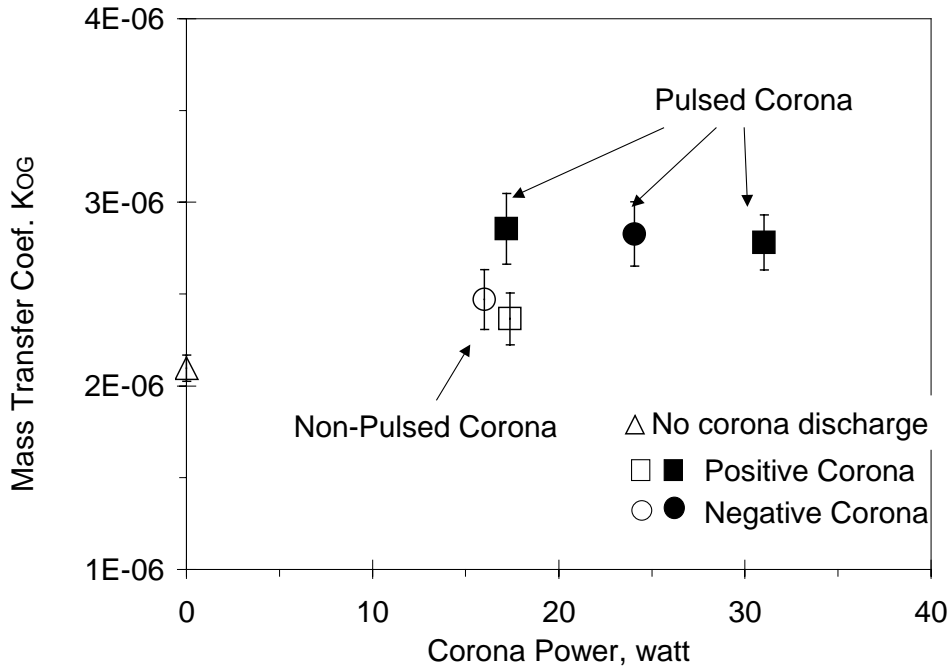


Figure 7.4 The Effect of Pulsing on the SO₂ Mass Transfer in Batch Reactor

Batch reactor test condition: 5200 ppm SO₂ in plexi-glass reactor, in pure N₂ and boiled de-ionized water, room temp.

7.4 Polarity

The condition of the corona was observed both in the wESP system and in the batch reactor. A schematic of corona processes can be seen in Figure 7.5 [6, 61, 78]. For a positive discharge, the corona may appear to be a tight, sheath moving around the electrode or a streamer moving away from the electrode. A blue glowing around the electrode was generally observed with a higher power level. A negative discharge may produce tufts of corona. A fuzzier corona can be visually observed with a higher power level. The type of corona also depended on the surface condition of the wire. As more disformities were made on the wire, a fuzzier, more uniform corona was produced. In general, negative corona requires the presence of an electron-absorbing gas in the surrounding region while positive corona can be used anytime [31]. Negative corona is more stable, but it generates more ozone.

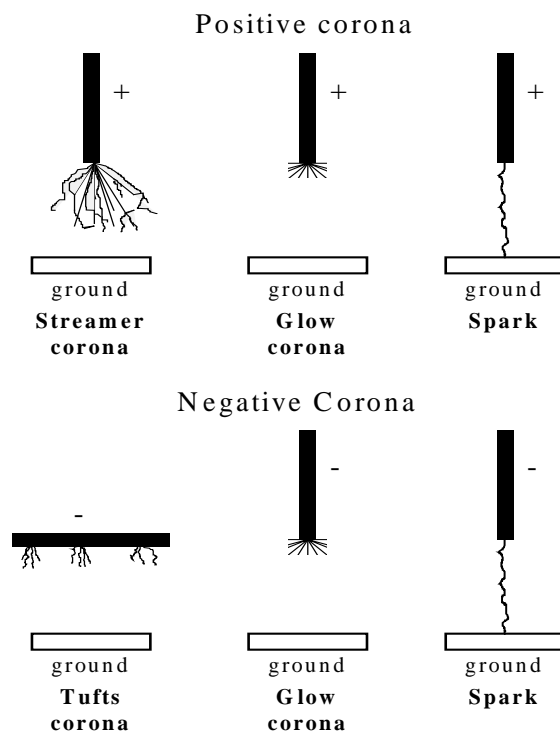


Figure 7.5. Schematic of Corona Discharge Processes

The results of batch reactor tests (Figure 7.6) show that the SO_2 mass transfer rates are enhanced more by positive corona discharge at the same corona power level. These results are similar to Masuda's works which showed that the De- NO_x rate in positive pulsing corona is more than one order of magnitude higher than that with negative pulsing [16].

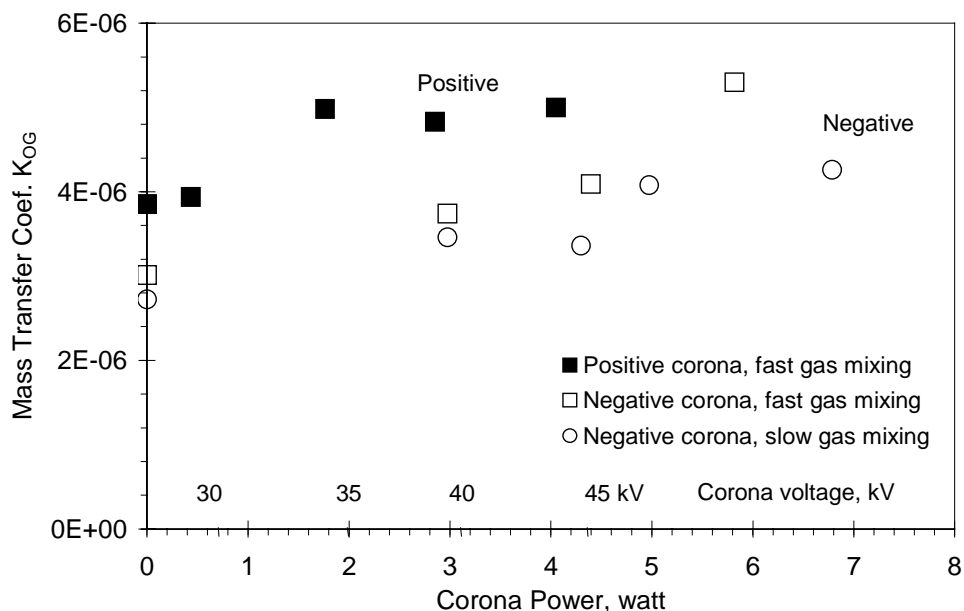


Figure 7.6 Mass Transfer Coefficient vs. Corona Polarity and Power in Batch Reactor

Batch reactor test condition: 3200 ppm SO₂ in pure N₂, boiled de-ionized water, pulsed corona discharge, room temp. Input power of gas mixer: 0.360 w for fast gas mixing, 0.015w for slow gas mixing.

7.5 Corona Power

The theoretical discussion of SO₂ mass transfer affected by corona power are presented in detail in section 4.7. The experimental results of overall mass transfer coefficient, K_{OG} , are summarized in Table 7.1 and Figure 7.7. In the N₂/DI water system, the mass transfer was enhanced by 50% in a corona of 6 watts (40 kV, power density: 205 watt/ m³), by about 160% in a corona of 20 watts (45 kV, 684 watt/m³). This means that the overall gas side mass transfer resistance was effectively reduced by 160%, or the overall mass transfer flux was enhanced by 160%. In the air/tap water system, corona power was limited within 17 watt due to the sparking. The results show that the mass transfer was enhanced by 58% in a corona of 17 watts (53 kV, 581 watt/m³).

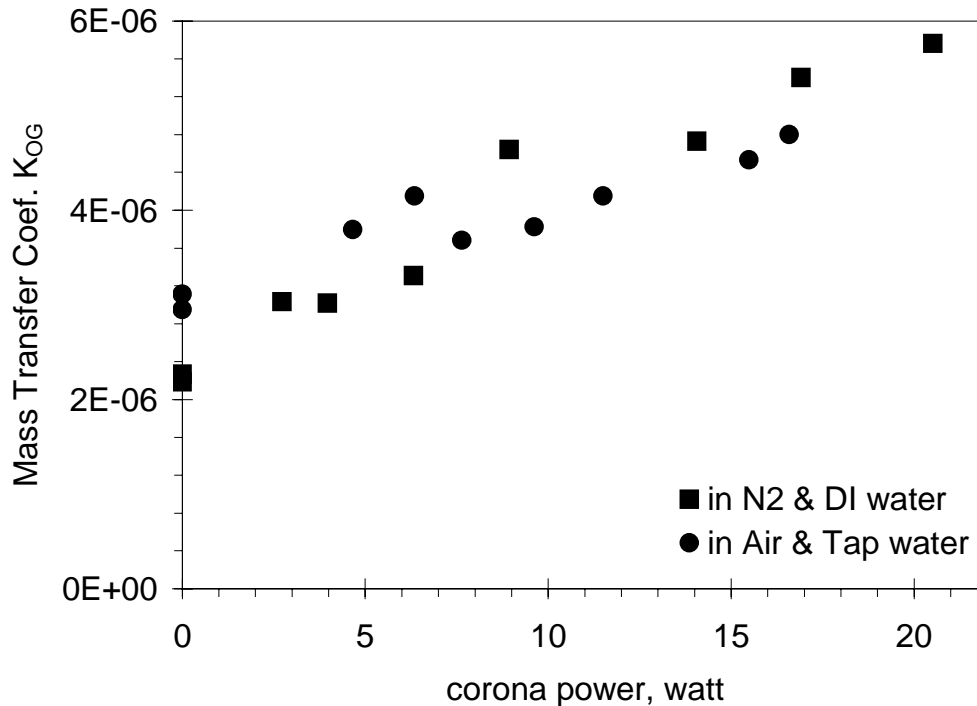


Figure 7.7 Overall Mass Transfer Coefficients vs. Corona Power of Batch Tests

Batch Reactor Test Condition: 3300 ppm SO₂ in air and pure N₂, tap and de-ionized water, at room temperature, with positive pulsed corona.

The purpose of NaOH solution tests is to remove the liquid mass transfer resistance. The results show that the corona-reduced total mass transfer resistance (from test #225a to #328) could be greater than the gas mass transfer resistance (test #302). This implies that the corona discharge not only reduce the gas side mass transfer resistance, but also reduce the liquid side resistance. The mass transfer resistances on both phases will be studied in detail in section 7.6.

These relative K_{OG} values obtained from the batch tests might not be applied to the wESP flowing system because these values depend on system geometries and experimental conditions. Maximuk and Bologna indicated that the mass transfer enhancement in a stationary system is greatly different from that in a flowing system. When external gas flow is absent, the intensification of mass transfer by an electric wind is about 40 to 100 times for the evaporation of stationary liquid. In the case of the motion of both

phases, however, the intensification is about 1.5 to 2 times. The effect of electric field decreased when the flow rate of the liquid increased [79].

Table 7.1 Summary of Overall Mass Transfer Coefficients of Batch Tests

Test #	Corona Power	Overall Mass Transfer Coefficients K_{OG}	Total Mass Transfer Resistance	Mass Transfer Enhancement by Electrostatics
	watt	mol/s-cm ² -atm	s-cm ² -atm/mol	
In N₂ + DI water				
225a	0	2.27E-06	440,717	0%
225	0	2.19E-06	457,473	0%
223	2.7	3.03E-06	329,594	36%
224	4.0	3.02E-06	331,456	35%
309	6.3	3.31E-06	302,127	49%
328az	8.9	4.64E-06	215,521	108%
328a	14.1	4.73E-06	211,454	112%
328z	16.9	5.40E-06	185,058	143%
328	20.5	5.76E-06	173,505	159%
In N₂ + NaOH solution				
302	0	1.25E-05	80,794	0%
317	6.1	6.14E-05	16,359	394%
318	18.7	6.30E-05	15,880	409%
In Air + Tap water				
227a	0	3.11E-06	321,059	0%
327	0	2.95E-06	338,881	0%
227	4.7	3.79E-06	263,525	25%
307	6.4	4.15E-06	241,035	37%
228	7.6	3.68E-06	271,450	21%
227b	9.6	3.82E-06	261,506	26%
307a	11.5	4.15E-06	240,900	37%
328b	15.5	4.53E-06	220,629	49%
228a	16.6	4.80E-06	208,374	58%
In Air + NaOH solution				
302a	0	1.27E-05	78,616	0%
318a	7.4	6.86E-05	14,583	439%
329	15.3	6.58E-05	15,190	418%

Batch Reactor Test Condition: 3300 ppm SO₂ in air and pure N₂, tap and de-ionized water, at room temperature, with positive pulsed corona.

7.6 Chemical Dissociation Enhancements and Electrostatic Enhancements

The results of mass transfer coefficients and resistances and chemical dissociation enhancement factor for non-corona tests are shown in Table 7.2. The NaOH greatly reduced the liquid mass transfer resistance. The difference between K_{OG} and k_g of NaOH tests is less than 0.7%. The absorption of SO_2 to pure water (or tap water) is liquid phase limited. The liquid resistance is around 3.2 and 4.5 times of the gas resistance in N_2 /DI water and air/tap water system, respectively. The gas resistances of N_2 and of air are about the same, while the liquid resistance of tap water is less than that of pure water due to the higher alkalinity.

Table 7.2 Mass Transfer Coefficients and Resistances and Chemical Dissociation Enhancement Factor for Non-Corona Tests

Test #	K_{OG}	ϕ_c	k_l^o	k_l	k_g	Liquid resistance	Gas resistance	Total resistance
	mol/s-cm ² -atm		cm/s	cm/s = $\phi_c k_l^o$	mol/s-cm ² -atm	= H / kl	= I / kg	s-cm ² -atm/mol
In N₂ + DI water								
225a	2.27E-06	4.88	0.000409	0.00199	1.25E-05	360,416	80,302	440,717
225	2.19E-06	4.83	0.000395	0.00190	1.25E-05	377,172	80,302	457,473
In N₂ + NaOH solution								
302	1.24E-05	3627	0.000402	1.45657	1.25E-05	493	80,301	80,794
In Air + Tap water								
227a	3.12E-06	5.21	0.000567	0.00295	1.28E-05	243,137	77,922	321,059
327	2.95E-06	5.10	0.000540	0.00275	1.28E-05	260,959	77,922	338,881
In Air + NaOH solution								
302a	1.27E-05	1868	0.000553	1.03368	1.28E-05	695	77,921	78,616

Batch Reactor Test Condition: 3300 ppm SO_2 in air and pure N_2 , tap and de-ionized water, at room temperature, with positive pulsed corona.

The results of mass transfer coefficients and resistances, chemical dissociation enhancements and electrostatic enhancement factors in corona discharges are shown in Table 7.3, Figure 7.8 and Figure 7.9.

The gas side electrostatic enhancement factors rapidly reached to 5.0 for air and N₂ as corona power increased, but seemed to stop enhancing anymore when the power was greater than 7 watts (power density: 240 watt/m³). The minimum gas mass transfer resistance that can be reduced by corona was about 15,000 s-cm²-atm/mol.

However, the liquid electrostatic enhancement factors were gradually increasing as corona power before the sparking occurred. From the Figure 7.9, the liquid mass transfer resistances continuously decreased as corona power increased, and the reduction was greater in DI water tests. If the corona power can be increased by higher pulsing frequency, the enhancement of liquid side mass transfer might be even greater. As corona power greater than 7 watts (240 watt/m³) in this batch system, most mass transfer enhancement occurred in the liquid phase. It is believed that both the gas side and the liquid side boundary layer thicknesses were reduced by the corona discharge. And the electrical potential gradient in the liquid phase enhanced the liquid phase mass transfer.

Table 7.3 Mass Transfer Coefficients and Resistances and Electrostatic enhancement Factors

Test #	Power	K_{OG}	ϕ_c	k_l°	Total k_l	$\phi_{e,l}$	Total k_g	$\phi_{e,g}$	Liquid resistance	Gas resistance	Total resistance
	watt	mol/s-cm ² -atm		cm/s	cm/s		mol/s-cm ² -atm		s-cm ² -atm/mol	s-cm ² -atm/mol	s-cm ² -atm/mol
In N₂ + DI water											
225a	0	2.27E-06	4.873	0.000409	0.00199	1.00	1.25E-05	1.00	360,416	80,302	440,717
225	0	2.19E-06	4.831	0.000394	0.00190	1.00	1.25E-05	1.00	377,172	80,302	457,473
223	2.7	3.03E-06	4.806	0.000402	0.00248	1.29	2.50E-05	2.01	289,594	40,000	329,594
224	4.0	3.02E-06	4.745	0.000402	0.00238	1.25	3.33E-05	2.68	301,456	30,000	331,456
309	6.3	3.31E-06	4.649	0.000402	0.00251	1.35	6.14E-05	4.93	285,837	16,289	302,127
328a	14.1	4.73E-06	4.582	0.000402	0.00367	2.00	6.26E-05	5.02	195,473	15,981	211,454
328	20.5	5.76E-06	4.677	0.000402	0.00455	2.42	6.36E-05	5.11	157,781	15,724	173,505
In N₂ + NaOH solution											
302	0	1.24E-05	3,627	0.000402	1.45657	1.00	1.25E-05	1.00	493	80,301	80,794
317	6.1	6.11E-05	19,032	0.000402	10.2867	1.35	6.14E-05	4.93	70	16,289	16,359
318	18.7	6.30E-05	4,722	0.000402	4.59607	2.42	6.36E-05	5.11	156	15,724	15,880
In Air + Tap water											
227a	0	3.12E-06	5.210	0.000567	0.00295	1.00	1.28E-05	1.00	243,137	77,922	321,059
327	0	2.95E-06	5.100	0.000540	0.00275	1.00	1.28E-05	1.00	260,959	77,922	338,881
227	4.7	3.80E-06	4.934	0.000553	0.00306	1.12	3.45E-05	2.69	234,525	29,000	263,525
307	6.4	4.15E-06	4.781	0.000553	0.00320	1.21	6.14E-05	4.78	224,735	16,300	241,035
228	7.6	3.68E-06	4.778	0.000553	0.00279	1.06	6.99E-05	5.45	257,149	14,301	271,450
227b	9.6	3.82E-06	4.833	0.000553	0.00291	1.09	6.83E-05	5.32	246,856	14,650	261,506
307a	11.5	4.15E-06	4.807	0.000553	0.00317	1.19	6.83E-05	5.32	226,250	14,650	240,900
328b	15.5	4.53E-06	4.766	0.000553	0.00349	1.32	6.67E-05	5.19	205,629	15,000	220,629
228a	16.6	4.80E-06	4.880	0.000553	0.00371	1.38	6.67E-05	5.19	193,374	15,000	208,374
In Air + NaOH solution											
302a	0	1.27E-05	1,868	0.000553	1.03368	1.00	1.28E-05	1.00	695	77,921	78,616
318a	7.4	6.86E-05	4,337	0.000553	2.53533	1.06	6.99E-05	5.45	283	14,300	14,583
329	15.3	6.58E-05	5,149	0.000553	3.77340	1.32	6.67E-05	5.19	190	15,000	15,190

* Total $k_g = \phi_{e,g}$ * k_g of non-corona tests ; Total $k_l = \phi_{e,l}$ * ϕ_c * k_l°

Batch Reactor Test Condition: 3300 ppm SO₂ in air and pure N₂, tap and de-ionized water, at room temperature, with positive pulsed corona.

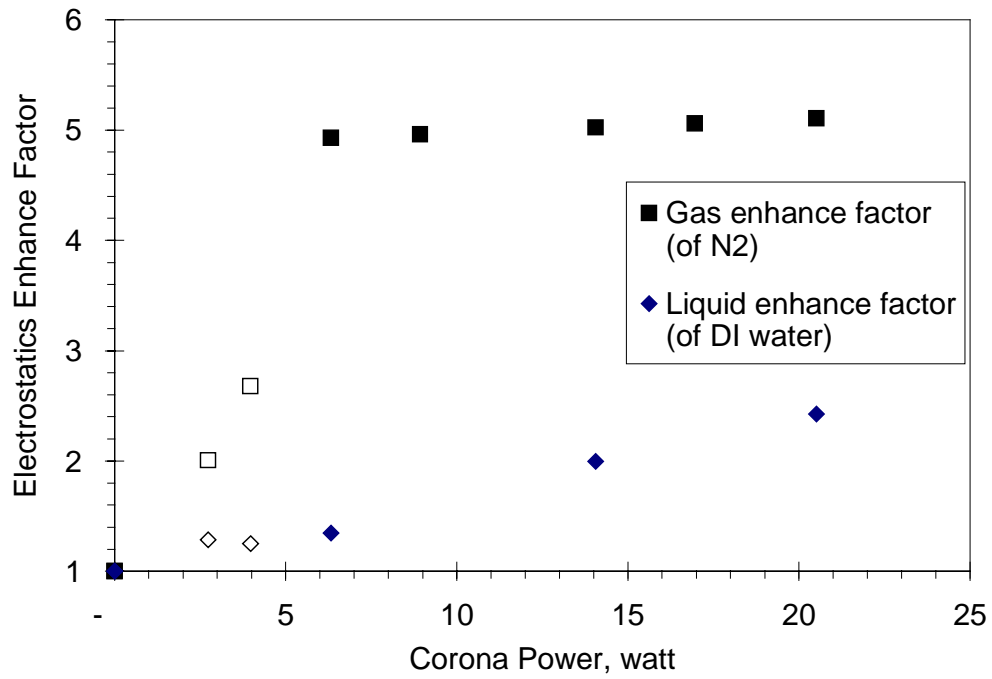
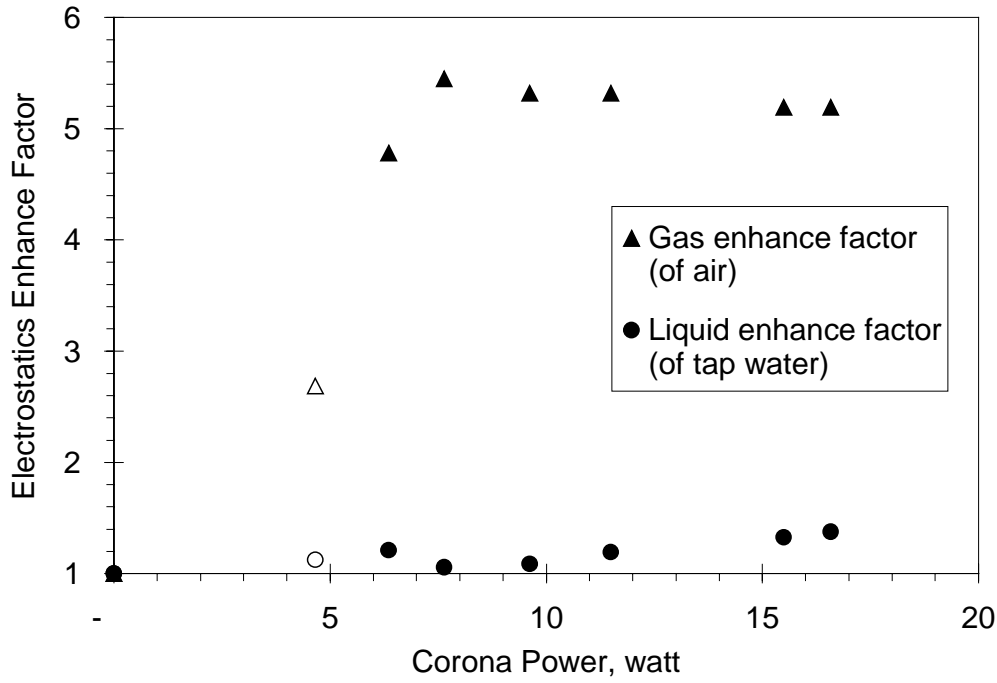


Figure 7.8 Electrostatic Enhancement Factors vs. Corona Power

Batch Reactor Test Condition: 3300 ppm SO₂ in air and pure N₂, tap and de-ionized water, at room temperature, with positive pulsed corona.

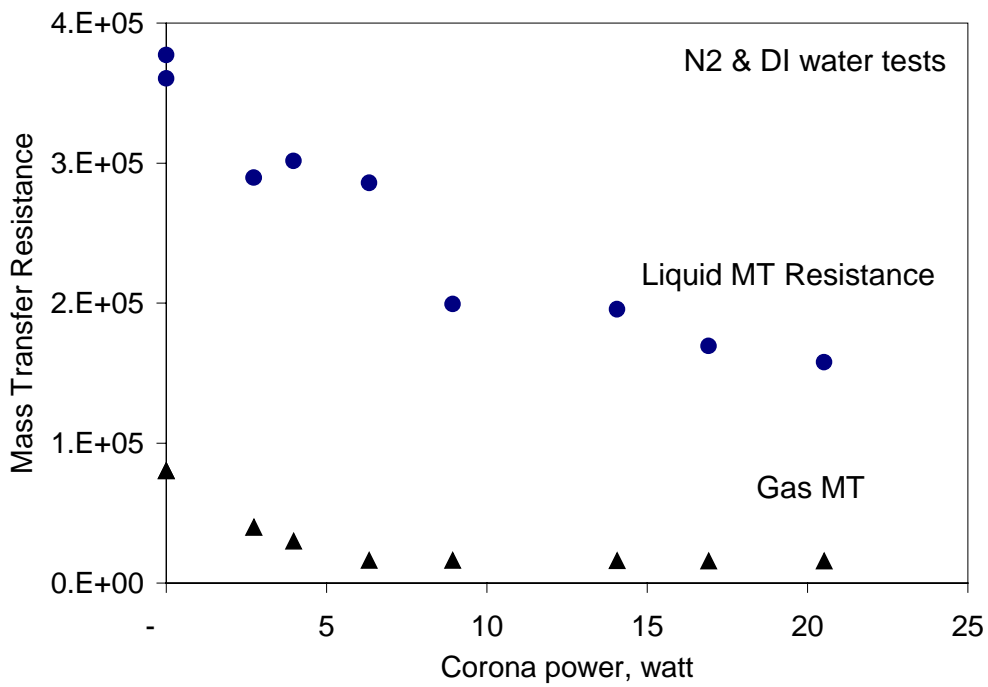
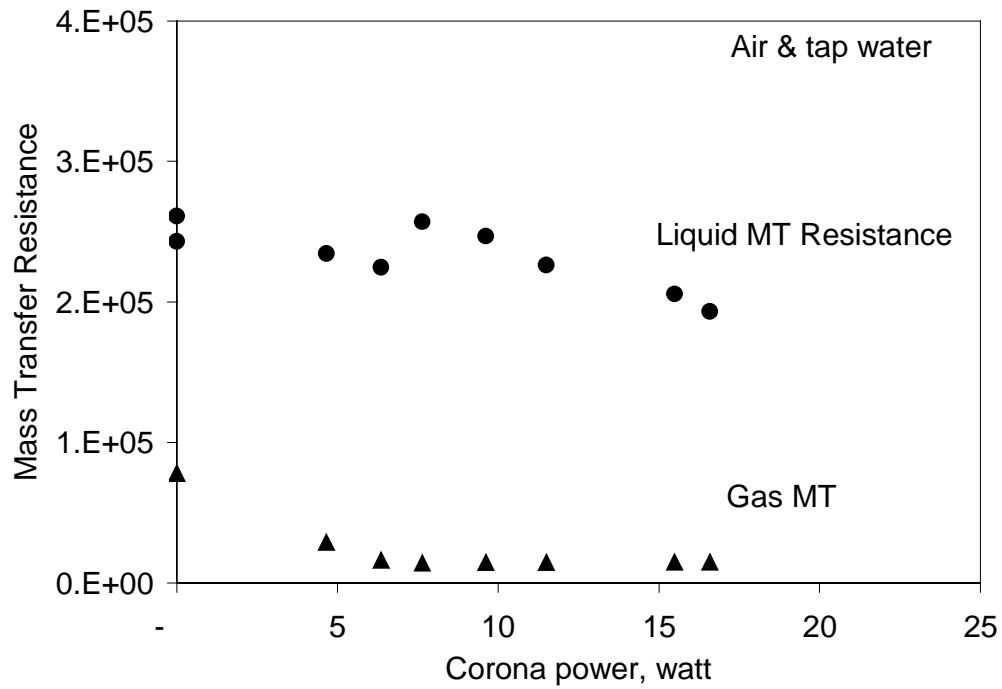


Figure 7.9 Mass Transfer Resistances vs. Corona Power

Batch Reactor Test Condition: 3300 ppm SO₂ in air and pure N₂, tap and de-ionized water, at room temperature, with positive pulsed corona.

7.7 Comparison of the Mass Transfer Enhancement due to the Corona Effect and the Physical Gas-Phase Mixing

The mass transfer enhancements due to the corona effect and due to the physical gas-phase mixing are studied by comparing the results in sections 7.1 and 7.5. Unlike there was an upper limit of mass transfer enhancement due to physical mixing in Figure 7.2, corona continuously enhanced the mass transfer till the sparks occurred. The maximum enhancement of overall mass transfer coefficient due to the physical gas-phase mixing was 1.6 times, which was less than the maximum enhancement due to corona discharge (2.6 times). The decrease of mass transfer resistance due to physical mixing in Figure 7.2 ($108\text{k s-cm}^2\text{-atm/mol}$) was about the same level of the gas phase mass transfer resistance shown in Table 7.2 ($80\text{k s-cm}^2\text{-atm/mol}$). The physical mixing in the gas phase enhanced only the gas phase mass transfer, while the corona discharge was able to enhance the mass transfer of both the gas phase and the liquid phase.

It is assumed that the physical mixing effect caused by corona wind was similar to the fan mixing effects although the wind produced by the gas mixer is different from the wind produced by a corona. Therefore, the mass transfer enhancement in a corona discharge is not only due to the physical mixing caused by corona wind, but also due to the selective charge of SO_2 gas molecules and the electrical potential gradient in the gas phase and liquid phase.

Tests were conducted with no power and with power in Figure 7.1. It can be seen that the corona discharge further enhanced the SO_2 mass transfer, even when the enhancement of fan mixing existed, and vice versa.

8. CONCLUSIONS

Wet ESP

A bench-scale pulse-enhanced wESP system was constructed to study the combined removal of SO₂ and NO_x in the presence of a pulsed corona. This wESP has been designed to operate wet or dry, positive and negative, and with the optional injection of ammonia and/or ozone for comparison purposes. Simulated combustion flue gases with SO₂ (up to 3000 ppm) and/or NO_x (up to 1200 ppm) were tested to determine the feasibility of SO₂ and NO_x removal in the wESP.

SO₂ Removal

High level of SO₂ (up to 70%) was removed by using water and pulsed corona discharge (45 kV, 40 watt) without any additives. The SO₂ removal efficiency was compared well with equilibrium predictions for the system when the inlet SO₂ concentration and corona power levels were above critical levels. SO₂ removal efficiency increased with gas residence time, water flow rate, inlet SO₂ concentration, and applied corona power. It was experimentally found that higher the input SO₂ concentration, higher the removal efficiency, even for the trials without power. Corona discharge forced the charged SO₂ to reach equilibrium with the water. It is believed that the primary removal mechanisms for SO₂ are the selective charging (electron attachment) of SO₂ molecules and the wet wall absorption.

The sulfite concentrations were greater than the increased sulfate concentrations in the corona-discharge phases, which indicated that the electron attachment might be the primary removal mechanism rather than oxidizing SO₂ to SO₃.

Ammonia injection could improve the SO₂ removal approaching to 100%. White NH₄HSO₄ aerosols are clearly observed inside the ESP. The amount of in-situ ozone is not enough to be considered a major SO₂ removal mechanism in this process. Injected ozone improved the SO₂ removal a little in non-corona case but inhibited the effect of corona discharge on SO₂ removal when NO was not present.

Any ozone injection for gaseous pollution control should be placed before the ESP facility. Water was more acidic in the first two sections which also had the highest sulfite concentration, showing most of the SO₂ removal took place in the first one-third of the wESP.

A n-CSTR/mass transfer model was developed for this wESP system. The overall SO₂ removal efficiency and the overall SO₂ mass transfer coefficient of the wESP can be predicted from wESP system parameters and operational conditions.

NO_x Removal

There was no appreciable amount of NO removal in pure N₂ stream, although there were corona discharge and water film in the wESP. NO has to be oxidized into NO₂ before any removal takes place. NO_x removal efficiency increased with gas residence time, inlet NO_x concentration, and applied corona power. In an air stream, 20% De-NO_x efficiency was the maximum limit when the gas residence time was less than 8.5 seconds.

Ammonia injection did not improve the NO_x removal in both corona and non-corona cases in air. The amount of in-situ ozone was not enough to be considered as a major NO_x removal mechanism in a wESP. NO and total NO_x removal are improved with ozone injection because NO is oxidized by ozone. The presence of 300 ppm ozone improves both the NO (from ~18% to 50%) and NO_x removal (from ~10% to 20%).

In a 3%-O₂ simulated flue gas, the De-NO efficiency was only 5% without any additives. Adding NH₃ (NH₃/NO_x ratio 1, no ozone) at 32 watts corona discharge, NO_x removal was increased to 10%. In 6%-O₂ simulated flue gas, NH₃ injection (NH₃/NO_x ratio 1) increased NO_x removal from 10% to 13%. A 200 ppm ozone injection (no ammonia) increased NO removal from 13% to 36% by oxidation, but total NO_x removal was increased only from 10% to 17%. The maximum NO_x removal in simulated flue gas

was 40% due to the formation of NH_4NO_3 aerosols with the injection of 312 ppm O_3 and 5800 ppm NH_3 (without ammonium sulfur aerosols).

Enhanced Effect of In-situ Ammonium Sulfur Aerosols

High NO_x removals were measured when the in-situ ammonium sulfur aerosols were formed in simulated flue gas that contained NH_3 , SO_2 , and ozone. With the 2400 ppm SO_2 , 200 ppm ozone, and 2500 ppm NH_3 (ammonia to pollutants stoichiometry ratio 0.45), total NO_x removal increased to 66% in 3%- O_2 simulated flue gas. Further increasing the additives to 312 ppm ozone and 2900 ppm NH_3 (stoichiometry ratio 0.53), total NO_x removal increased to 80%. Higher ozone or ammonia input did not further increase the NO_x removal efficiency.

It was determined that the in-situ ammonium sulfur aerosols served as a highly efficient adsorbent with tremendous surface area which enhanced the oxidation of NO, as well as the formation of NH_4NO_3 . Ozone, NO, H_2O , and NH_3 were adsorbed to the surface of aerosols. These aerosols enhanced the NO oxidation and the reaction between NO_2 , H_2O , and NH_3 .

Batch SO_2 Absorption Reactor

A batch reactor was also constructed to provide a controlled environment to study the SO_2 mass transfer and removal mechanisms. The maximum mass-transfer enhancement by gas-phase mechanical mixing is around 1.60 times with less than 0.8 watt (power density: 27.4 watt/ m^3) input of mixing power. The results showed that a positive pulsed corona achieved the maximum pollutant removal rate in this experimental system at the same corona discharge power as compared to any other types of coronas. The overall mass transfer was enhanced by 160% in the experimental system with 20 watts of pulsed positive corona (power density: 685 watt/ m^3).

A thin film mass transfer model was developed to study the mass transfer coefficient by introducing electrostatic enhancement factors to both the gas and liquid side mass transfer coefficients.

The gas side electrostatic enhancement rapidly reached to 5 times as corona power increased, but stop enhancing anymore when the power was greater than 7 watts (power density: 240 watt/m³). The minimum gas mass transfer resistance that can be reduced by corona was about 15000 s-cm²-atm/mol. The liquid electrostatic enhancement factors were gradually increasing as corona power before the sparking occurred. The liquid mass transfer resistances continuously decreased as corona power, and the reduction was greater in de-ionized water. As corona power is greater than 7 watts, most mass transfer enhancement occurred in the liquid phase. It is believed that both the gas side and the liquid side boundary layer thicknesses were reduced by the corona discharge. And the electrical potential gradient in the liquid phase enhanced the liquid phase mass transfer.

9. REFERENCE

- 1 *1997 National Air Quality and Emissions Trends Report*, US EPA, Office of Air Quality Planning and Standards, EPA 454/R-98-016, <http://www.epa.gov/oar/aqtrnd97> , 1998.
- 2 Nevers, Noel De; *Air Pollution Control Engineering*, 2nd Ed., McGraw-Hill Co., 2000.
- 3 Ellison, W; "Limiting of SO₂ and NO_x Emissions In Worldwide Coal-Power Production," *Radiation Physics and Chemistry*, Vol. 45, No. 6, pp. 1003-1011, 1995.
- 4 Griffin, Roger D.; *Principles of Air Quality Management*, CRC Press, 1994.
- 5 Masuda, Senichi; "Non-Equilibrium Plasma Chemical Process PPCP and SPCP for Control of NO_x, SO_x and Other Gaseous Pollutants", *4th International Conference on Electrostatic Precipitation*, Chap. 9, pp. 615-623, 1990.
- 6 Chang, Jen-Shih; Phil A Lawless; Toshiaki Yamamoto; "Corona Discharge Processes", *IEEE Transactions on Plasma Science*, Vol. 19, No. 6, pp. 1152-1166, 1991.
- 7 Masuda, Senichi; "Control Strategies and Applicable Technologies", *Managing Hazardous Air Pollutants*, pp. 380-396, 1992.
- 8 Yamamoto, Isao; Kochi Yamamoto; Kotaro Shimizu; Yuichi Fujiyama; Kazuhiko Tsunoda and Akira Mizuno; "Wet Type Plasma Reactor for Incinerator," *IAS Annual Meeting (IEEE Industry Applications Society)*, Vol. 3, pp. 1861-1864, 1998.
- 9 Penetrante, B. M.; J. N. Bardsley and M.C. Hsiao, "Effect of Electrical Parameters on the Chemical Kinetics of Plasma-Based Pollution Control", *Workshop on Applications of Electrostatics for Control of Gas Phase Air Pollutants*, The University of Cincinnati, Cincinnati, Ohio, August 22, 1997.
- 10 Hinds, William C.; *Aerosol Technology, Properties, Behavior, and Measurement of Airborne Particles*, John Wiley & Sons, 1982.
- 11 Mizuno, Akira; Judson Sideny Clements and Robert H. Davis; "A Method for the Removal of Sulfur Dioxide from Exhaust Gas Utilizing Pulsed Streamer Corona for Electron Eenergization", *IEEE Transactions on Industry Applications*, Vol. 1A-22, No. 3, pp. 516-521, 1986.
- 12 Dean, John A.; *Lange's Handbook of Chemistry*, 13th edition, McGraw Hill Book Co., NY., 1985.
- 13 Bradbury, Norris E. and H. E. Tatel, "The Formation of Negative Ions in Gases, Part II. CO₂, N₂O, SO₂, H₂S and H₂O," *Journal of Chemical Physics*, Vol. 2, pp. 835-840, 1934
- 14 H. J. White; "A Pulse Method for Supplying High-Voltage Power for Electrostatic Precipitation", *AIEE Trans*, Vol. 71, pp. 326-329, 1952.
- 15 Dinelli, Giorgio; Luigi Civitano and Massimo Rea, "Industrial Experiments on Pluse Corona Simultaneous Removal of NO_x and SO₂ from Flue Gas", *IEEE Transactions on Industry Applications*, Vol. 26, No. 3, pp. 535-541, 1990.
- 16 Masuda, Senichi and Hideyuki Nakao; "Control of NO_x by Positive and Negative Pulsed Corona Discharges", *IEEE Transactions on Industry Applications*, Vol. 26, No. 2, pp. 374-83, 1990.
- 17 Penetrante, B. M. "Pollution Control Applications of Pulsed Power Technology", *9th IEEE International Pulsed Power Conference*, New Mexico, Jun 1993.
- 18 Chakrabarti, Alokumar; Akira Mizuno; Kazuo Shimizu; Tsutomu Matsuoka and Satoshi Furuta; "Gas Cleaning with Semi-Wet Type Plasma Reactor", *IEEE Transactions on Industry Applications*, Vol. 31, pp. 500-506, 1995.

- 19 Masuda, Senichi; Kensuke Akutsu and Mitsuhiro Ishida; "Generation of NO_x from Heated Corona Wires", *IAS Annual Meeting* (Ieee Industry Applications Society). No. 79, CH1484-51A, New York, NY, pp. 61-65, 1979.
- 20 Mizuno, Akira; Kazuo Shimizu; Tsutomu Matsuoka and Satoshi Furuta; "Reactive Absorption of NO_x using Wet Discharge Plasma Reactor", *IEEE Transactions on Industry Applications*, Vol. 31, No. 6, pp. 1463-1467, 1995.
- 21 Chang, Jen-Shih; "Role of H₂O and NH₃ on the Formation of NH₄NO₃ Aerosol Particles and De-NO_x under the Corona Discharge Treatment of Combustion Flue Gases", *Journal of Aerosol Science*, Vol. 20, No. 8, pp. 1087-1090, 1989.
- 22 Chang, Jen-Shih; "Chemical Reactions Leading to an Aerosol Particle Formation and Growth by an Irradiation of High Energy Electron Beam", *Aerosol Formation and Reactivity, Second International Aerosol Conference*, West Berlin, 22-26 Sept. 1986; G. Israel et al., Pergamon Press, Oxford, pp. 867-870.
- 23 Chang, Jen-Shih and Senichi Masuda; "Mechanism of Pulse Corona Induced Plasma Chemical Process for Removal of NO_x and SO₂ from Combustion Gases," *1988 IEEE Industry Applications Society 23rd Annual meeting*, Pittsburgh, Pennsylvania, October 2-7, 1988; Vol. 2, pp. 1628-1635.
- 24 Bradbury, Norris E, "Formation of Negative Ions in Gases by Electron Attachment, Part I. NH₃, CO, NO, HCl and Cl₂," *Journal of Chemical Physics*, Vol. 2, p. 827, 1934.
- 25 Lakdawala, Vishnukumar K. and J. L. Moruzzi; "Attachment, Detachment and Ion-Molecule Reactions in SO₂ and SO₂-O₂ Mixtures", *J. Phys. D : Appl. Phys.*, Vol. 14, pp. 2015-26, 1981.
- 26 Tamon, Hajime, Noriaki Sano and Morio Okazaki, "Influence of Oxygen and Water Vapor on Removal of Sulfur Compounds by Electron Attachment", *AIChE Journal*, Vol. 42, No. 5, pp. 1481-6, May 1996.
- 27 A. W. Castleman, Jr.; "Nucleation Processes and Aerosol Chemistry," *Space Science Rev.*, Vol. 15, pp. 547-589, 1974.
- 28 Simachev, V. Yu; S S. Novoselov; V. A. Svetlichnyi; A. F. Gavrilov; M. V. Gorokhov; V. I. Semenov; V. A. Ryzhikov and V. V. Demchuk; "Investigation of the Ozone-Ammonia Method of Simultaneous Desulphurisation and Denitrification of Flue Gases when Burning Donetsk Coals", *Thermal Engineering*. Vol. 35, No. 3, pp. 171-175, 1988.
- 29 Lozovskii, V. A.; S. S. Novoselov; V. A. Svetlichnyi; V. A. Ryzhikov and V. Y. Simachev; "The Role of Ozone in Oxidising Reactions when it Interacts with the Flue Gases from Thermal Power Stations", *Thermal Engineering*. Vol. 35, No. 8 pp. 442-444, 1988.
- 30 Ohtsuka, K.; T. Yukitake and M. Shimoda; "Oxidation Characteristics of Nitrogen Monoxide in Corona Discharge Field", *Proc. Inst. Electrostat Japan*, Vol. 9, No. 5, pp. 346-351, 1985.
- 31 Crawford, Martin; *Air Pollution Control Theory*, McGraw hill, Inc. 1976.
- 32 Saporov, M. I.; S. S. Novoselov; S. A. Fadeev and T. S. Gerasimova; "Reducing Pollutant Emissions to Atmosphere from Future Coal-Fired Power Stations," *Thermal Engineering (English translation of Teploenergetika)*, Vol 37, No. 8., pp. 413-416, Aug 1990.
- 33 Liu, Linmao; Jingfu Guo, Jie Li and Lianxi Sheng "The Effect of Wire Heating and Configuration on Ozone Emission in A Negative Ion Generator," *Journal of Electrostatics*, Vol. 48, No. 2, pp 81-91, Jan 2000.
- 34 Slater, Steven M. and Mark S. Rissone; "Simultaneous Oxidation of SO₂ and NO in Flue Gas by Ozone Injection," *Fuel*, Vol. 59, No. 12, pp. 897-899, 1980.
- 35 Kerr, J. Alistair and Stephen J. Moss, *CRC Handbook of bimolecular and Termolecular Gas Reactions*, CRC Press, Inc., Boca Raton, Florida, 1982.

- 36 Eichwald, O.; M. Yousfi; A. Hennad and M. D. Benabdessadok; "Coupling of Chemical Kinetics, Gas Dynamics, and Charged Particle Kinetics Models for the Analysis of NO Reduction from Flue Gases," *Journal of Applied Physics*, Vol. 82, pp. 4781-94, 1997.
- 37 Onda, K.; Y. Kasuga; K. Kato; M. Fujiwara and M. Tanimoto; "Electric Discharge Removal Of SO₂ And NO_x From Combustion Flue Gas By Pulsed Corona Discharge", *Energy Conversion and Management*, Vol.38, Issue 10-13, pp. 1377-1387, 1997.
- 38 Baranchicov, E. I.; G. S. Belenky; M. A. Deminsky; V. P. Dorovsky; E. M. Erastov; V. A. Kochetov; D. D. Maslenicov; B. V. Potapkin; V. D. Rusanov; V. V. Severny and A. A. Fridman; "Plasma-Catalysis SO₂ Oxidation in an Air Stream by a Relativistic Electron Beam and Corona Discharge," *Radiation Physics and Chemistry*, Vol. 40, No. 4., pp. 287-294; 1992.
- 39 Vasishtha, Niraj. and Arun V. Someshwar, "Absorption Characteristics of Sulfur Dioxide in Water in the Presence of a Corona Discharge", *Industrial & Engineering Chemistry Research*, Vol. 27, No. 7, pp. 1235-1241, 1988.
- 40 Chang, Jen-Shih; "Simultaneous Removal of NO_x and SO₂ from a Combustion Flue Gas by Corona Discharge Radical Shower Systems", *Workshop on Applications of Electrostatics for Control of Gas Phase Air Pollutants*, The University of Cincinnati, Cincinnati, Ohio, August 22, 1997.
- 41 Masuda, Senichi; Shunsuke Hosokana; Xiang-Ling Tu, Kaichi Sakakibara, Shigehiro Kitoh and Shigeo Sakai, "Destruction of Gaseous Pollutants by Surface-Induced Plasma Chemical Process (SPCS)", *IEEE Transactions on Industry Applications*, Vol. 29, No. 4, pp. 781-786, 1993.
- 42 Kanazawa, S.; J. S. Chang; G. F. Round; G. Sheng; T. Ohkubo; Y. Nomoto and T. Adachi; "Removal of NO_x from Flue Gas by Corona Discharge Activated Methane Radical Showers," *Journal of Electrostatics*, Vol. 40-41, pp. 651-656, 1997.
- 43 Boyle, J.; A. Russell; S. C. Yao; Q. Zhou; J. Ekmann; Y. Fu and M. Mathur; "Reduction of Nitrogen-Oxides from Postcombustion Gases Utilizing Molecular Radical Species," *Fuel*, Vol. 72, No. 10, pp. 1419-1427, 1993.
- 44 Helfritch, Dennis J.; "Plasma Technologies Applied to Air Pollution Control", *Workshop on Applications of Electrostatics for Control of Gas Phase Air Pollutants*, The University of Cincinnati, Cincinnati, Ohio, August 22, 1997.
- 45 Yabe, Akira; Yasuo Mori and Kunio Hijikata; "EHD Study of the Corona Wind between Wire and Plate Electrodes," *American Institute of Aeronautics and Astronautics Journal*, Vol. 16, No. 4, pp. 340-345, 1978.
- 46 Franke, M. E. and L. E. Hogue; "Electrostatic Cooling of a Horizontal Cylinder," *Journal of Heat Transfer, Transactions ASME*, Vol. 113, no. 3, pp. 544-548, 1991
- 47 Khang, Soon-Jai, Karen Larkin, Tim C. Keener and Steve Khang; "The Effect of Nonthermal Plasmas on Mass Transfer Coefficients for Gas Cleaning", *Workshop on Applications of Electrostatics for Control of Gas Phase Air Pollutants*, The University of Cincinnati, Cincinnati, Ohio, August 22, 1997.
- 48 Crowley, Joseph M.; "Dimensionless Ratios in Electrohydrodynamics," *Handbook of Electrostatic Discharge Processes*. edited by Jen-Shih Chang, Arnold J. Kelly, and Joseph M. Crowley, Marcel Dekker, Inc., Chap. 7, pp. 99~119, 1995.
- 49 Gregory N. Brown "Ammonia Scrubbing Makes High Sulfur Fuels Economical," Marsulex Environmental Technologies, Lebanon, Pennsylvania, USA, 1999.
- 50 Ellison, W.; "Update on major commercial advancements by ammonia FGD," *24th International Technical Conference on Coal Utilization and Fuel Systems*, Clearwater, FL, USA, 8-11 Mar 1999.

- 51 Borio, D.; P. Rader and M. Walters; "Ammonia Scrubbing: Creating Value from SO₂ Compliance," ABB Environmental Systems, Knoxville, Tennessee, USA, 1999
- 52 Bai, Hsunling; Pratim Biswas and Tim C Keener; "SO₂ Removal by NH₃ Gas Injection: Effects of Temperature and Moisture Content", *Industrial & Engineering Chemistry Research*, Vol. 33, pp. 1231-6, May 1994.
- 53 Bai, Hsunling; "Fundamental Study of Ammonium-Sulfur Dioxide Reactions to Form Solid Particles," Doctoral Dissertation, University of Cincinnati, Jan. 1992.
- 54 Ning, C. et al., "Experimental Studies on Removal of SO₂ and NO by Positive Pulse Corona and Ammonia Water," *Huanjing Kexue (Environmental Science)*, Vol. 15, No. 1, pp. 15-18, 1994.
- 55 Penetrante, Bernie M.; Hsiao, Mark C.; Merritt, Bernard T.; Vogtlin, George E.; Wallman, P. Henrik "Comparison of electrical discharge techniques for nonthermal plasma processing of NO in N₂," *IEEE Transactions on Plasma Science*, Vol. 23, no. 4, pp. 679-687, 1995.
- 56 Hasegawa, T. and M. Sato; "Study of Ammonia Removal from Coal-Gasified Fuel," *Combustion and Flame*, Vol. 114, Issue: 1-2, pp. 246-258, 1998.
- 57 Suchak, Naresh J., Kanhaiya R. Jethani and Jyeshthraj B. Joshi, "Absorption of Nitrogen Oxides In Alkaline Solutions: Selective Manufacture of Sodium Nitrite", *Industrial & Engineering Chemistry Research*, Vol. 29, pp. 1492-502, 1990.
- 58 Ohkubo, Toshikazu; Seiji Kanazawa; Yukiharu Nomoto; Jen-Shih Chang and Tokayoshi Adachi; "NO_x Removal by a Pipe with Nozzle-Plate Electrode Corona Discharge System", *IEEE Transactions on Industry Applications*, Vol. 30, No. 4, pp. 856-861, 1994.
- 59 John H. Seinfeld, "Aqueous-Phase Chemical Equilibria", *Atmospheric Chemistry and Physics of Air Pollution*, 1986
- 60 Yang, Xinjian; *Ammonia regeneration for a combined lime/ammonia spray dryer FGD process*, M.S. Theses, University of Cincinnati, Civil and Environmental Engineering, 1991.
- 61 Abdel-Salam, M "Influence of Humidity on Charge Density and Electric Field in Electrostatic Precipitators," *Journal of Physics. D, Applied Physics*, Vol. 25, pp. 1318-22, 1992.
- 62 Fouad, L.; Elhazek, S. "Effect of Humidity on Positive Corona Discharge in a Three Electrode System," *Journal of Electrostatics*, Vol. 35, No. 1, pp. 21-30, 1995
- 63 Clements, Judson Sideny; Akira Mizuno; Wright C. Finney and Robert H. Davis; "Combined Removal of SO₂, NO_x, and Fly Ash from Simulated Flue Gas Using Pulsed Streamer Corona", *IEEE Transactions on Industry Applications* Vol. 25, No. 1, pp. 62-69, 1989.
- 64 Tamon, Hajime, Hirotohi Mizota and Noriaki Sano, "New Concept of Gas Purification by Electron Attachment", *AIChE Journal*, Vol. 41 No.7, p1701-11, 1995
- 65 Larkin, Karen, Chao-heng Tseng; Tim C. Keener and Soon-Jai Khang; "Sulfur Dioxide Removal by Enhanced Electrostatics", *Air & Waste Management Association's 90th Annual Meeting*, Toronto, Ontario, Canada, June 8-13, 1997.
- 66 Greenberg, Arnold E., *Standard Methods for the Examination of Water and Wastewater*, 19th edition, by American Public Health Association, American Water Works Association, Water Pollution Control Federation, New York, 1995.
- 67 Lide, David R.; *CRC Handbook of Chemistry and Physics*, 79st edition, CRC Press, 1999
- 68 Perry, Robert H.; Don W. Green and James O. Maloney, *Perry's Chemical engineers' handbook*, 6th ed., McGraw-Hill, New York, 1984.
- 69 Talaie, M. R.; J. Fathikalajahi and M. Taheri "Mathematical Modeling of SO₂ Absorption in a Venturi Scrubber," *Journal of the Air & Waste Management Association*, Vol. 47, pp. 1211-15, 1997.

- 70 Calvert, Jack G.; *SO₂, NO, and NO₂ oxidation mechanisms : atmospheric considerations, Acid precipitation series* ; Vol. 3, Ann Arbor science book, 1984.
- 71 James F. Pankow, *Aquatic Chemistry Concepts*, Lewis Publishers, 1991.
- 72 Pradhan, M. P. and Joshi, J. B. "Absorption of NO_x gases in Aqueous NaOH Solutions: Selectivity and Optimization," *AIChE Journal*. Vol. 45, No. 1, pp. 38-50, 1999.
- 73 Thomas, D. and J. Vanderschuren; "Effect of Temperature on NO_x Absorption into Nitric Acid Solutions containing Hydrogen Peroxide," *Ind. Eng. Chem. Res.* Vol. 37, pp. 4418-4423, 1998.
- 74 Rohrer, Jr., Wesley M.; John M. Koltick, Jr.; Naresh J. Suchak; Julius Brown and Arthur P. Skelley, "Slip Stream Test of Cannon Technology's Low Temperature Oxidation (LTO) System at Duquesne Light Company's Elrama Plant: Demonstration of an Oxidative Process."
- 75 Chung-Shih Chang and Gary T. Rochelle, "SO₂ Absorption into NaOH and Na₂SO₃ Aqueous Solutions," *Ind. Eng. Chem. Fundam.*, vol. 24, pp. 7-11, 1985.
- 76 Olausson, S.; Mats Wallin and I. Bjerle, "A Model for the Absorption of Sulphur Dioxide into a Limestone Slurry," *Chem. Eng. J.*, Vol. 51, pp. 99-108, 1993.
- 77 Chung-Shih Chang and Gary T. Rochelle, "SO₂ Absorption into Aqueous Solutions," *AIChE Journal*, Vol. 27, No. 2, pp. 292-298, 1981.
- 78 Chang, Jen-shih; Arnold J. Kelly and Joseph M. Crowley; *Handbook of Electrostatic Processes*, New York : M. Dekker, 1995.
- 79 Maximuk, E. P. and M. K. Bologna; "Some Mechanisms of Electric Field Influence Onmass Transfer Processes in the Gas-Liquid System," *Journal of Electrostatics*, Vol. 40-41, pp. 663-668, 1997.
- 80 Hjuler, K. and K. Dam-johansen; "Mechanism and Kinetics of the Reaction between Sulfur-Dioxide and Ammonia in Flue-Gas," *Industrial and Engineering Chemistry Research*, Vol. 31, No. 9, pp. 2110-2118, 1992
- 81 Welty, James R.; Charles E. Wicks, and Robert E. Wilson; *Fundamentals of Momentum, Heat, and Mass Transfer*, 3rd ed., Wiley, New York, 1984

10. APPENDICES

Table 10.1 Summary of Literature Reviews

Ref.	Technology	Year	Country	Scale	Wet	O2 %	CO2 %	SO2/NOx	NH3 ppm	O3 ppm	Other additive	Temp oC	Gas Flow in cm3/sec	Res. Time sec	Primary Mechanism	Final Removal
UC	Enhanced Wet-ESP	1999	USA	Lab	wESP 63cm3/s, 2.2%v, wESP 63cm3/s, 2.2%v.	3%	11%	both	2900	312 ppm = 0.53 g/hr		room	2017	8.6	Ozone oxidize NO, NH3 remove NO2 and SO2	water absorption and aerosol removal
UC	Enhanced Wet-ESP plasma corona induced	1999	USA	Lab		0%	0%	SO2	0	0	0	room	1888	10.0		
5	Plasma PPCP	1995	Japan	Lab	dry	21%	0%	both	180			room			radicals from e-	NH4 aerosol
58	pipe electrode	1994		Lab	dry		yes	NOx	30000						radicals from e-	NH4 aerosol&radical decompose to N2, O2
11	corona + E-Beam pulse streamer, tubular PEER	1986	Japan & US	Lab	2.5%, 100% RH			SO2				room	20	6.7	radicals oxidation or aerosol formation	NH3 + acid mist form aerosol
63	Pulse-induced Plasma Chemical Process, PPCP+EBeam	1989		Lab	2.5%, 100% RH	20%	0%	SO2			fly ash	22, 80, 110	75	5.2	radicals oxidation radical OH, O... oxidize NO; corona wind reduced boundary layer	
16		1990	Japan	Lab	dry			both				10	4.03 sec/m			
81	Pulse energization system DC corona, tubular wet- ESP	1988			dry			SO2								
30		1985	Japan	Lab	WESP, 10%	5%		SO2			ethanol, hydrazine, H2O2	55		4	oxidation	water absorption
B13	double dielectric barrier discharge		USA	Lab	2%			NOx					17		radicals OH, O, HO2 from e-	
15	Pulse Corona ESP	1990	Italy	pilot	8%	6%	13%	both	1000		fly ash	100	277778	5.4-6.9	radicals from e-	form aerosol
15					8%	6%	13%	both			fly ash	70				
15					8%	6%	13%	both			Ca(OH)2	90		200 mins	improved mass transfer/oxidation radical decompose or oxidized	water absorption
39	Non-Pulse Corona	1988	USA	Batch	water bottom 30 cm3			SO2				room	6240 cm3			
41	SFCP, streamer	1993	Japan	Lab	dry	4%	0%	NOx				room	250	4.3		
41						15%	0%	NOx				room	667	0.002		
41						flue gas		NOx				25	833	0.6		
41						flue gas		NOx				400	194	1.5		
37	Pulse Corona	1997	Japan	Lab	0%	2%	10%	both	yes			100	117		radical OH oxidation + corona wind	NH4 aerosol
37					18%	2%	10%	both	yes				117			
B23	TecoLytic(TM) array corona wet scrubber	1997	USA	pilot	wet scrubber			both			CaO, MgO in Liquid CH4		25 ft/sec		radicals from e- methane radicals	scrubber
80	corona + CH4/NH3 corona + CH4/NH3	1997		Lab	dry			NOx					50	282		NH4NO3 aerosol, N2O NH4 aerosol&radical decompose to N2, O2
40	Radical shower	1997	Canada	Lab	dry	3%	8%	both	ratio	1.2 ~ 2	CH4		83		radicals from e- 90% oxidized	
B30	Corona in jet engine	1997	USA	pilot	dry			NOx			CaCl2 solution on filter		141550	0.87		
18	Semi-wet cylindrical ESP	1995	Japan	Lab	Semi-wet ESP	21%		NOx				room	16	0.6 ~ 2.4	NOx reduction	water absorption
B36	WESP	1981	USA	paten	wet			SO2				53	2.5E+08	45 ft/sec		

Ref.	Technology	Year	Country	Scale	Wet	O2 %	CO2 %	SO2/NOx	NH3 ppm	O3 ppm	Other additive	Temp oC	Gas Flow in cm3/sec	Res. Time sec	Primary Mechanism	Final Removal
21	Dry negative streamer pulsed corona	1989			17-20%			SO2	1000			90		25	half decompose, half oxidized to NO2	salts aerosol
20	Wet, Semi-wet, spay cylindrical ESP	1995	Japan	Lab	wet			NOx	800				33	2		water absorption
B47	pulsed corona + NH3	1998	China	Pilot	dry			SO2	2200			70	388889			
B47				Math Mode				SO2	1750	insitu, 10 ppm@40k V	500 ppm ethylene, C2H4	65	333333			
B54	streamer pulsed corona	1999	USA	industrial	dry	21%	0%	NOx				room	83-166	15	NO->N by e-@N2; insitu O3 oxidation@air	NO2, NO3+OH from VOC or H2O=HNO2
B55	pulsed corona reactor	1998	Netherlands	Lab	16%	6%	8%	both	900	0	no	80	83333	30	NO oxidized to NO2	salts aerosol
28	Ozone-NH3 method+wet scrubber	1988	USSR	Pilot	wet scrubber			both	5.3kg/h	4000 g/hr	no		1388889	0.45 ~ 0.9	Ozone-NH3	wet scrubber
29	Ozone method, Venturi	1988	USSR	Pilot	wet scrubber			both	7000 g/hr	7000 g/hr	no	67	2777778	0.5	Ozone	wet scrubber
HA3	Hot Ammonia Radical Injection	1995	USA	Lab	Semi-wet ammonia water injection, dry	4%	flue gas	NOx	1-5 ratio		no	777			Ammonia Radical Reduction	Reduction
54	Positive Pulse Corona and Ammonia Water	1994	China	Lab	out-gas wet scrubber	21%	0%	SO2	1564	0	0	16	3695	2	radicals oxidation	+NH3 = salt Aerosol
54					49-61%RH	21%	0%	SO2		0	0	141	3695			
54					63%RH	21%	0%	NOx	506	0	0	12	3695	2		
43	HN3/CH4 Radical Injection Reduction	1993	USA	Lab	dry			NOx			CH4	757			Ammonia Radical Reduction	Reduction
17	Pulse Corona & E-beam	1993		Review	-	-	-	both								
9	Pulse Corona & E-beam	1997	USA	Review	-	-	-	both								
44	Pulse Corona & E-beam	1997	USA	Review	-	-	-	both								
26	Hg removal: Pulse-induced Plasma Chemical Process	1996									no					
7	CFCs removal: Surface-discharge Plasma Chemical Process	1992	Japan	Lab	18%	11%	9%	Hg			no	150 ~ 350	1453	2, 2-10		Hg removal (HgO, HgCl, HgCl2 solids)
7	VOC removal: dielectric barrier discharge	1992	Japan	Lab	dry	air	0%	CFC			no	room	8	8		decomposed
T05	Wet-type plasma reactor	1998	Taiwan	Lab	dry	air		VOC			no	room	8			
8	Heat transf.	1998	Japan		WESP			Dioxin								
47	Generation of Nox from Heated Corona Wires	1979						both								
19	Heated Corona Wires	1979			dry			no		no	no					
49	NH3 scrubbing	1997	USA	polit	wet scrubber	flue gas		SO2	in	no	no					

Ref.	+/-	Wire-Plate	Peak Voltage	Average Power	Energy density	SO2 level	Best SO2	g(SO2)/kWh	eV/#	NOx level	Best NOx	g(NO)/kWh	eV/#	Post treatment	O3 power	Note
		cm	KV	watts	Wh/nm3	ppm	%	Wh		ppm	%	Wh			watt	
21			40-75			2800	99%									
20			20	40	333.25											
B47			120	6000	4.29	2200	80%	1175	2.0	400	99%	2		bag		
B47				3000	2.50	1750	86%	1723	1.4							
B54	+		40	300000						100	30% @ N2; 50% @ air					
B55	?	10	60 + DC bios		4	300	95%	184	13	300	80%			ESP		
28																
29						655	96%	146	16	378	85%	44			61,538	L/G=1-0.5L/m3
HA3				215						326-490	96%	58			107,692	L=0.5L/m3
										flue gas	80%					
54	+	190	45	118	8.87	635	96.90%	199	12							
54	+	190	4.85			624	98.90%									high temp is bad for SO2
54	+	190	4.85													
43				1.5						260	31%					
17										600	94%					
9																
44																
26																
7	-	50 ~ 250	55	10	1.91											99%+ Mercury
7	AC	10k	4	40	1,388.89											
T05			26													
8																
47																
19																
49							93-98%									NH3 slip<10ppm

Table 10.2 Molecular Reactions

SO ₂ Reactions in the gas phase	Equilibrium Constant K or Activate Energy E (kJ/mol)	Reaction rate constant log k cm ³ /mol-sec $\log k = \log A - 0.434 \frac{E}{RT}$	Temp (K)	Reference No.
2SO ₂ + O ₂ → 2SO ₃ + O ₂	[SO ₃]/[SO ₂] = 8*10 ¹¹ at equilibrium	very slow under catalyst-free conditions in the gas phase 0.5~2%/hr field measurements	300	59 p164 59 p197
NO _x Reactions in the gas phase				
2NO + O ₂ → 2NO ₂		log k = 652.1/T-0.7356 kN/m ² = 1450 N/m ² or 1/atm? k = 1.4E-38 cm ⁶ /sec	298	57 eq1, 28 eq4, 73 36 eq207
2NO ₂ → 2NO + O ₂	E = 112.6 kJ/mol logA=12.6	log k = 0.17 log k = 12.6-5878/T	473 473-823	35
2NO ₂ ↔ N ₂ O ₄	K = 6.57 kN/m ² log K = 2993/T - 9.226		298	57
NO + NO ₂ ↔ N ₂ O ₃	K = 0.52 kN/m ² log K = 2072/T - 7.234		298	57
NO _(g) + NO _{2(g)} + H ₂ O _(g) ↔ 2HNO _{2(g)}	K = 1.41 kN/m ² log K = 2051.17/T - 6.7328		298	57
3NO _{2(g)} + H ₂ O _(g) ↔ 2HNO _{3(g)} + NO _(g)	K = 9.272*10 ⁻³ kN/m ² log K = 2003.8/T - 8.757		298	57
4NO _{2(g)} + O _{2(g)} + 2H ₂ O _(g) ↔ 4HNO _{3(g)}				28 eq5
NO + O ₂ → NO ₂ + O	E = 19.5 kJ/mol log A = 12.23	log k = 8.83 12.23 - 0.434 $\frac{19500}{8.314T}$ = 12.23 - $\frac{1018}{T}$	300 300 ~ 550	35
2NO ₂ → NO ₃ + NO	E = 100 kJ/mol log A=11.89	log k = 0.85 log k = 11.89-5220/T	473 473-703	35
NO ₃ + NO ₂ → NO + NO ₂ + O ₂	E = 13.4 kJ/mol log A = 11.15	log k = 8.82 log k = 11.15-700/T	300 300-850	35
NO ₃ + NO ₂ + M → N ₂ O ₅ + M M: particle		k = 8.4*10 ¹¹ cm ³ /mol-sec k = 6.6*10 ¹¹ cm ³ /mol-sec	340, M = 0,1 Mpa	29, 74 eq3 36 eq213
N ₂ O ₅ + M → NO ₃ + NO ₂ + M M: particle		k = 5.22 sec ⁻¹ k = 73 sec ⁻¹	340	29 36 eq221
2NO ₃ ↔ 2NO ₂ + O ₂		k = 3.78*10 ⁸	340	29

		$k = 7.2 \cdot 10^8$		36, eq218
$\text{NO} + \text{NO}_3 \leftrightarrow 2\text{NO}_2$		$k = 7.8 \cdot 10^{12}$	340	29
NOx Reactions in the liquid phase				
$\text{NO}_{(g)} + \text{NO}_{2(g)} + \text{H}_2\text{O} \rightarrow 2\text{H}^+ + 2\text{NO}_2^-$	$K = 3.28 \cdot 10^{-5} \text{ M}^4/\text{atm}^2$		298	59 p209, 72 eq28
$\text{N}_2\text{O}_{3(g)} + 2\text{H}_2\text{O} \rightarrow 2\text{H}^+ + 2\text{NO}_2^-$				72 eq29
$\text{N}_2\text{O}_{4(g)} + 2\text{H}_2\text{O} \rightarrow 2\text{H}^+ + \text{NO}_2^- + \text{NO}_3^-$				72 eq30
$3\text{NO}_{2(g)} + \text{H}_2\text{O} \rightarrow 2\text{H}^+ + 2\text{NO}_3^- + \text{NO}_{(g)}$				28 eq3
$2\text{NO}_{2(g)} + \text{H}_2\text{O} \rightarrow 2\text{H}^+ + \text{NO}_2^- + \text{NO}_3^-$	$K = 244 \text{ M}^4/\text{atm}^2$		298	59 p209
$\text{N}_2\text{O}_5 + \text{H}_2\text{O} \leftrightarrow 2\text{HNO}_3$		$k = 5 \cdot 10^{-21} \text{ cm}^3/\text{sec}$		36 eq224, 74 eq4
O ₃ Reactions in the gas phase				
$\text{O}_3 + \text{O}_3 \rightarrow 3\text{O}_2$	$E = 78.6 \text{ kJ/mol}$ $\log A = 12.65$	$\log k = 0.69$ $\log k = 12.65 - 4103/T$	343 343 ~ 373	35
$2\text{SO}_2 + \text{O}_2 \rightarrow 2\text{SO}_3$	$[\text{SO}_3]/[\text{SO}_2] = 8 \cdot 10^{11}$		298	70
$\text{SO}_2 + \text{O}_3 \rightarrow \text{SO}_3 + \text{O}_2$	$\Delta H = -57.8 \text{ kcal/mol}$	$\log k < 1.8$ $k < 120$ $k \leq 4.8$	300 340 300	35 p182, 70 29 29, 70 p42
$\text{NO} + \text{O}_3 \rightarrow \text{NO}_2 + \text{O}_2$	$E = 10.5 \sim 11 \text{ kJ/mol}$	$\log k = 9.88 \sim 10.18$ $\log k = 10 \sim 11$ $k = 1.92 \cdot 10^{10}$	298 300 340	35 74 eq1 29
$3\text{NO} + \text{O}_3 \rightarrow 3\text{NO}_2$				28 eq2
$2\text{NO} + 3\text{O}_3 \rightarrow \text{N}_2\text{O}_5 + 3\text{O}_2$				30
$\text{NO}_2 + \text{O}_3 \rightarrow \text{NO}_3 + \text{O}_2$	$E = 20, 29 \text{ kJ/mol}$	$\log k = 7.29 \sim 7.67$ $k = 5.34 \cdot 10^7$ $k = 10 \cdot 10^7$	289-299 340	35, 74 eq2 29 36
$\text{N}_2\text{O} + \text{O}_3 \rightarrow 2\text{NO} + \text{O}_2$				
NOx Reactions with SOx				
$\text{NO}_{2(g)} + \text{SO}_{2(g)} \rightarrow \text{NO}_{(g)} + \text{SO}_{3(g)}$	$E = 110.9 \text{ kJ/mol}$ $\log A = 14.4$ $\Delta H = -9.9 \text{ kcal/mol}$	$\log k = 0.57$ $\log k = 14.4 - 5789/T$	297 434~504	35
		$\log k = -5.28$	298	70 p9, 59 p166
$\text{NO}_{3(g)} + \text{SO}_{2(g)} \rightarrow \text{NO}_{2(g)} + \text{SO}_{3(g)}$	$\Delta H = -32.6 \text{ kcal/mol}$	$< \log k = 3.62$	298	70 p9, 59 p166
$\text{N}_2\text{O}_{5(g)} + \text{SO}_{2(g)} \rightarrow \text{N}_2\text{O}_{4(g)} + \text{SO}_{3(g)}$	$\Delta H = -24 \text{ kcal/mol}$	$< \log k = 1.38$	298	70 p9

Reaction rate: $1 \text{ cm}^3/\text{molecule-sec} = 6 \cdot 10^{23} \text{ cm}^3/\text{mol-sec}$

Table 10.3 Reactions of Ammonia with SO₂

Product	Reaction	Equilibrium Expressions	Temp °C	Log K @25°C	Reference No.
Ammonium sulfite	$2\text{NH}_3(\text{g}) + \text{SO}_2(\text{g}) + \text{H}_2\text{O}(\text{g}) \rightarrow (\text{NH}_4)_2\text{SO}_3(\text{s})$	$K = \exp(-76.6+32630/T)$	0~23	14.3	52, 53, 54 eq1
		$K = \exp(-73.8+30601/T)$	60~110	12.5	52
		$\text{Log } K = -33.27+14171/T$		14.3	80 tab.Ib
Ammonium bisulfite	$\text{NH}_3(\text{g}) + \text{SO}_2(\text{g}) + \text{H}_2\text{O}(\text{g}) \rightarrow \text{NH}_4\text{HSO}_3(\text{s})$	$K = \exp(-54.7+22928/T)$	0~23	9.7	52
		$K = \exp(-53.8+22116/T)$	60~110	8.9	52
		$\text{Log } K = -23.77+9958/T$		9.7	80 tab.Id
	$(\text{NH}_4)_2\text{SO}_3(\text{s}) + \text{SO}_2(\text{g}) + \text{H}_2\text{O}(\text{g}) \rightarrow 2\text{NH}_4\text{HSO}_3(\text{s})$				54 eq2
Hydrated Ammonium sulfite	$2\text{NH}_3(\text{g}) + \text{SO}_2(\text{g}) + 2\text{H}_2\text{O}(\text{g}) \rightarrow (\text{NH}_4)_2\text{SO}_3 \cdot \text{H}_2\text{O}(\text{s})$	$K = \exp(-96.7+40090/T)$	0~23	16.4	52
		$K = \exp(-93.8+38062/T)$	60~110	14.7	52
		$\text{Log } K = -42+17411/T$		16.4	80 tab.Ic
Hydrated Ammonium sulfite	$(\text{NH}_4)_2\text{SO}_3(\text{s}) + \text{H}_2\text{O}(\text{g}) \rightarrow (\text{NH}_4)_2\text{SO}_3 \cdot \text{H}_2\text{O}(\text{s})$				52
Ammonium pyrosulfite	$2\text{NH}_3(\text{g}) + 2\text{SO}_2(\text{g}) + \text{H}_2\text{O}(\text{g}) \rightarrow (\text{NH}_4)_2\text{S}_2\text{O}_5(\text{s})$	$K = \exp(-96.5+40767/T)$	0~23	17.5	52
		$K = \exp(-94.6+39144/T)$	60~110	16.0	52
		$\text{Log } K = -41.89+17705/T$		17.5	80 tab.Ic
Ammonium sulfate	$2(\text{NH}_4)_2\text{SO}_3(\text{s}) + \text{O}_2(\text{g}) \rightarrow 2(\text{NH}_4)_2\text{SO}_4(\text{s})$				
		$\text{NH}_4\text{HSO}_3(\text{s}) + \frac{1}{2} \text{O}_2(\text{g}) + \text{NH}_3(\text{g}) \rightarrow (\text{NH}_4)_2\text{SO}_4(\text{s})$			52
		$\text{SO}_2(\text{g}) \rightarrow ?\text{H}_2\text{SO}_4 + \text{NH}_3(\text{g}) \rightarrow (\text{NH}_4)_2\text{SO}_4(\text{s})$			32 eq2
		$\text{SO}_2(\text{g}) + \frac{1}{2} \text{O}_2(\text{g}) + \text{NH}_3(\text{g}) + \text{H}_2\text{O}(\text{g}) + \text{corona} \rightarrow (\text{NH}_4)_2\text{SO}_4(\text{s})$			54 eq3

Table 10.4 Henry's Constants into Water

	Henry's Constants, H , $C = H \cdot P$	Temp (K)	Ref.
	Difficult to dissolve into water		
$O_{2(g)} \rightarrow O_{2(aq)}$	$\log H = -2.89$ mol/L-atm	298	59 p199
$NO_{(g)} \rightarrow NO_{(aq)}$	$\log H = -2.72$ mol/L-atm	298	59 p209
$O_{3(g)} \rightarrow O_{3(aq)}$	$\log H = -2.03$ mol/L-atm for $Y = H X$, $H = 2.59$	298	59 p199 p219 O8
$NO_{2(g)} \rightarrow NO_{2(aq)}$	$\log H = -2$ mol/L-atm	298	59 p209
$SO_{2(g)} \rightarrow SO_{2(aq)}$	$\log H = 0.095$ mol/L-atm $K_H = 7.1 \cdot 10^{-4} \exp(3145/T)/RT$ mol/L-atm	298	59 p199 p204
$NH_{3(g)} \rightarrow NH_{3(aq)}$	$\log H = 1.79$ mol/L-atm	298	59 p199
$SO_{3(g)} \rightarrow SO_{3(aq)}$	$\log H =$ large $H = 10^{-25}$ atm, (molar fraction $x = H \cdot P$)	298	2 p407
$NO_{3(g)} \rightarrow NO_{3(aq)}$	$\log H = ??$		
	Easy to dissolve into water		

Table 10.5 Henry's Constant of SO_2

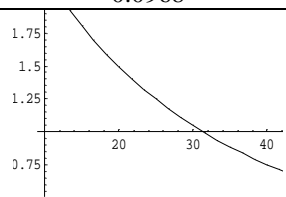
Definition	$C = H P_{SO_2}$	$P_{SO_2} = H C$	$C = H P_{SO_2}$	$Y = H X$
H		$33189000/10^{1376.1/T}$	$(7.1 \cdot 10^{-4} e^{3145/T})/RT$	$1054500 \cdot \exp(-3050.73/T)$
Unit	M/atm	atm-cm ³ /mol	M/atm	dimensionless
log H	$1376.1/T - 4.521$	$7.521 - 1376.1/T$		
H @298K	1.24	803 atm-cm ³ /mol	1.113	34.026
log H @298K	0.0968			
Vs. Temperature		$H = 666$ atm-cm ³ /mol @ 20°C		
Reference	[59 p199 p204]	From [59 p199 p204] (Used in this paper)	[69, eqA-5]	[A7-1]

Table 10.6 Liquid Phase Reactions

SO ₂ Reactions in the gas phase	Equilibrium Constant K or E (kJ/mol)	Rate const log k cm ³ /mol-sec $\log k = \log A - 0.434 \frac{E}{RT}$	Temp (K)	Ref.
Oxidation in the Liquid Phase				S3, p826
$2\text{SO}_3^{2-}(\text{aq}) + \text{O}_2(\text{aq}) \rightarrow 2\text{SO}_4^{2-}(\text{aq})$				
$\text{SO}_2(\text{aq}) + \text{O}_3(\text{aq}) \rightarrow \text{SO}_4^{2-}(\text{aq})$	-	log k = 4.38	298	59 p227
$\text{HSO}_3^-(\text{aq}) + \text{O}_3(\text{aq}) \rightarrow \text{SO}_4^{2-}(\text{aq})$	-	log k = 5.57	298	59 p227
$\text{SO}_3^{2-}(\text{aq}) + \text{O}_3(\text{aq}) \rightarrow \text{SO}_4^{2-}(\text{aq})$	-	log k = 9.18	298	59 p227
$\text{NO}_2^-(\text{aq}) + \text{O}_3(\text{aq}) \rightarrow \text{NO}_3^-(\text{aq}) + \text{O}_2(\text{aq})$	-	200 sec ⁻¹	298	59 p231
$\text{NH}_4^+ + \text{OH}^- \rightarrow \text{NH}_3(\text{g}) + \text{H}_2\text{O}$	Log K = 6.83			60 p18
Dissociation Reactions in the liquid phase				
$\text{SO}_2(\text{g}) + \text{H}_2\text{O} \rightarrow \text{S[IV]}(\text{aq})$	$H_{\text{S[IV]}} = H_{\text{SO}_2} \left[1 + \frac{K_1}{[\text{H}^+]} + \frac{K_1 K_2}{[\text{H}^+]^2} \right]$			59 p203
$\text{H}_2\text{O} \rightarrow \text{H}^+ + \text{OH}^-$	log K = -14		298	
$\text{HNO}_3 \rightarrow \text{H}^+ + \text{NO}_3^-$	log K = 1		298	71 p58, 72
$\text{HNO}_2 \rightarrow \text{H}^+ + \text{NO}_2^-$	log K = -3.15		298	71 p58, 72
$\text{H}_2\text{SO}_4 \rightarrow \text{H}^+ + \text{HSO}_4^-$	log K = 3		298	71 p58
$\text{HSO}_4^- \rightarrow \text{H}^+ + \text{SO}_4^{2-}$	log K = -1.99		298	71 p58
$\text{H}_2\text{SO}_3 \rightarrow \text{H}^+ + \text{HSO}_3^-$	log K ₁ = -1.91 K ₁ = 1.9*10 ⁻⁵ exp(2022/T) mol/L		298	71 p58, 69
$\text{HSO}_3^- \rightarrow \text{H}^+ + \text{SO}_3^{2-}$	log K ₂ = -7.18 K ₂ = 2.4*10 ⁻¹⁰ exp(1671/T) mol/L		298	71 p58, 69
$2\text{NO}_2(\text{aq}) + \text{H}_2\text{O} \rightarrow 2\text{H}^+ + \text{NO}_2^- + \text{NO}_3^-$				57 eq24
$\text{N}_2\text{O}_3(\text{aq}) + \text{H}_2\text{O}(\text{aq}) \rightarrow 2\text{H}^+ + 2\text{NO}_2^-(\text{aq})$				57 eq25
$\text{N}_2\text{O}_4(\text{aq}) + \text{H}_2\text{O}(\text{aq}) \rightarrow 2\text{H}^+ + \text{NO}_2^- + \text{NO}_3^-$				57 eq26
$\text{NO}_2(\text{aq}) + \text{SO}_2(\text{aq}) \rightarrow \text{NO}(\text{aq}) + \text{SO}_3(\text{aq})$	-	log k = 6.3	298	59 p227

Table 10.7 Dissociation Reactions of Sulfite and Sulfate

Source	[69 eqA-6&7]	[59 p199, p204]	[71 p.58]	Vs. Temperature
$H_2SO_3 \rightarrow H^+ + HSO_3^-$				
K_{a1} ; mol/L	$1.9 \cdot 10^{-5} \exp(2022/T)$	$10^{(853/T - 4.74)}$		
pK_{a1}		1.89 @298K	1.91 @298K	
ΔH_{298} ; kcal/mol		-4.16		
$HSO_3^- \rightarrow H^+ + SO_3^{2-}$				
K_{a2} ; mol/L	$2.4 \cdot 10^{-10} \exp(1671/T)$	$10^{(621.9/T - 9.278)}$		
pK_{a2}		7.22 @298K	7.18 @298K	
ΔH_{298} ; kcal/mol		-2.23		
$H_2SO_4 \rightarrow 2H^+ + SO_4^{2-}$				
K_{a1} ; mol/L			-3 @298K	
K_{a2} ; mol/L			1.99 @298K	

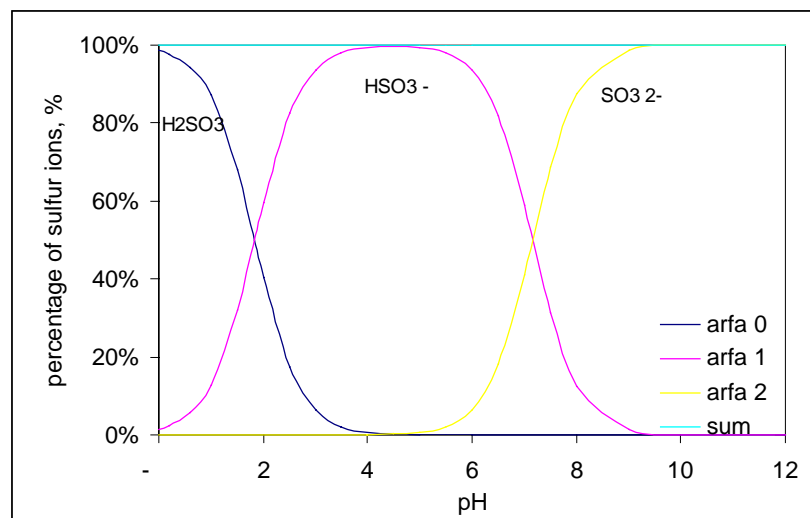


Figure 10.1 Distribution of Sulfite Ions vs. pH of solution

Table 10.8 Solubility of Gases in water

	Solubility of NH ₃ in water	Solubility of SO ₂ in water	Solubility of NO in water	Solubility of NO ₂ in water
	529 g/L @ 20°C	89.7 g/L @ 20°C (estimated from $\ln X = -25.2629 + 0.457552 \cdot T + 5.6855 \cdot \ln(T/100)$ $X = 2.46 \cdot 10^{-2}$ @ 20°C where X: mole fraction solubility at SO ₂ partial pressure 1 atm)	0.063 g/L	1.26 g/L
Ref #	68 Tab 3-123	67	3 p1008	3 p1008

Table 10.9 Diffusivity of Ions in Water

$$D_{H^+} = 9.31 \cdot 10^{-5} \text{ cm}^2/\text{s} [75, 76]$$

$$D_{H_2SO_3} = 1.76 \cdot 10^{-5} \text{ cm}^2/\text{s} [33, 36]$$

$$D_{HSO_3^-} = 1.33 \cdot 10^{-5} \text{ cm}^2/\text{s} [75, 76]$$

$$D_{SO_3^{2-}} = 0.958 \cdot 10^{-5} \text{ cm}^2/\text{s} [75, 76]$$

$$D_{HCO_3^-} = 1.18 \cdot 10^{-5} \text{ cm}^2/\text{s} [75, 76]$$

$$D_{OH^-} = 5.24 \cdot 10^{-5} \text{ cm}^2/\text{s} [37]$$

Table 10.10 Solubility Study of Calcium and Ammonium Salts

		Ref #
$\text{CaO} + 2\text{H}_2\text{O} + \text{SO}_2 \rightarrow \text{CaSO}_3 \cdot 2\text{H}_2\text{O}$	Log K = 32.8	S3, p823
$\text{CaCO}_3 + 2\text{H}_2\text{O} + \text{SO}_2 \rightarrow \text{CaSO}_3 \cdot 2\text{H}_2\text{O} + \text{CO}_2$	Log K = 10.9	S3, p823
$\text{CaSO}_{4(s)} \rightarrow \text{Ca}^{2+} + \text{SO}_4^{2-}$	Log K_{sp} = -4.15	67
$\text{CaSO}_4 \cdot 2\text{H}_2\text{O}_{(s)} \rightarrow \text{Ca}^{2+} + \text{SO}_4^{2-} + 2\text{H}_2\text{O}$	Log K_{sp} = -4.6 $\log(\text{Ca}^{2+}) = -4.6 - \log(\text{SO}_4^{2-})$ 2.08~2.54 g/L	71 p224
$\text{Ca}(\text{OH})_{2(s)} \rightarrow \text{Ca}^{2+} + 2\text{OH}^-$	Log K_{sp} = -5.31 0.18 g/100mL	67 A6
$\text{Ca}(\text{OH})_{2(s)} + 2\text{H}^+ \rightarrow \text{Ca}^{2+} + 2\text{H}_2\text{O}$	Log K_{sp} = 22.8 = 2*14-5.31 $\log(\text{Ca}^{2+}) = 22.8 - 2\text{pH}$	71 p232

	Sulfate SO_4^{2-}	Sulfite SO_3^{2-}	Nitrate NO_3^-	Nitrite NO_2^-	OH^-
Ca^{2+}	Calcium Sulfate	Calcium Sulfite	Calcium Nitrate	Calcium Nitrite	Calcium Hydroxide
	0.208g/100mL [68] 0.205% [67] = 0.205 g/100mL	0.0054 % [67] = 0.0054 g/100mL	141 g/100mL [68] 59 % [67] = 144 g/100mL	76.7 g/100mL [68] 48.6 % [67] = 94.6 g/100mL	0.16 g/100mL [68]
log K_{sp}	-4.3 [67] -3.64*	-6.69*	3.43*	3.17*	-5.31 [67] -4.39*
NH_4^+	Ammonium Sulfate	Ammonium Sulfite	Ammonium Nitrate	Ammonium Nitrite	Ammonium Hydroxide
	76.7g/100mL [68] 43.3 % [67] = 76.4 g/100mL	39.1% [67] = 64.2 g/100mL	217g/100mL [68] 68 % [67] = 213 g/100mL	68.8 % [67] = 221 g/100mL	Soluble
log K_{sp}	2.89*	2.83*	2.87*	3.07*	?

Solubility data of sulfate, sulfite, nitrate, nitrite compounds at 25°C

* Estimated Ksp from g/100mL solubility data

Table 10.11 Radicals and Electrons Related Reactions

Three Body Attachment :	E	rate const : log A or log k (cm³/mol.sec)	Temp (K)	Ref.
$e^- + NO + NO \rightarrow NO^- + NO$				N1, p340
$e^- + SO_2 + X \rightarrow SO_2^- + X + \text{energy}$	Exothermic, electron affinity of $SO_2^- = 1.097 \text{ eV}$	at $E/N < 40 \text{ Td}$, 1 torr		25 p2017 p2024
Dissociative attachment:	E	rate const : log A or log k (cm³/mol.sec)	Temp (K)	Ref. #
$e^- + SO_2 \rightarrow O + SO^-$ (most probable)	4.52 eV	at 1 torr		25 p2024
$e^- + SO_2 \rightarrow SO + O^-$	4.15 eV	at 1 torr		25 p2024
$e^- + SO_2 \rightarrow O_2 + S^-$	3.63 eV	at 1 torr		25 p2024
associative detachment	E	rate const : log A or log k (cm³/mol.sec)	Temp (K)	Ref. #
$O^- + SO_2 \rightarrow SO_3 + e + \text{energy}$	exothermic, 2.1 eV	at 1 torr SO_2 - O_2 mixture		25 p2025
	at $E/N=117.2 \text{ Td}$	reaction rate = $2 \cdot 10^{-9} \sim 8 \cdot 10^{-10} \text{ cm}^3/\text{s}$		
$O_2^- + SO_2 \rightarrow SO_2^- + O_2$	at 1 torr SO_2 - O_2 mixture	reaction rate = $3.9 \cdot 10^{-9} \text{ cm}^3/\text{s}$		25 p2015
$e (18.9 \text{ eV}) + H_2O \rightarrow OH^+ + H + 2e$	ionization of OH^+ from H_2O	$k = 2.6 \cdot 10^{-14} \text{ cm}^3/\text{s}$		37, 36
$e (13.8 \text{ eV}) + OH \rightarrow OH^+ + 2e$	ionization of OH^+ from OH			37
$NH_3 + e \rightarrow NH^* + H_2 + e$				18 eq4
$NH_3 + e \rightarrow NH_2^* + H + e$				18 eq5
$NH^* + NO \rightarrow N_2 + OH^*$				18 eq6
$NH_2^* + O_2 \rightarrow HNO + OH^*$				18 eq7
$NH_2^* + NO \rightarrow N_2 + H_2O$				18 eq8

X = the third body

1 eV = $1.6 \cdot 10^{-19}$ watt-sec = $1.6 \cdot 10^{-19}$ J = about 96 kJ/mol for a mole molecules

Reaction rate: $\text{cm}^3/\text{molecule-sec} = 6 \cdot 10^{23} \text{ cm}^3/\text{mol-sec}$